

University of Alberta

PRECISION CALCULATIONS IN HEAVY FERMION DECAYS

by

Alexey Pak



A thesis submitted to the Faculty of Graduate Studies and Research in partial fulfillment of the requirements for the degree of **Doctor of Philosophy**.

Department of Physics

Edmonton, Alberta  
Fall 2008



Library and  
Archives Canada

Bibliothèque et  
Archives Canada

Published Heritage  
Branch

Direction du  
Patrimoine de l'édition

395 Wellington Street  
Ottawa ON K1A 0N4  
Canada

395, rue Wellington  
Ottawa ON K1A 0N4  
Canada

*Your file* *Votre référence*  
*ISBN: 978-0-494-46402-1*  
*Our file* *Notre référence*  
*ISBN: 978-0-494-46402-1*

**NOTICE:**

The author has granted a non-exclusive license allowing Library and Archives Canada to reproduce, publish, archive, preserve, conserve, communicate to the public by telecommunication or on the Internet, loan, distribute and sell theses worldwide, for commercial or non-commercial purposes, in microform, paper, electronic and/or any other formats.

The author retains copyright ownership and moral rights in this thesis. Neither the thesis nor substantial extracts from it may be printed or otherwise reproduced without the author's permission.

**AVIS:**

L'auteur a accordé une licence non exclusive permettant à la Bibliothèque et Archives Canada de reproduire, publier, archiver, sauvegarder, conserver, transmettre au public par télécommunication ou par l'Internet, prêter, distribuer et vendre des thèses partout dans le monde, à des fins commerciales ou autres, sur support microforme, papier, électronique et/ou autres formats.

L'auteur conserve la propriété du droit d'auteur et des droits moraux qui protègent cette thèse. Ni la thèse ni des extraits substantiels de celle-ci ne doivent être imprimés ou autrement reproduits sans son autorisation.

---

In compliance with the Canadian Privacy Act some supporting forms may have been removed from this thesis.

Conformément à la loi canadienne sur la protection de la vie privée, quelques formulaires secondaires ont été enlevés de cette thèse.

While these forms may be included in the document page count, their removal does not represent any loss of content from the thesis.

Bien que ces formulaires aient inclus dans la pagination, il n'y aura aucun contenu manquant.

■ ■ ■  
**Canada**

*Let no one, therefore, expect from us a complete history and theory of the Glass Bead Game. Even authors of higher rank and competence than ourself would not be capable of providing that at the present time. That task must remain reserved to later ages, if the sources and the intellectual prerequisites for the task have not previously been lost. Still less is our essay intended as a textbook of the Glass Bead Game; indeed, no such thing will ever be written. The only way to learn the rules of this Game of games is to take the usual prescribed course, which requires many years; and none of the initiates could ever possibly have any interest in making these rules easier to learn.*

*(“The Glass Bead Game”, Hermann Hesse)*

# Abstract

This thesis is devoted to precision perturbative calculations in field theory. Supplementing accurate experimental data, they improve the knowledge of fundamental parameters and provide the basis for searches of unknown physics effects.

The results of two original theoretical calculations are presented. Both describe the decays of heavy fermions, such as the top quark and the muon, but chiefly relevant to the important case of bottom-to-charm quark transitions.

The first calculation corresponds to a special kinematic limit of maximum recoil momentum of the final quark. Mass-dependent next-to-next-to-leading order (NNLO) corrections due to strong interaction found in this work complement and extend a series of published results obtained in other limits.

The second and the major calculation of this thesis provides charm mass effects in the total semi-leptonic decay rate of the bottom quark, also at NNLO. Used as an input to fitting precision measurements, these results reveal a mistake in previous approximations, thus leading to a shift in the value of one of Cabibbo-Kobayashi-Maskawa matrix elements.

When applied to muon decays, these expressions describe an important but previously overlooked correction to muon life time. Significant for ongoing experiments, this correction results in a slight shift of the measured Fermi constant.

The techniques and methods used in those projects are explained in detail, with attention to practical issues. The algorithms are implemented as computer programs, applicable to a wide variety of other challenging problems.

To Olga and Masha.

# Table of Contents

<b>1</b>	<b>Introduction</b>	<b>1</b>
<b>2</b>	<b>Multi-scale problems</b>	<b>5</b>
2.1	Effective theories . . . . .	5
2.2	Asymptotic expansions . . . . .	8
2.3	Conclusion . . . . .	14
<b>3</b>	<b>Recurrence relations</b>	<b>15</b>
3.1	One-loop example . . . . .	15
3.2	Laporta algorithm . . . . .	17
3.3	Epsilon-finite bases . . . . .	24
3.4	Gröbner bases . . . . .	25
<b>4</b>	<b>Numerical evaluation of master integrals</b>	<b>29</b>
4.1	Alpha-representation . . . . .	30
4.2	Sector decomposition . . . . .	37
4.3	Mellin-Barnes transformation . . . . .	42
4.4	Conclusion . . . . .	46
<b>5</b>	<b>Evaluation of integrals by differential equations</b>	<b>47</b>
5.1	Simple one-loop example . . . . .	48
5.2	Harmonic polylogarithms . . . . .	51
5.3	Simple four-loop example . . . . .	52
5.4	The gory details of a four-loop calculation . . . . .	55
<b>6</b>	<b>Semi-leptonic <math>b</math>-quark decay near maximum recoil</b>	<b>58</b>
6.1	Maximum recoil limit . . . . .	58
6.2	Tree-level decay rate . . . . .	60
6.3	One-gluon corrections . . . . .	62
6.4	Two-gluon corrections . . . . .	64
6.5	Applications of the result . . . . .	70
<b>7</b>	<b>Semi-leptonic <math>b</math>-quark decay and muon decay</b>	<b>74</b>
7.1	Tree-level decay rate and first-order correction . . . . .	75
7.2	Calculation of two-loop corrections . . . . .	77
7.3	Evaluation of master integrals . . . . .	79

7.4	Integrated decay rate . . . . .	79
7.5	Moments of distributions and axial current . . . . .	82
7.6	Charm mass in $b \rightarrow u$ decays and vector couplings . . . . .	84
7.7	Conclusion: semi-leptonic results . . . . .	85
<b>8</b>	<b>Conclusion</b>	<b>86</b>
	<b>Bibliography</b>	<b>88</b>
<b>A</b>	<b>Selected integration formulas</b>	<b>94</b>
A.1	Exactly known integrals . . . . .	94
A.2	Phase space parameterizations . . . . .	95
<b>B</b>	<b>Topologies and master integrals</b>	<b>98</b>
B.1	Three-loop on-shell master integral . . . . .	98
B.2	Four-loop on-shell topologies . . . . .	99
B.3	Four-loop master integrals . . . . .	100
B.4	Three-loop eikonal topologies . . . . .	110
B.5	Three-loop eikonal master integrals . . . . .	111
<b>C</b>	<b>Semi-leptonic <math>b</math>-quark decay results</b>	<b>114</b>
C.1	Integrated decay rate . . . . .	114
C.2	Moments of lepton energy distribution . . . . .	116
C.3	Moments of hadronic energy distribution . . . . .	121
C.4	Decay rate in model with vector couplings . . . . .	125
C.5	Charm mass in $b \rightarrow u$ transitions . . . . .	128

# List of Figures

2.1	One-loop double-scale propagator-type integral . . . . .	9
2.2	“Soft” loop momentum limit, $q \sim m$ . . . . .	9
2.3	“Hard” loop momentum limit, $q \sim M$ . . . . .	9
2.4	Topology contributing to $\mathcal{O}(\alpha)$ corrections to the muon decay rate . . . . .	12
2.5	Region 1: $k_1, k_2 \gg m$ . . . . .	13
2.6	Region 2: $k_2 \gg k_1 \sim m$ . . . . .	13
2.7	Region 3: $k_1 \gg k_2 \sim m$ . . . . .	13
2.8	Region 4: $k_1, k_2 \sim m$ . . . . .	13
3.1	Sketch of a system convenient for Gauss elimination. Each line corresponds to a single relation. Filled boxes represent non-zero coefficients. . . . .	20
3.2	Sketch of Gauss elimination steps (the first equation is at the top). Light grey boxes represent non-zero coefficients, dark grey – coefficient $-1$ . . . . .	21
3.3	Work flow for reducing an expression $X$ . . . . .	23
3.4	Laporta work flow re-using the existing solution. . . . .	23
3.5	Appending new lines after the reduced system. . . . .	23
4.1	Numbering and line directions in a a two-loop graph. . . . .	31
4.2	Spanning trees of the graph with labeled chords. . . . .	32
4.3	Spanning 2-trees of the graph. Chords and entering external momenta are labeled. . . . .	32
4.4	Example of trees corresponding to form <b>B</b> . Chords and momenta are labeled. . . . .	33
4.5	Trees-with-a-cycle contributing to <b>K</b> . Cycle direction, cycle lines and chords are labeled. . . . .	34
5.1	Generic topology T. Dashed lines represent massless, and solid lines – massive propagators. Index $1\epsilon$ denotes the $\epsilon$ -power of line 1. . . . .	52
5.2	Three regions contributing to the imaginary part of topology T in the expansion about $x = 0$ . . . . .	54
5.3	Different topologies having the same on-shell ( $x = 1$ ) limit. Thin solid line represents mass 1, thick lines – squared mass $1/x$ . . . . .	56



5.4	Topology leading to $V30$ in the on-shell limit. . . . .	57
6.1	Tree-level decay $b \rightarrow cW^*$ . . . . .	60
6.2	Self-energy diagram related to the tree-level decay $b \rightarrow cW^*$ . . . . .	60
6.3	Diagrams contributing to $\mathcal{O}(\alpha_s)$ corrections . . . . .	62
6.4	Common double-scale topology . . . . .	62
6.5	$\mathcal{O}(\alpha_s)$ renormalization contributions . . . . .	63
6.6	Quark loop contribution to $b$ -decay at $\mathcal{O}(\alpha_s^2)$ . . . . .	67
6.7	Abelian contributions to $b$ -decay at $\mathcal{O}(\alpha_s^2)$ . . . . .	68
6.8	Non-abelian contributions to $b$ -decay at $\mathcal{O}(\alpha_s^2)$ . . . . .	70
6.9	$\mathcal{O}(\alpha_s^2)$ mass expansions of the semi-leptonic heavy quark decay rate $\Gamma(Q \rightarrow q\ell\bar{\nu})$ in various kinematic limits. Allowed kinematic configurations are inside the triangle. On the lower side, recoil momentum of $q$ is the largest. . . . .	71
6.10	Matching of expansions around $\rho = 0$ (thick line) and $\rho = 1$ (thin line) for maximum quark recoil, $M_{W^*} = 0$ . Matching point corresponds to the smallest difference between the two approximations. . . . .	72
7.1	Diagram corresponding to the tree-level decay rate . . . . .	75
7.2	Region 1: $q \sim m_b \gg m_c$ . . . . .	75
7.3	Region 2: $q \sim m_c$ . . . . .	75
7.4	One-gluon corrections to the semi-leptonic decay rate . . . . .	76
7.5	Wave function and mass renormalization contributions . . . . .	76
7.6	Examples of $\mathcal{O}(\alpha_s^2)$ diagrams . . . . .	77
7.7	Expansion of a double-scale topology (a) in all contributing asymptotic regions (b-l). Thick lines represent mass $m_b$ , thin – mass $m_c$ , dashed lines are massless, double lines correspond to eikonal propagators. . . . .	77
7.8	Double-scale topologies with artificial large mass $1/x$ (thick lines), unit mass (thin solid lines), and massless propagators (dashed lines). $\epsilon$ denotes non-integer propagator power from integration of a massless sub-loop. . . . .	79
7.9	Mass-dependent corrections to $X_2$ of Eq. 7.4. . . . .	80
7.10	Tree-level and $\mathcal{O}(\alpha_s)$ matrix elements of the four-quark operator . . . . .	80
7.11	Renormalization contribution of the axial current . . . . .	83
7.12	First two moments of lepton and hadron energy distributions . . . . .	84
7.13	Charm contributions to semi-leptonic decay $b \rightarrow u$ . . . . .	84

# Chapter 1

## Introduction

Our present understanding of the microscopic structure of the universe is summarized in an extremely successful framework – the Standard Model (SM)<sup>1</sup>. It consists of three major ingredients:

**Quantum Electrodynamics (QED)**, built from late 1920s to 1950s, describes electromagnetic interactions of charged particles. Its development involved P. Dirac, V. Fock, W. Pauli, H. Bethe, S. Tomonaga, J. Schwinger, R. Feynman, F. Dyson and other prominent physicists. Since then, it has been verified down to sub-atomic scales by the collider experiments (e.g., LEP tested the QED at  $10^{-17}$  m), and up to galactic distances through astronomical observations (the most stringent limits on the photon mass [1, 2] correspond to the Compton wavelength of  $10^{20}$  m). This makes the QED by far the most well-established physics theory.

**Quantum Chromodynamics (QCD)** describes the short-range “strong” interactions, including, e.g., nuclear forces. In an effort to understand the “ordinary” matter, M. Gell-Mann and G. Zweig in 1964 identified the special role of SU(3) triplet representations in hadronic spectroscopy [3, 4]. After the discovery of asymptotic freedom by Gross, Wilczek and Politzer in 1973 [5, 6, 7], QCD was established [8, 9] as a theory of interacting quarks.

The first direct evidence for quarks appeared in a 1969 experiment led by J. Friedman, H. Kendall, and R. Taylor [10, 11]; but it was not until 1995 that

---

<sup>1</sup>Neutrino oscillations, while not part of the SM, can be accommodated relatively easily.

(presumably) the last and the heaviest top quark was found in Fermilab [12].

**Electro-weak (EW)** theory through the so-called Higgs mechanism provides explanation for the masses of other particles, also introducing heavy gauge bosons mediating “weak” interactions. Suppressed compared to QED at distances larger than  $10^{-17}$  m, this force is nevertheless responsible for nuclear beta-decays and the muon decay. In 1956, T.-D. Lee and C.-N. Yang predicted [13] that certain nuclei may decay differently in our universe and the one reflected in a mirror; and that was observed in C.-S. Wu’s experiment in 1957 [14] (several observations by other groups followed immediately). In 1967, S. Weinberg, S. Glashow, and A. Salam suggested an elegant generalization [15, 16] of that theory providing answers to many theoretical concerns, valid through distances of the order  $10^{-18}$  m. It found a spectacular confirmation when  $W$  and  $Z$ -bosons were directly observed in 1983 at CERN [17].

The Standard Model, unifying these three forces, was formulated in 1970-73. After the discovery of the tau-neutrino in 2000 [18], the last remaining unobserved piece of the SM is the Higgs boson.

While this thesis is being written, the Large Hadron Collider (LHC) is about to start taking data. To interpret its results and fully utilize its potential, large efforts are being put into evaluating quantum corrections to many processes in the SM and its hypothesized extensions.

As an alternative to huge particle accelerators, low-energy experiments aim at tiny indirect manifestations of the New Physics. For example, trapped ion measurements reach accuracy of fractions of parts-per-trillion (ppt) in testing QED [19], while the muon anomalous magnetic moment [20], measured to parts-per-million (ppm), tests EW theory. Such experiments provide the best accuracy for fundamental constants, such as the fine structure constant  $\alpha$ .

To match the progress of the experimental technology, theoretical calculations need to account for next-to-leading, next-to-next-to-leading or even further effects, thus becoming increasingly difficult. The most advanced computational framework for such calculations is the perturbation theory based on Feynman diagrams [21, 22]. Successive approximations in this method

correspond to the greater number of nested “loop” integrations.

This thesis deals with the perturbative corrections to heavy fermion decays within the Standard Model. In addition to the complexity of multiple loops they involve several different energy scales, thus necessitating a careful resolution of their contributions. Recent progress in related techniques made possible the calculations that constitute the heart of this thesis. Together with accurate measurements, those results may ultimately lead to better accuracy for fundamental constants, such as the Fermi constant  $G_F$  and the Cabibbo-Kobayashi-Maskawa matrix element  $V_{cb}$ <sup>2</sup>.

The structure of this thesis is as follows. The leading chapters present a detailed overview of computational techniques and frameworks. Chapter 2 introduces a systematic approach to multiple-scale problems, Chapter 3 describes the methods to reduce the number of integrals in a calculation. Chapters 4 and 5 demonstrate, respectively, numerical and analytical tools used in practice to evaluate multi-loop integrals.

The chapters that follow are devoted to the results of the original research projects completed using those instruments. Chapter 6 presents a calculation of QCD effects in semi-leptonic  $b \rightarrow c$  transitions obtained in a special kinematic limit. This result builds upon and complements a series of related published results. Finally, Chapter 7 contains the most important and challenging result of this work, which describes both the QCD corrections to the semi-leptonic  $b$ -quark decays, and the QED effects in the muon ( $\mu$ ) decays.

Following the conclusions in Chapter 8, the Appendices A, B and C summarize the auxiliary results and formulas needed to accomplish this work. Some of the results presented in this thesis have already been published [26, 27].

---

<sup>2</sup>The flavour is a property of quarks of well-defined mass (which may be not known well). The charged weak interactions connect up-type quarks with linear combinations of down-type quarks of various masses (flavours). The coefficients of these combinations form a three-by-three matrix, called the CKM matrix [23, 24, 25].

## Notations

Throughout this thesis, we use the “natural” system of units in which  $\hbar = c = \epsilon_0 = 1$ . Dimensional regularization with  $D = 4 - 2\epsilon$  is used to consistently treat divergent integrals. A factor of  $\mathcal{F} = \Gamma(1+\epsilon)/(4\pi)^{2-\epsilon}$  per loop is explicitly extracted in all loop integrals to avoid the proliferation of Euler’s constant  $\gamma_E$  in the expressions and results. Following the notations of Ref. [28], the integration measure over momentum  $k$  is denoted as  $d^D k/(2\pi)^D \equiv [d^D k]$ . Since this thesis significantly uses the developments of Ref. [28], the concepts and methods mentioned but not described here can be found in that reference.

# Chapter 2

## Multi-scale problems

A fundamental physical theory, describing phenomena at the smallest distances, is usually not appropriate for calculations at much lower energy scales. For instance, the dynamics of fluids is impossible to describe in terms of interacting quarks and leptons. However, effects of quark theory, atomic structure, and molecular interactions can be hidden in a few measurable parameters, resulting in what is known as an effective low-energy theory.

Finding quantum corrections in problems involving several energy scales is usually simpler within an effective theory. A complementary approach is to separate the scales inside the loop integrals, and build the corresponding expansion. Although less general, this technique is very well suited for computer-aided calculations.

This chapter introduces the basics of effective field theories (EFTs), mostly following Refs. [29, 30]. After that, we discuss several examples of asymptotic expansions in loop integrals.

### 2.1 Effective theories

All the properties of an arbitrary field  $\phi$  are encoded in its generating functional, or vacuum-to-vacuum transition matrix element:

$$W \equiv \langle 0|0 \rangle = \int \mathcal{D}\phi e^{iS[\phi]}, \quad S[\phi] = \int d^D x \mathcal{L}(\phi, \partial_\mu \phi), \quad (2.1)$$

where the path integral is taken over all configurations of field  $\phi$ , and the action  $S$  is an integral of the Lagrangian density  $\mathcal{L}$ .

The basic idea due to Wilson [31] consists of integrating out the high-energy modes  $\phi_H$  with energy (frequency)  $E > \Lambda$  from this path integral. The remaining integral over modes  $\phi_L$  (with  $E < \Lambda$ ) is then expressed in terms of an effective cutoff-dependent action  $S_\Lambda$ :

$$W = \int \mathcal{D}\phi e^{iS[\phi]} = \int \mathcal{D}\phi_L \mathcal{D}\phi_H e^{iS[\phi_L, \phi_H]} = \int \mathcal{D}\phi_L e^{iS_\Lambda[\phi_L]}. \quad (2.2)$$

$S_\Lambda$  can be expanded in an (infinite) sum in terms of all operators  $\mathcal{O}_i$ , allowed by the symmetries of the problem. They are non-local at the scale  $1/\Lambda$ , but since the fields  $\phi_L$  vary only weakly over such distances, this non-locality does not influence physical results:

$$S_\Lambda = \int d^D x \sum_i g_i \mathcal{O}_i. \quad (2.3)$$

If an operator  $\mathcal{O}_i$  scales with energy as  $E^{\delta_i}$  (where  $E$  characterizes the low-energy process), then to keep  $S_\Lambda$  dimensionless, the coupling constant  $g_i$  should offset the dimension by  $D - \delta_i$ . Since  $g_i$ 's connect our theory to the “fundamental” high-energy theory, they can only depend on  $\Lambda$ , and we can assume  $g_i = \Lambda^{D-\delta_i} \lambda_i$  with  $\lambda_i \sim 1$ . Integration over  $d^D x$  introduces a factor scaling as  $E^{-D}$ , so that

$$\int d^D x g_i \mathcal{O}_i \sim \lambda_i \left( \frac{E}{\Lambda} \right)^{\delta_i - D}. \quad (2.4)$$

Each operator  $\mathcal{O}_i$  now can be classified based on its scaling as  $E \rightarrow 0$ . If  $\delta_i < D$ , then its contribution to  $S$  grows, and  $\mathcal{O}_i$  is called “relevant”. Terms with  $\delta_i > D$  are “irrelevant”, and those with  $\delta_i = D$  are “marginal”. Usually there is only a finite number of relevant and marginal terms that determine the low-energy physics. Irrelevant terms are considered to the order dictated by the chosen precision. Constants  $g_i$  then are fixed by a calculation in the “full” theory.

**Example 1.** A simple example of an effective theory is Fermi’s four-fermion interaction, describing the muon decay. In the electroweak theory the propagator of a  $W$ -boson with four-momentum  $q$  is  $P^{\alpha\beta} \sim \frac{g^{\alpha\beta}}{q^2 - M_W^2}$ , where  $W$ -boson

mass  $M_W \approx 80.4$  GeV. However, the characteristic momentum transfer in the muon decay is  $\sqrt{q^2} \sim m_\mu \approx 105.6$  MeV  $\ll M_W$ . The  $W$ -exchange amplitude  $g_w^2 P^{\alpha\beta} \cdot \bar{\mu}\gamma_\alpha \frac{1-\gamma_5}{2}\nu \cdot \bar{e}\gamma_\beta \frac{1-\gamma_5}{2}\nu$  can then be substituted with an effective vertex  $G_F \cdot \bar{\mu}\gamma_\alpha(1-\gamma_5)\nu \cdot \bar{e}\gamma^\alpha(1-\gamma_5)\nu$ , where  $G_F = \frac{\sqrt{2}g_w^2}{8M_W^2}$  is the Fermi constant. This constant absorbs all the weak physics, thus  $W$ - and  $Z$ -bosons are absent in this theory. Note that although this operator is “irrelevant” by our classification (its scaling dimension is  $[\bar{\mu}(1-\gamma_5)\nu \cdot \bar{e}(1-\gamma_5)\nu] = 6 > 4$ ), it is responsible for the leading contribution to the decay.

**Example 2.** To demonstrate the practical approach to building an effective theory, let us try to explain why the sky is blue. We consider the elastic scattering of photons off neutral atoms, with photon energy  $E_\gamma$  much smaller than atomic excitation energy  $\Delta$ . The latter is small compared to the inverse Bohr radius,  $a_0^{-1}$ , which in turn is smaller than the atomic mass  $M$ :

$$E_\gamma \ll \Delta \ll a_0^{-1} \ll M. \quad (2.5)$$

It is not difficult to determine the relevant degrees of freedom. First, gauge invariance dictates that the photonic field  $A_\mu$  can only enter as  $F_{\mu\nu} = \partial_\mu A_\nu - \partial_\nu A_\mu$ . Second, the atomic field  $\Phi$ , satisfying Klein-Gordon equation  $(\partial_\mu\partial^\mu - M^2)\Phi = 0$ , can be decomposed to factor out the fast oscillations due to its large rest mass:  $\Phi = e^{-iMv_\mu x^\mu} \phi$ , where  $v_\mu$  is the atomic four-velocity. Being neutral,  $\phi$  can only couple to  $F_{\mu\nu}$  but not to  $A_\mu$ .

Let us now construct the most general Lagrangian, satisfying Lorentz and gauge symmetries, from all possible monomials containing  $v_\mu$ ,  $\partial_\mu$ ,  $\phi^\dagger\phi$ , and  $F_{\mu\nu}$ . Some combinations vanish, simplifying the task: for instance,  $\partial_\mu F^{\mu\nu} = 0$  due to Maxwell’s equations,  $\partial_\mu\partial^\mu\phi = 0$  is the equation of motion for the field  $\phi$ . In addition, in the atomic rest frame  $v_\mu = (1, 0, 0, 0)$ , which together with zero-recoil condition  $\partial_t\phi = 0$  leads to  $v_\mu\partial^\mu\phi = 0$ .

Thus, our interaction Lagrangian is<sup>1</sup>

$$\mathcal{L}_{\text{eff}} = c_1\phi^\dagger\phi F_{\mu\nu}F^{\mu\nu} + c_2\phi^\dagger\phi v^\alpha F_{\alpha\mu}v_\beta F^{\beta\mu} + c_3\phi^\dagger\phi(v^\alpha\partial_\alpha)F_{\mu\nu}F^{\mu\nu} + \dots \quad (2.6)$$

<sup>1</sup>There are more operators scaling as the third term, e.g.,  $\phi^\dagger\partial^\mu\phi F_{\mu\nu}v_\alpha F^{\alpha\nu}$ , which we do not include here since the first two terms will be found to dominate at low energies.



Now we establish the operator dimensions:  $[\partial_\mu] = 1$  (scaling as 1/length); the photon kinetic term,  $\mathcal{L}_\gamma = -\frac{1}{4}(F^{\mu\nu})^2$ , requires  $[F_{\mu\nu}] = 2$ . Finally, the dimension of operator  $\phi$  is determined from the normalization of atomic wave functions  $\Psi$ :  $\phi^\dagger|0\rangle = \Psi|1\rangle$  ( $|0\rangle$  and  $|1\rangle$  being the states with zero and one atoms). Since  $\langle 1|1\rangle = 1$ , and we normalize for one atom per volume,  $\int d^3x|\Psi|^2 = 1$ , then  $[\phi] = 3/2$ .

Since  $\mathcal{L}_{\text{eff}}$  has dimension 4, then  $[c_1] = [c_2] = -3$ ,  $[c_3] = -4$ , and only the two lowest order terms determine the scattering cross-section. To decide whether  $\Delta$  or  $a_0^{-1}$  set the scale of  $c_1$  and  $c_2$ , we may notice that low-frequency photons cannot probe the structure of atomic levels; thus, the cross-section has to be determined by the scatterer's size,  $a_0$ . Our effective Lagrangian now becomes

$$\mathcal{L}_{\text{eff}} = a_0^3 (\lambda_1 \phi^\dagger \phi F_{\mu\nu} F^{\mu\nu} + \lambda_2 \phi^\dagger \phi v^\alpha F_{\alpha\mu} v_\beta F^{\beta\mu}), \quad (2.7)$$

where  $\lambda_{1,2} \sim \mathcal{O}(1)$  have to be determined from a high-energy calculation. The scattering amplitude then scales as  $a_0^3$ , and the cross-section  $\sigma$  as  $a_0^6$ . Since  $\sigma$  has dimension of area,  $-2$ , we finally have:

$$\sigma \sim a_0^6 E_\gamma^4, \quad (2.8)$$

thus blue light scatters stronger than red, and the sky looks blue.

## 2.2 Asymptotic expansions

These examples demonstrate the power of effective theories in identifying the most prominent effects. However, extending the calculations in an EFT beyond the leading order may prove not much simpler than in the more general “fundamental” theory. A powerful approach to evaluating multiple-scale effects in loop corrections, the method of asymptotic expansions [32, 33, 34, 35, 36, 37, 38, 39, 40, 41, 42, 43] is completely systematic and thus convenient for computerized calculations.

A naive approach to determine the asymptotic behavior of an integral depending on a parameter  $x$  in the limit  $x \rightarrow 0$  would be to Taylor expand the integrand about  $x = 0$ , and integrate each term. However, since loop

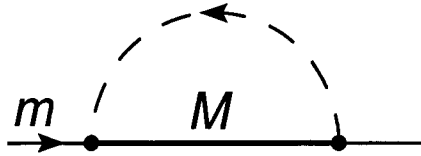


Figure 2.1: One-loop double-scale propagator-type integral

momenta are integrated over all scales, “soft” subgraphs can give a nontrivial contribution in some corners of the integration space. Thus, a more careful treatment would be to identify all contributing regions, expand the integrands, and integrate the result in each region separately, respecting the boundaries between the regions – impossible for any realistic problem. The solution comes from a non-intuitive statement: once the expansion is done in every region, the boundaries may be discarded and integration performed over all momentum space in each region. Due to mathematical properties of this operation, no double-counting occurs in the overlapping integrals.

We will demonstrate the power of asymptotic expansion with a few examples of varying complexity.

**Simple one-loop example.** Consider the integral in Fig. 2.1, where the dashed line is massless and carries loop momentum  $q$ .

With  $M \gg m$ , the integral may get contributions from the two regions of loop momentum  $q$ :  $q \sim m$  and  $q \sim M$ . In the former case, the heavy line

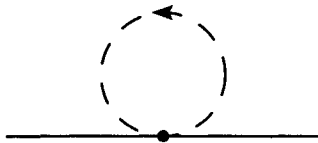


Figure 2.2: “Soft” loop momentum limit,  $q \sim m$



Figure 2.3: “Hard” loop momentum limit,  $q \sim M$

shrinks to a point (similarly to the  $W$ -boson propagator in muon decay) as in

Fig. 2.2, and the integral becomes a massless tadpole – zero in dimensional regularization:

$$I(1, 1; x) = \int \frac{[d^D q]}{(q+p)^2 (q^2 + M^2)} \quad (2.9)$$

$$\stackrel{q \sim m}{=} \sum_{i=0}^{\infty} \int \frac{[d^D q] (-q^2)^i}{(q+p)^2 (M^2)^{i+1}} = 0. \quad (2.10)$$

In the region  $q \sim M \gg m$ , the expansion in powers of  $x = m^2/M^2$  results in every term being a massive vacuum loop (Fig. 2.3):

$$\begin{aligned} I(1, 1; x) &= \int \frac{[d^D q]}{(q+p)^2 (q^2 + M^2)} \stackrel{q \sim M}{=} \sum_{i=0}^{\infty} \int_{q \sim m} \frac{[d^D q] (-2qp - p^2)^i}{(q^2)^{i+1} (q^2 + M^2)} \quad (2.11) \\ &= \sum_{i=0}^{\infty} \sum_{k=0}^i \int_{q \sim M} \frac{[d^D q] (-1)^i (p^2)^{i-k}}{(q^2)^{i+1} (q^2 + M^2)} \frac{i!}{k! (i-k)!} (2qp)^k \end{aligned}$$

Extending the integration to the whole range of  $q$ , we can apply the averaging formula Eq. A.5 to the powers of  $(2pq)$  in the numerator. As integrals with odd powers of  $q$  vanish, we can change the summation index:

$$\begin{aligned} I(1, 1; x) &\stackrel{k=2j}{=} \sum_{i=0}^{\infty} \sum_{j=0}^{\lfloor i/2 \rfloor} \int \frac{[d^D q] (-1)^i (p^2)^{i-2j}}{(q^2)^{i+1} (q^2 + M^2)} \quad (2.12) \\ &\times \frac{i!}{(2j)! (i-2j)!} \frac{(q^2 p^2)^j (2j)! \Gamma(2-\epsilon)}{j! \Gamma(2-\epsilon+j)} \end{aligned}$$

Now, vacuum bubbles can be integrated with Eq. A.1:

$$\begin{aligned} I(1, 1; x) &= \sum_{i=0}^{\infty} \sum_{j=0}^{\lfloor i/2 \rfloor} G_{m2}(1+i-j, 1; M^2) \frac{(-1)^i (p^2)^{i-j} i! \Gamma(2-\epsilon)}{j! (i-2j)! \Gamma(2-\epsilon+j)} \quad (2.13) \\ &= \frac{\mathcal{F}}{\Gamma(1+\epsilon)} \sum_{i=0}^{\infty} \sum_{j=0}^{\lfloor i/2 \rfloor} \frac{(-1)^j (m^2)^{i-j} \Gamma(\epsilon+i-j) \Gamma(1-\epsilon-i+j) i!}{(M^2)^{i-j+\epsilon} j! (i-2j)! \Gamma(2-\epsilon+j)} \\ &\stackrel{i=n+j}{=} \frac{\mathcal{F}(m^2)^{-\epsilon}}{\Gamma(1+\epsilon)} \sum_{n=0}^{\infty} \sum_{j=0}^n \frac{(-1)^j x^{n+\epsilon} \Gamma(n+\epsilon) \Gamma(1-\epsilon-n) (n+j)!}{j! (n-j)! \Gamma(2-\epsilon+j)}. \end{aligned}$$

In the last line we used the transformation

$$\sum_{i=0}^{\infty} \sum_{j=0}^{\lfloor i/2 \rfloor} = \sum_{j=0}^{\infty} \sum_{i=2j}^{\infty} = \sum_{j=0}^{\infty} \sum_{n=j}^{\infty} = \sum_{n=0}^{\infty} \sum_{j=0}^n.$$

The inner summation can now be performed using the formula

$$\sum_{j=0}^n \frac{(-1)^j \Gamma(a+j)}{j! (n-j)! \Gamma(b+j)} = \frac{\Gamma(a) \Gamma(b-a+n)}{n! \Gamma(n+b) \Gamma(b-a)}, \quad (2.14)$$

and our final answer is:

$$\begin{aligned}
\frac{I(1, 1; x)}{\mathcal{F}(m^2)^{-\epsilon}} &= \frac{\Gamma(1 - \epsilon)}{\Gamma(1 + \epsilon)} \sum_{n=0}^{\infty} x^{n+\epsilon} \frac{\Gamma(n + \epsilon)}{\Gamma(2 - \epsilon + n)} \\
&= \frac{1}{\epsilon} + 1 + \ln x + \frac{x}{2} + \epsilon \left[ 1 + \ln x + \frac{\ln^2 x}{2} + x \left( \frac{3}{4} + \frac{\ln x}{2} \right) \right] \\
&\quad + \epsilon^2 \left[ 1 + \ln x + \frac{\ln x^2}{2} + \frac{\ln x^3}{6} + x \left( \frac{7}{8} + \frac{3}{4} \ln x + \frac{\ln x^2}{4} \right) \right] + \dots
\end{aligned} \tag{2.15}$$

The sum in Eq. 2.15 can be expressed in terms of the hyper-geometric function and analytically continued outside the region  $M \gg m$ . For  $x = 1$  it, of course, reproduces  $\text{Onshell}(1, 1; 1)$  (Eq. A.3).

**Another one-loop example.** The following example is again related to the integral in Fig. 2.1. This time we consider the real decay threshold limit  $0 < \delta^2 = m^2 - M^2 \ll m^2$ . The imaginary part of that loop integral then corresponds through the optical theorem to the two-body phase space (Eq. A.8):

$$\begin{aligned}
\text{Im} \int \frac{[d^D k]}{k^2(k^2 + 2kp - \delta^2 - i0)} &= \frac{1}{2} \int d\Phi(P \rightarrow P_1, P_2) \\
&= \frac{\pi^{3/2} \mathcal{F}}{2^{1-2\epsilon} \Gamma(1 + \epsilon) \Gamma(3/2 - \epsilon)} \frac{(\delta^2)^{1-2\epsilon}}{(m^2)^{1-\epsilon}},
\end{aligned} \tag{2.16}$$

where capital letters denote momenta in the Minkowski space of the decaying and final particles, such that  $P^2 = m^2$ ,  $P_1^2 = M^2$ , and  $P_2^2 = 0$ . The  $-i0$  term here is shown explicitly, since the imaginary part of the integral vanishes when contour is not deformed. It is also implicit in the expressions below.

The same result can be obtained by the asymptotic expansion. Reasoning similarly to the previous example, we find that the only non-zero region in this configuration corresponds to  $k \sim \delta^2/m$ :

$$\int \frac{[d^D k]}{k^2(k^2 + 2kp - \delta^2)} \stackrel{k \sim \delta^2/m}{=} \int \frac{[d^D k]}{k^2(2kp - \delta^2)} \sum_{i=0}^{\infty} \left( \frac{-k^2}{2kp - \delta^2} \right)^i. \tag{2.17}$$

Inspecting Eq. 2.17, we notice that all terms except the first ( $i = 0$ ) vanish – if  $k^2$  cancels in the denominator,  $2kp - \delta^2$  can be written as  $2k'p$  by shifting the integration momentum. The latter form has no relevant scale (since the scale of  $p$  can be factored out of the integral), and corresponding integrals vanish.

Introducing the Tomonaga parameter  $\lambda$ , we unite the denominators, complete the square, and apply Eq. A.1:

$$\begin{aligned} \int \frac{[d^D k]}{k^2(2kp - \delta^2)} &= \int_0^\infty d\lambda \int \frac{[d^D k]}{(k^2 + \lambda(2kp - \delta^2))^2} \\ &= \frac{\mathcal{F} \Gamma(\epsilon)}{\Gamma(1 + \epsilon)} \int_0^\infty d\lambda (m^2 \lambda^2 - \delta^2 \lambda)^{-\epsilon} \\ &= \frac{\mathcal{F} \Gamma(\epsilon)}{\Gamma(1 + \epsilon)} \frac{\Gamma(1 - \epsilon)}{\Gamma(\epsilon)} \frac{\Gamma(-1 + 2\epsilon)}{\Gamma(\epsilon)} \frac{(-\delta^2)^{1-2\epsilon}}{(m^2)^{1-\epsilon}}. \end{aligned} \quad (2.18)$$

The only non-trivial factor in this formula, the power  $(-1)^{-2\epsilon}$ , is uniquely determined by the above mentioned term  $-i0$ , allowing the expansion  $(-1 - i0)^{-2\epsilon} = e^{-i\pi(-2\epsilon)} = 1 + 2i\pi\epsilon - 2\pi^2\epsilon^2 + \dots$ . Imaginary terms in this expansion give rise to the imaginary part of the integral above which order by order reproduces the expansion of Eq. 2.16.

**Three-loop example.** In the Fermi effective theory, next-to-leading order QED corrections to muon decay give rise to the following integrals (Fig. 2.4):

$$I(a_1, a_2, a_3, a_4, a_5, a_6) = \int \frac{[d^D k_1][d^D k_2][d^D k_3]}{D_1^{a_1} D_2^{a_2} D_3^{a_3} D_4^{a_4} D_5^{a_5} D_6^{a_6}}, \quad (2.19)$$

with  $D_1 = (p+k_3-k_2)^2$ ,  $D_2 = k_2^2+m^2$ ,  $D_3 = k_1^2+m^2$ ,  $D_4 = k_3^2$ ,  $D_5 = (k_1-k_2)^2$ , and  $D_6 = (p+k_1-k_2)^2+M^2$ . Here  $m$  is the electron mass, and  $M$  is muon mass,  $M \gg m$ , and the external momentum is on-shell,  $p^2 = -M^2$ . Each Feynman diagram, contributing to the muon decay process, can be expressed in terms of integrals of Eq. 2.19 with various indices  $a_1, \dots, a_6$ . Since this topology involves two different mass scales, we should analyze how to factorize it into single-scale contributions. In what follows, we only discuss the contributing expansion regions and sketch calculations (following Ref. [44]), without showing explicit results (those will be discussed later in Chapter 7).

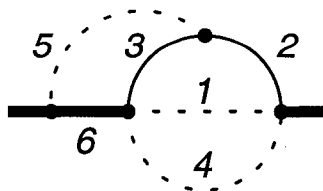


Figure 2.4: Topology contributing to  $\mathcal{O}(\alpha)$  corrections to the muon decay rate

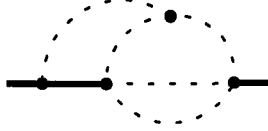


Figure 2.5: Region 1:  $k_1, k_2 \gg m$

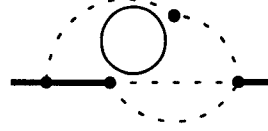


Figure 2.6: Region 2:  $k_2 \gg k_1 \sim m$

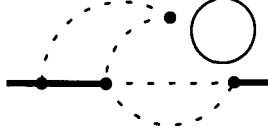


Figure 2.7: Region 3:  $k_1 \gg k_2 \sim m$

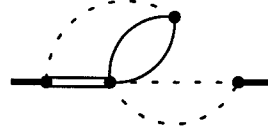


Figure 2.8: Region 4:  $k_1, k_2 \sim m$

Four contributing regions of virtualities for integrals of Eq. 2.19 are:

Region 1 (Fig. 2.5)	$ k_1  \gg m,  k_2  \gg m$	$D_2 \rightarrow k_2^2$ $D_3 \rightarrow k_1^2$
Region 2 (Fig. 2.6)	$ k_1  \sim m,  k_2  \gg m$	$D_2 \rightarrow k_2^2$ $D_5 \rightarrow k_2^2$ $D_6 \rightarrow (p - k_2)^2 + M^2$
Region 3 (Fig. 2.7)	$ k_1  \gg m,  k_2  \sim m$	$D_3 \rightarrow k_1^2$ $D_1 \rightarrow (p + k_3)^2$ $D_5 \rightarrow k_1^2$ $D_6 \rightarrow (p + k_1)^2 + M^2$
Region 4 (Fig. 2.8)	$ k_1  \sim m,  k_2  \sim m$	$D_1 \rightarrow (p + k_3)^2$ $D_6 \rightarrow 2p(k_1 - k_2) + i\delta$

In Region 1, the one-loop subgraph with massless propagators  $D_1$  and  $D_4$  can be integrated. After that, we have a two-loop topology which has been solved in Ref. [28]. This region is technically the hardest. In all remaining ones there is some degree of factorization which simplifies the calculations.

In Region 2, after averaging over the directions of momentum  $k_1$  according to Eq. A.5, we can integrate the one-loop massive bubble  $D_3$ . The remainder is a two-loop diagram, in which again we can first integrate the massless propagators  $D_1$  and  $D_4$ . The last integral belongs to a one-loop massive propagator-type topology, Eq. A.3.

Region 3 can be calculated by averaging over the directions of  $k_2$ , and integrating the massive bubble with  $D_2$ . The rest factorizes into two one-loop integrals, which can be found with Eqs. A.3 and A.2.

The most interesting is Region 4. After we integrate  $D_1$  and  $D_4$ , we are left with an “eikonal” integral [45], which gives rise to odd powers of  $m$  in the final answer. Again, a solution was found in Ref. [28].

In every region, we can evaluate a few first terms in the  $m/M$  expansion. When this procedure is applied to the muon decay, the sum of contributions from all four regions (properly renormalized) reproduces term by term the expansion of the exact formula [46].

## 2.3 Conclusion

Examples above demonstrate the strong sides of the effective theories and the asymptotic expansions. The basic properties of the low-energy interactions can easily be established by inspecting a few first terms in an effective theory. To include higher order corrections, one has to list the terms in the effective Lagrangian with higher scaling dimensions. Manual construction of this list (and accounting for the appearing Feynman rules) quickly becomes impossible. The techniques of asymptotic expansions then solve this problem and at the same time eliminate the necessity for a separate calculation of the Wilson coefficients. Limited only by the available computer resources, an expansion scheme must be developed once to produce any required number of terms.

# Chapter 3

## Recurrence relations

Integrals arising from Feynman diagrams are in general not independent. Linear equations between integrals (recurrence relations) resulting from integration by parts [47, 48, 49] can be used to reduce thousands of integrals in a problem to a few “master integrals”. Only the latter then need to be explicitly evaluated. This method becomes indispensable when asymptotic expansions to high orders are involved. However, finding the proper combination of recurrence relations may be challenging. While the relations for one- and two-loop integrals could be solved manually for arbitrary values of indices, reduction of three- and four-loop topologies requires automated algorithms, turning this step into the most computationally demanding part of the problem.

This chapter starts with a simple one-loop example, followed by the discussion of the popular method suggested by Laporta [50], with emphasis on details relevant for its practical implementation. Next, we briefly describe an interesting modification of Laporta method based on switching to the so-called epsilon-finite basis. The chapter concludes with an introduction to the very promising general method related to the so-called Gröbner bases.

### 3.1 One-loop example

Consider again the one-loop topology in Fig. 2.1, this time assuming arbitrary positive integer powers of denominator factors  $D_1 = k^2$ ,  $D_2 = (k + p)^2 + M^2$ ,



where  $p^2 = -m^2$ :

$$I(a_1, a_2) = \int \frac{[d^D k]}{D_1^{a_1} D_2^{a_2}}. \quad (3.1)$$

It is possible to prove the following relations:

$$\int [d^D k] \frac{\partial}{\partial k^\mu} \left[ k^\mu \frac{1}{D_1^{a_1} D_2^{a_2}} \right] = 0, \quad (3.2)$$

$$\int [d^D k] \frac{\partial}{\partial k^\mu} \left[ p^\mu \frac{1}{D_1^{a_1} D_2^{a_2}} \right] = 0. \quad (3.3)$$

For instance, Eq. 3.2 follows from the Stokes theorem:

$$\int [d^D k] \frac{\partial}{\partial k^\mu} \frac{k^\mu}{D_1^{a_1} D_2^{a_2}} = \oint_{|k| \rightarrow \infty} [d^{D-1} S_\mu] \frac{k^\mu}{D_1^{a_1} D_2^{a_2}} \rightarrow \oint [d^{D-1} S_\mu] \frac{k^\mu}{(k^2)^{a_1+a_2}} = 0,$$

the last integral vanishing due to absence of scale in dimensional regularization.

Let us explicitly take derivatives in Eq. 3.2:

$$\begin{aligned} 0 &= \int \left[ D - a_1 \frac{2k^2}{D_1} - a_2 \frac{2k^2 + 2kp}{D_2} \right] \frac{[d^D k]}{D_1^{a_1} D_2^{a_2}} \\ &= [(D - 2a_1 - a_2) - a_2 \mathbf{2}^+ (\mathbf{1}^- - M^2 + m^2)] I(a_1, a_2). \end{aligned} \quad (3.4)$$

The operator  $\mathbf{2}^+$  increases the second index, and operator  $\mathbf{1}^-$  decreases the first index by a unit. This recurrence relation may be symbolically written as

$$R_1 : \quad (D - 2a_1 - a_2) + a_2(M^2 - m^2)\mathbf{2}^+ - a_2\mathbf{2}^+\mathbf{1}^- = 0. \quad (3.5)$$

By analogy, we can derive the relation from Eq. 3.3:

$$\begin{aligned} R_2 : \quad &(a_1 - a_2) + a_1(M^2 - m^2)\mathbf{1}^+ + a_2(M^2 + m^2)\mathbf{2}^+ \\ &- a_1\mathbf{1}^+\mathbf{2}^- + a_2\mathbf{1}^-\mathbf{2}^+ = 0. \end{aligned} \quad (3.6)$$

Relation  $R_1$  can be brought to a more useful form by multiplying it with  $\mathbf{2}^-$  (which shifts the index  $a_2 \rightarrow a_2 - 1$ ), and moving all operators to the left hand side:

$$1 = \frac{1}{(a_2 - 1)(M^2 - m^2)} ((a_2 - 1)\mathbf{1}^- - (D + 1 - 2a_1 - a_2)\mathbf{2}^-). \quad (3.7)$$

When both  $a_1$  and  $a_2$  are positive, this identity can be applied to an integral  $I(a_1, a_2)$  as many times as necessary to either reduce to zero  $a_1$ , corresponding topology being a massive vacuum bubble, or reduce  $a_2$  to unity.

## 3.2 Laporta algorithm

Integration-by-parts relations found in the previous section can be easily generalized to an arbitrary  $L$ -loop Feynman integral

$$I(a_1, \dots, a_n) \equiv I(\{a\}) = \int \frac{[d^D p_1] \dots [d^D p_L]}{D_1^{a_1} \dots D_n^{a_n}}. \quad (3.8)$$

Here denominators  $\{D\} \equiv D_1, \dots, D_n$  are at most quadratic in loop momenta  $p_1, \dots, p_L$  and external momenta  $p_{L+1}, \dots, p_{L+M}$ , and may depend on other parameters (masses). We can also require that they form a complete basis, i.e. that any scalar product  $p_i p_j$  can be expressed in terms of  $\{D\}$ 's and masses.

For any set of indices  $\{a\}$  we have:

$$\begin{aligned} 0 &= \int [d^D p_1] \dots [d^D p_L] \frac{\partial}{\partial p_i^\mu} \left[ p_j^\mu \frac{1}{D_1^{a_1} \dots D_n^{a_n}} \right] \\ &= \int \left\{ \delta_{ij} D - \sum_{k=1}^n p_j^\mu \frac{\partial D_k}{\partial p_i^\mu} \frac{a_k}{D_k} \right\} \frac{[d^D p_1] \dots [d^D p_L]}{D_1^{a_1} \dots D_n^{a_n}}, \end{aligned} \quad (3.9)$$

where  $1 \leq i \leq L$  and  $1 \leq j \leq L + M$ . But  $\{D\}$  form a complete basis,

$$p_j^\mu \frac{\partial D_k}{\partial p_i^\mu} = c_{ijk0} + \sum_{l=1}^n c_{ijkl} D_l, \quad (3.10)$$

and the relations are completely determined by coefficients  $c_{ijkl}$ .

Re-arranging identities Eq. 3.9 to a useful form, such as Eq. 3.7, however, is not easy. Ref. [50] introduced a practical solution method, suitable for reducing multi-loop integrals in very large calculations (two public implementations are presently available [51, 52]).

Instead of finding the general solution to the reduction problem for any exponents  $\{a\}$ , that reference suggests considering recurrence relations originating from a finite number of specific index vectors (“seeds”). This system of uniform linear equations can be solved in a computer algebra program by Gauss elimination so that “complicated” integrals are expressed in terms of “simpler” master integrals. The challenging part is the proper choice of the seeds: on the one hand, the system should be large enough to reduce all integrals in the problem, on the other hand, it should fit in the memory of available computers.

**Complexity function.** We start the discussion by trying to define what exactly the “complexity” of an integral is, i.e. find some “natural” empirical criteria of integral  $I(\{a\})$  being more “complicated” than integral  $I(\{b\})$ :

1. An integral with fewer denominators (lines in the corresponding graph) is simpler. With  $N_+(\{a\}) \equiv \sum_{a_i > 0} 1$  – the number of positive  $a_i$ 's – this criterion is then  $N_+(\{a\}) > N_+(\{b\})$ .
2. An integral with smaller powers of  $D_i$ 's in the denominator (or, equivalently, with fewer dots on the lines) is simpler. With  $S_+(\{a\}) \equiv \sum_{a_i > 0} a_i$  being the sum of positive indices, it reads  $S_+(\{a\}) > S_+(\{b\})$ .
3. An integral with smaller powers of numerators is simpler. If  $S_-(\{a\}) \equiv -\sum_{a_i < 0} a_i$  is the negated sum of negative indices, we have  $S_-(\{a\}) > S_-(\{b\})$ .

The ordering done by  $N_+$ , then by  $S_+$ , and then by  $S_-$  is not yet complete, i.e. in general it is still possible to have different integrals with the same values of  $N_+$ ,  $S_+$ , and  $S_-$ . To apply Laporta algorithm, we need to eliminate this ambiguity, for instance, by imposing in such cases lexicographic comparison of indices  $\{a\}$  and  $\{b\}$ . This means that we find the lowest  $i$  such that  $a_i \neq b_i$ , and if  $a_i > b_i$ , then  $I(\{a\})$  is more complex.

The choice of complexity criteria is by no means unique. Different criteria may lead to different master integral sets identified through the reduction (but, of course, the number of master integrals will be the same).

In practice, it is convenient to encode those criteria in a single-valued complexity function  $O(\{a\})$ , producing a unique (positive integer) number for any set of integer indices  $\{a\}$  so that  $O(\{a\}) > O(\{b\})$  if and only if  $I(\{b\})$  is “simpler” than  $I(\{a\})$ . For implementation purposes, to avoid keeping large mapping tables, it is also convenient if the function  $O$  has a (relatively simple) inverse:  $O^{-1}(O(\{a\})) = \{a\}$ . As a simple (not necessarily the best) example of such function we can use numbers base  $2N > 0$ , where  $N$  is larger than any required values of indices  $a_i$  and functions  $N_+$ ,  $S_{\pm}$ . The order of “digits” then

reproduces the relative importance of corresponding parameters:

$$\begin{aligned} O_{2N}(\{a\}) &= N_+(\{a_i\})(2N)^{n+2} + S_+(\{a_i\})(2N)^{n+1} + S_-(\{a_i\})(2N)^n \\ &+ (a_1 + N)(2N)^{n-1} + \dots + (a_n + N). \end{aligned} \quad (3.11)$$

In every relation  $C_1 I(\{a\}_1) + \dots + C_k I(\{a\}_k) = 0$  we substitute integrals  $I(\{a\})$  with symbolic variables  $V[O(\{a\})]$ . Solution of the system then consists in expressing variables  $V[i]$  with higher index  $i$  in terms of those with lower  $i$ .

**Generation of recurrence relations.** Now that we defined the ordering of integrals, we consider the central problem of Laporta algorithm – the choice of seeds. When constraining the set of seeds  $\{a\}_i$  needed to reduce integrals with exponents  $\{b\}_j$ , it is quite natural to start from the properties of  $\{b\}_j$ . As the first guess, we may find maximal and minimal limiting values for each index over the set  $\{b\}_j$ ,  $\{b\}^{\min}$  and  $\{b\}^{\max}$ . It is possible to generate all vectors  $\{a\}_i$  with components limited by  $\{b\}^{\min}$  and  $\{b\}^{\max}$ . Each of these  $\prod_{i=1}^n (b_i^{\max} - b_i^{\min})$  seeds then produces  $L(L + M)$  relations. For a three-loop ( $L = 3$ ) propagator-type on-shell ( $M = 1$ ) topology, there are  $n = L(L + 3)/2 = 9$  independent denominator factors, and restricting each exponent to values  $-1, 0, 1$ , we find 236196 equations. This system is large but manageable, and from the experience with several real topologies of this type we find that in all practical cases it was sufficient for the reduction. However, extending this calculation is not easy.

Asymptotic expansion of some multi-scale topology generates integrals with higher positive or lower negative indices. If we roughly assume that every order in expansion results in a unit change in several factors  $(b_i^{\max} - b_i^{\min})$ , and that we usually need at least 7-8 terms in that expansion, the numbers quickly reach tens of millions of equations and solution of that system becomes impossible.

How can we limit this growth without compromising the completeness of the solution? A possible approach is to further investigate the set  $\{b\}_j$ . As we established, an important property of a particular integral is  $N_+$ , the number of lines. A Feynman diagram which has some line  $i$  removed results in scalar integrals with non-positive index  $a_i$ . The asymptotic expansion of double-scale

denominators, as follows from the previous chapter, cannot restore missing lines in the expanded integrals.

Another useful observation comes from the structure of recurrence relations (Eq. 3.9). Since the power of  $D_k$  in the denominator only increases through a factor  $\frac{a_k}{D_k}$ , recurrence relations for seeds with  $a_k \leq 0$  will not contain integrals with  $a_k > 0$ .

Thus, a subset of integrals with specific  $N_+(\{b\}) = k$  will be reduced only through integrals with the number of lines  $\leq k$ .

For every integral of such a subset, we may determine the values  $S_+$  and  $S_-$ , and find their maxima:  $S_{\pm}^{max}(k) = \max[S_{\pm}(\{b\}) | N_+(\{b\}) = k]$ ,  $0 \leq k \leq n$ . In all studied cases, generating the seeds  $\{a\}$  with the requirement that  $S_{\pm}(\{a\}) \leq S_{\pm}^{max}(N_+(\{a\}))$  also results in a valid reduction table, but the generation is now strongly constrained: expansion of a non-planar three-loop diagram to the 10-th order (with some indices as high as 8) now requires a system of  $\approx 200000$  equations. Thus, a working description of the set of seeds consists of  $n$  numbers  $\{a\}^{\min}$ ,  $n$  numbers  $\{a\}^{\max}$ ,  $n + 1$  numbers  $\{S_+^{\max}\}$  and  $n + 1$  numbers  $\{S_-^{\max}\}$  (for generality, we do not exclude the case with all negative indices).

The ordering of relations is also important. Ideally, the most “convenient” system for Gauss elimination should have a close-to-diagonal shape, or RRs be ordered by the “characteristic” complexity of the involved integrals (Fig. 3.1).

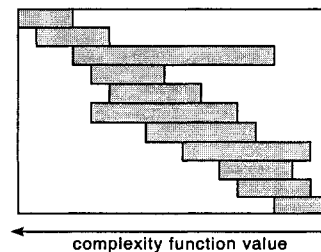


Figure 3.1: Sketch of a system convenient for Gauss elimination. Each line corresponds to a single relation. Filled boxes represent non-zero coefficients.

However, the complexity of integrals in a single relation may be very different, and corresponding values of the complexity function cover a large range. While there is no simple way to determine the optimal ordering, a good practical approach is to order seeds by complexity. Although far from ideal, the resulting system still requires significantly less resources during elimination than a system generated with some arbitrary ordering of seeds. With generation limits defined in terms of  $N_+(\{a\})$ , and  $S_{\pm}^{max}(N_+(\{a\}))$ , the corresponding algorithm of ordered and constrained seeds generation is relatively straightforward.

**Gauss elimination.** The basic procedure of solving a system of equations transforms the system as sketched in Fig. 3.2.

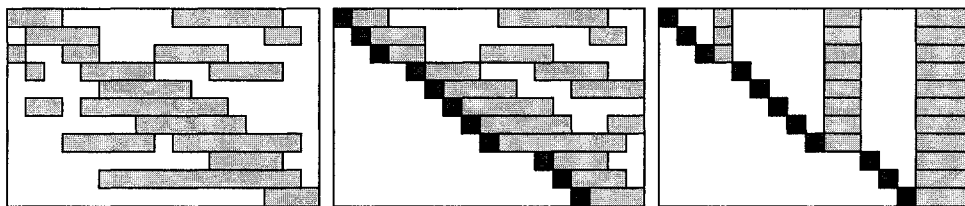


Figure 3.2: Sketch of Gauss elimination steps (the first equation is at the top). Light grey boxes represent non-zero coefficients, dark grey – coefficient  $-1$ .

First, we normalize the first equation so that its highest (corresponding to the most complicated index vector) coefficient is  $-1$ , then substitute this line in the lines below. Continuing this process, we arrive at the “triangular” table. Next, we do the backward substitution, or “diagonalization”: starting from the last line, we eliminate corresponding coefficients higher in the table, finally obtaining the “diagonal” shape. Each line has a leading coefficient  $-1$ ; remaining non-zero coefficients correspond to the master integrals.

Depending on the problem, we may or may not require the “diagonalization” step. The triangular system may already be applied to the expression appearing after evaluating the sum of Feynman diagrams, starting from the

top of the table. Substitution is then done only in the integrals appearing in the expression, rather than in every line of the table, which may considerably speed up the process. However, sometimes it is convenient to have the table where each integral is immediately expressed in terms of master integrals.

The steps outlined above are open for multiple improvements. Considerable speed-up may happen due to a re-ordering of rows during Gauss elimination, a separation of the table into “bunches” processed in parallel mode, and other ideas originating from numerical methods and facilitated by advanced available computing environments.

Another notable point in discussing the Gauss method is the algebra of coefficients. In case of a single-scale topology, the coefficients are rational functions of space dimension  $D$ . Gauss elimination requires multiplication, addition, and normalization of those functions. The most CPU-intensive task then becomes finding the greatest common divisor (GCD) of two polynomials in  $D$  with integer coefficients. Efficient GCD algorithms, based on modular arithmetics and stochastic acceleration, such as those implemented in Ref. [53], may speed-up the calculation by an order of magnitude compared to less sophisticated algorithms. This advantage becomes much more pronounced for multi-scale topologies, when the coefficients in addition to  $D$  may depend on other kinematic parameters, and the GCD is calculated for multi-variate polynomials.

**Organization of calculation.** So far the work flow of our reduction step is as shown in Fig. 3.3. However, in a realistic calculation, taking weeks of computer time, once the reduction is done, it is desirable to re-use as much of it as possible in the following steps. For example, we may want to reduce another diagram belonging to the same topology, or expand the diagram to a higher degree, or slightly change the calculation – all of which may require a new iteration. During the work on this thesis, the following updated scheme proved useful (Fig. 3.4). At the seed generation stage, if a seed conforms to the limits used in previous iterations, related RRs will contribute nothing new to the table. Thus, we can only keep the new seeds, and store the new limits only

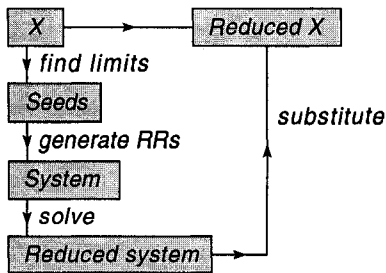


Figure 3.3: Work flow for reducing an expression  $X$ .

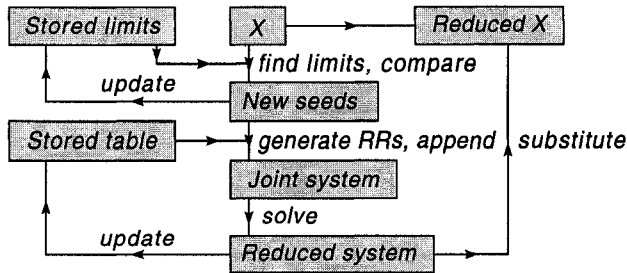


Figure 3.4: Laporta work flow re-using the existing solution.

if they produce any new seeds. New relations then can be simply appended to the end of the existing “diagonalized” table (Fig. 3.5).

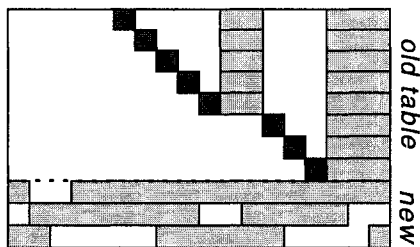


Figure 3.5: Appending new lines after the reduced system.

The effect of Gauss elimination, starting from the top, is then first to substitute all reduced integrals in the new table, and then reduce the new ones. (Of course, both new and old parts of the table have to use the same ordering function  $O(\{a\})$ .)

While this shortcut is very efficient in some cases, it should be used with care, as it effectively demands that updates to the table are done sequentially. When there are too many new seeds, it may be more efficient to use separate tables and update them in parallel. Also, growth of the table after several updates may slow down the consequent updates compared to starting a new table, so in general, one should try and choose the the best calculation strategy.



**Master integrals.** The complexity function  $O(\{a\})$  defines the “simplest” set of master integrals  $\{A\} \equiv A_1, \dots, A_m$  for a given topology. To be able to use a different basis  $\{B\} \equiv B_1, \dots, B_m$ , we should first reduce  $\{B\}$  in the basis  $\{A\}$  by running a separate Laporta reduction, resulting in system  $M_{ij}$ , and solve it for integrals  $\{A\}$ :

$$B_i = \sum_j M_{ij} A_j, \quad \implies \quad A_j = \sum_i (M^{-1})_{ji} B_i. \quad (3.12)$$

Now, we build the “large” Laporta table to reduce our expression to basis  $\{A\}$ , and then rotate the result to basis  $B$  by a “smaller” table  $M_{ji}^{-1}$ .

A slightly different procedure amounts to fewer steps. Let us assume that our complexity function is bounded from below, i.e.  $O(\{a_i\}) > K > m$ , where  $m$  is the number of master integrals for a given topology. Also, let us assume (quite naturally) that the expression of the new basis integrals  $\{B\}$  in terms of integrals  $I(\{a\})$  is known:

$$0 = -B_i + \sum W_{ij} I(\{a\}_j). \quad (3.13)$$

(Note that matrix  $W_{ij}$  is not reduced and  $I(\{a\}_j)$  are not necessarily master integrals.)

Now we can artificially assign the guaranteed lowest indices to the symbolic variables representing the master integrals:  $B_i \leftrightarrow V[i]$ ,  $1 \leq i \leq m$  (the reverse function should also be updated). The equations 3.13 now can be simply prepended to the “large” table as the new recurrence relations, and the following iteration of Gauss elimination will re-evaluate every line of the table in terms of the basis  $\{B\}$ .

### 3.3 Epsilon-finite bases

A simple but interesting observation about the choice of master integrals was made in Refs. [54, 55, 56, 57]. In  $D = 4 - 2\epsilon$  dimensions, it often happens that coefficients of master integrals  $\{A\}$  contain negative powers of  $\epsilon$  (“spurious poles”), which together with poles of  $\{A\}$  cancel in the final physical answer. Due to spurious poles, master integrals have to be evaluated to an

order in  $\epsilon$  higher than zero to find the finite contribution, and this is often very difficult. Here we can notice that the original expression, appearing from Feynman diagrams, has no such poles. Thus, it should contain an integral  $C = \sum M_j A_j$  with at least one reduction coefficient  $M_k$  divergent at  $\epsilon = 0$ . By changing the basis to  $\{A\}' = A_1, \dots, A_{k-1}, C, A_{k+1}, \dots, A_m$ , and substituting  $A_k = M_k^{-1} \left( C - \sum_{j \neq k} M_j A_j \right)$ , we can now express integral  $C$  with a trivial finite coefficient, while no new poles were introduced due to finiteness of  $M_k^{-1}$ . Repeating these steps for the remaining poles, we arrive to the so-called  $\epsilon$ -finite basis.

Every master integral now has to be evaluated to the order  $\epsilon^0$ . Also, the solution of the Laporta system can now be performed with coefficients represented as truncated series in  $\epsilon$  (which reduces the computational cost of operations). While the loss of meaningful orders in  $\epsilon$  can still happen in the intermediate steps, it is possible to deal with it by expanding the coefficients to high enough order.

### 3.4 Gröbner bases

The major drawbacks of the Laporta method are its limited universality and the large size of the tables. Also, as every integral is reduced separately, no cancellations occur until all integrals are substituted in the final expression.

An original method of finding a *general* solution of relations in Eq. 3.9, free from those problems, was suggested in Refs. [58, 59], based on the concept of Gröbner bases [60].

Consider a system  $\mathcal{P}$  of equations  $p_i = 0$ , where each  $p_i$  is a polynomial in  $x_1, \dots, x_n$ . If  $q$  is also a polynomial in  $x_i$ , we may check if it is compatible with  $\mathcal{P}$ . For that, we first identify the “highest” term in  $q$ . Then we choose some  $p_i$  and multiply it with a monomial  $u$  so that the “highest” term in  $up$  equals that in  $q$ , and subtract:  $q' = q - up$ . We repeat this step with  $q'$  until we reach the polynomial which can not be “simplified” further. This polynomial is said to be reduced with respect to system  $\mathcal{P}$ . If a polynomial is reduced to zero, it is compatible with system  $\mathcal{P}$ .

In general, applying  $p_i$ 's in different order, we obtain a different reduced polynomial; if this reduction is unique,  $\{p_i\}$  is said to be a Gröbner basis. Before discussing the method of creating such bases let us introduce some convenient notations.

First, we denote an *S-polynomial* (from “subtraction”) of polynomials  $p$  and  $q$  as  $S(p, q) \equiv up - vq$ , where  $u$  and  $v$  are the minimal monomials such that the “highest” terms of  $up$  and  $vq$  equal.

Second, we must finally define what the “highest” term is in a polynomial. In principle, any ordering of monomials would suffice as long as it satisfies several general conditions:

1. For any monomials  $u$  and  $v$ , either  $u < v$ , or  $v < u$ , or  $u = v$ .
2.  $1 \leq u$  for any monomial  $u$ .
3. If  $u < v$ , then  $wu < wv$  for any monomials  $u, v, w$ .

Common examples of allowed orderings include lexicographic, combined-power-then-lexicographic, etc.

Buchberger [60] found a general algorithm to build a Gröbner basis starting from an arbitrary set of polynomials  $\{p\}$ . He proved that the following algorithm terminates after a finite number of steps:

1. Let set  $W = \{(p_i, p_j)\}$  initially contain all pairs of polynomials from  $\{p\}$ .
2. Remove a pair  $(p_i, p_j)$  from  $W$  and find  $r = S(p_i, p_j)$ .
3. Reduce  $r$  with respect to  $\{p\}$  (in any order).
4. If  $r \neq 0$ , add  $r$  to the set  $\{p\}$  and all pairs  $\{(r, p_i)\}$  to  $W$ .
5. If  $W$  is not empty, go to step 2.
6. The final set  $\{p\}$  is a Gröbner basis.

In this form, the algorithm is not very useful since it can result in a *very* large set  $\{p\}$  (the definition of the basis does not imply its minimal size); practical implementations contain many improvements. Regardless of the way a Gröbner basis is found, it reduces any polynomial to its “simplest” form.

**Recurrence relations as polynomials.** To connect the problem of polynomial reduction with recurrence relations between integrals, let us recall index incrementing operators  $\mathbf{i}^+$ , such that  $\mathbf{i}^+ I(a_1, \dots, a_i, \dots) = I(a_1, \dots, a_i + 1, \dots)$ . We can identify an integral with positive indices  $\{a\}$  with a monomial built from operators  $\mathbf{i}^+$ , acting on the integral with zero indices:

$$I(a_1, a_2, \dots, a_n) = (\mathbf{1}^+)^{a_1} (\mathbf{2}^+)^{a_2} \dots (\mathbf{n}^+)^{a_n} I(0, \dots, 0). \quad (3.14)$$

Since the value of index  $a_i$  depends on whether it is calculated before or after the action of operator  $\mathbf{i}^+$ , we can also formally define an index operator  $\mathbf{i}$ :  $\mathbf{i} I(a_1, \dots, a_i, \dots) = a_i I(a_1, \dots, a_i, \dots)$ , satisfying obvious commutation relations:

$$[\mathbf{i}, \mathbf{j}^+] \equiv \mathbf{i}\mathbf{j}^+ - \mathbf{j}^+\mathbf{i} = \delta_{ij}, \quad [\mathbf{i}, \mathbf{j}] = [\mathbf{i}^+, \mathbf{j}^+] = 0. \quad (3.15)$$

With these commutation relations, we may always bring a monomial to the form when all increment operators are to the left of corresponding index operators. The following multiplication formula is easy to prove by induction:

$$(\mathbf{i})^n (\mathbf{i}^+)^m = \sum_{k=0}^{\min(m,n)} \frac{m!n!}{k!(m-k)!(n-k)!} (\mathbf{i}^+)^{m-k} (\mathbf{i})^{n-k}. \quad (3.16)$$

To avoid decrementing operators  $\mathbf{i}^-$  in the recurrence relations (Eq. 3.9), we multiply each relation with a needed number of operators  $\mathbf{i}^+$ . Finally, we arrive to the formulation of recurrence relations in terms of polynomials where each monomial has form  $(\mathbf{1}^+)^{a_1} (\mathbf{1})^{b_1} \dots (\mathbf{n}^+)^{a_n} (\mathbf{n})^{b_n}$ .

A Gröbner basis for those relations then uniquely reduces any monomial such as Eq. 3.14 to the simplest form, i.e. to the master integrals.

**Practical difficulties.** However, building this basis is a challenging task. A single-scale four-loop two-point topology has 14 indices and 20 recurrence relations. Allowing only powers of operators  $\mathbf{i}$ ,  $\mathbf{i}^+$  less or equal 2, we have 9 combinations for a single index, or  $\sim 10^{13}$  allowed monomials. At each step, due to formula Eq. 3.16, polynomials become more and more “dense”, and even storing them is a problem.

In Ref. [61], the problem was somewhat simplified by the introduction of S-bases, or separate bases for each sector. As already mentioned, positive and

non-positive values of an index represent different topologies, thus it is logical to consider separately the sectors with different combinations of indices being positive. Ordering the  $2^n$  sectors by “complexity”, it becomes sufficient in one sector to only build a basis reducing (not necessarily uniquely) any integral to simpler sectors. This is significantly easier than building a complete Gröbner basis.

The efficiency of S-basis construction is highly dependent on the chosen ordering of monomials and sectors, and there is no general answer for all topologies. Still, this approach already brought some non-trivial results [62].

For future applications, a combination of Laporta reduction algorithm with S-bases [61, 52] seems to be very promising – the sectors which are easy to reduce with S-bases are difficult for the Laporta method, and vice versa.

## Chapter 4

# Numerical evaluation of master integrals

After some physical quantity  $X(\epsilon)$  is calculated, dimensional regularization is removed by taking the limit  $\epsilon \rightarrow 0$ . The value of  $X(0)$  then is determined by the finite  $\mathcal{O}(\epsilon^0)$  term, while  $\mathcal{O}(\epsilon^{-n})$  poles and gauge parameter-dependent terms should identically cancel. This usually requires that for some master integral  $M = a_{p_{\min}}\epsilon^{p_{\min}} + \dots + a_{p_{\max}}\epsilon^{p_{\max}} + \mathcal{O}(\epsilon^{p_{\max}+1})$  the coefficients  $a_{p_{\min}}, \dots, a_{p_{\max}-1}$  must be known exactly, while the physically important answer is determined by  $a_{p_{\max}}$ .

The latter is usually so hard to find that an exact expression is either unavailable, or, if obtained, may require an independent cross-check for validation. An accurate numerical representation helps in either case, thus supplementing analytical methods. One can go further into an interesting field of experimental mathematics and reconstruct exact expressions based on high-precision approximations, but this path is beyond of scope of this thesis.

A major problem for numerical methods is dealing with divergences in a multi-dimensional integration. Knowing the structure of those divergences, one can analytically transform the integrand until it can be integrated numerically. This is the basic principle of the methods of sector decomposition and Mellin-Barnes transformation, described in this chapter, which have recently attracted much attention due to their versatility. The associated symbolic manipulations are relatively simple but have to handle large expressions, thus an efficient computer algebra package is required in addition to numerical code.

This chapter is organized as follows: first, we introduce the alpha-representation, which is an algorithmic version of Feynman parameterization. Next, we describe the method of sector decomposition, in the Euclidean regime and with a modification for infrared divergences. The chapter concludes with a brief overview of the technique employing Mellin-Barnes transformation.

## 4.1 Alpha-representation

Feynman parameterization is used to transform an integral over loop momenta to a parametric integral over a few variables, which can be evaluated analytically or numerically. The actual steps of transformation contain some freedom, which results in possible variations in the shape of intermediate and final expressions. A similar (and equivalent up to substitutions) parametric integral can be obtained through an algorithm which can be easily automated, leading to an expression called alpha-parameterization, or alpha-representation of the original loop integral.

While this representation per se may not be the most convenient one for the numerical evaluation, it serves as a starting point for many methods including those described later in this chapter. An overview presented below mostly follows the classical book by Bogolyubov [63].

Consider an arbitrary scalar  $L$ -loop integral with  $n$  denominator factors:

$$I(a_1, \dots, a_n) = \int \frac{[d^D k_1] \dots [d^D k_L] Z(q_1, \dots, q_n, p_1, \dots, p_M)}{(q_1^2 + m_1^2)^{a_1} \dots (q_n^2 + m_n^2)^{a_n}}, \quad (4.1)$$

where  $q_i$ , the momentum flowing through line  $i$ , is a linear combination of loop momenta  $k_1, \dots, k_L$  and external momenta  $p_1, \dots, p_M$ , and the numerator factor  $Z(q_1, \dots, p_M)$  is some polynomial built of scalar products  $q_i q_j$  or  $q_i p_j$ .

The corresponding alpha-representation has the form

$$\begin{aligned} I(a_1, \dots, a_n) &= \frac{\mathcal{F}^L \Gamma(N_a - LD/2)}{\Gamma^L(3 - D/2) \Gamma(a_1) \dots \Gamma(a_n)} \\ &\times \int_0^\infty d\alpha_1 \dots d\alpha_n \delta(1 - \alpha_1 - \dots - \alpha_n) \alpha_1^{a_1-1} \dots \alpha_n^{a_n-1} \\ &\times \frac{\mathbf{D}^{N_a - (L+1)D/2} \left( Z \left( \frac{1}{2i} \frac{\partial}{\partial \xi_1}, \dots, \frac{1}{2i} \frac{\partial}{\partial \xi_n}, p_1, \dots, p_M \right) e^{-i \left( \frac{2\mathbf{B} + \mathbf{K}}{\mathbf{D}} \right)} \Big|_{\xi_j=0} \right)}{[(\alpha_1 m_1^2 + \dots + \alpha_n m_n^2) \mathbf{D} + \mathbf{A}]^{N_a - LD/2}}, \end{aligned} \quad (4.2)$$

where  $\xi_1, \dots, \xi_n$  are auxiliary vectors and  $N_a = a_1 + \dots + a_n$ .

The expressions  $\mathbf{D}$ ,  $\mathbf{A}$ ,  $\mathbf{B}$ , and  $\mathbf{K}$ , depending on  $\alpha$ 's,  $\xi$ 's, and external momenta (but not on internal masses and exponents of propagators), first appeared in relation with Kirchhoff's rules for electric circuits. To illustrate their definitions, we use an example of a two-loop propagator-type graph in Fig. 4.1. To explore the structure of this graph, it is useful to introduce several

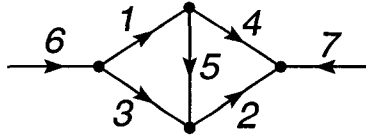


Figure 4.1: Numbering and line directions in a two-loop graph.

definitions:

- A *spanning tree* of a graph  $G$  is a connected subgraph of  $G$  containing all its vertices and no closed loops.
- A *spanning 2-tree* is a two-component subgraph containing all vertices of  $G$  and no loops.
- A *spanning tree-with-a-cycle* is obtained from a spanning tree  $T$  by supplementing it with one missing line of  $G$ .
- A *chord* of any of the subgraphs above is a line belonging to  $G$  but missing in the subgraph.

**Polynomial  $\mathbf{D}$ .** It is a sum of terms corresponding to all spanning trees of the graph. For each tree we build a product of  $\alpha$ 's with numbers corresponding to its chords. In our example, there are eight such terms (Fig. 4.2), and

$$\mathbf{D} = \alpha_1\alpha_2 + \alpha_1\alpha_4 + \alpha_1\alpha_5 + \alpha_2\alpha_3 + \alpha_2\alpha_5 + \alpha_3\alpha_4 + \alpha_3\alpha_5 + \alpha_4\alpha_5. \quad (4.3)$$



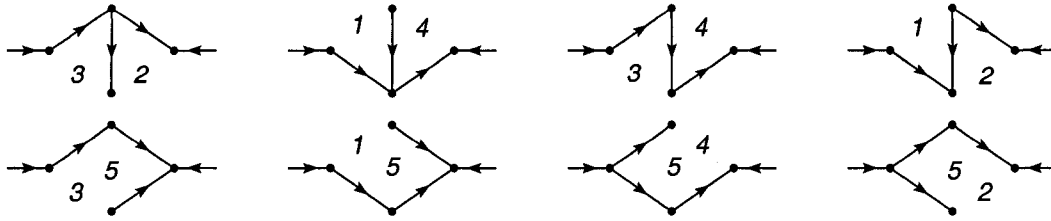


Figure 4.2: Spanning trees of the graph with labeled chords.

For the purpose of further discussion, notice that this polynomial is uniform in  $\alpha$ 's, each term containing  $L$  of them: exactly one line from each loop has to be removed to obtain a tree.

**Polynomial A.** Terms in **A** correspond to all spanning 2-trees of the graph. For each of them we build a product of  $\alpha$ 's corresponding to chords, and multiply by the squared total momentum entering any component of the 2-tree. Of ten 2-trees in our example (Fig. 4.3), eight are multiplied by  $p_6^2 (= p_7^2)$ ,

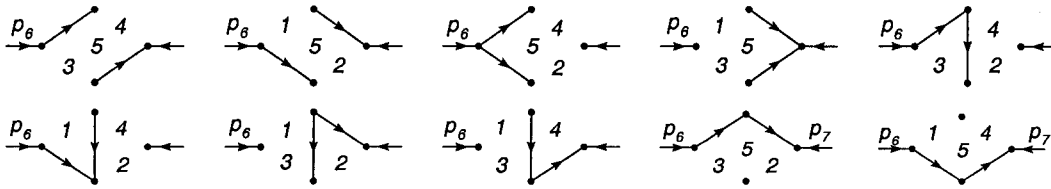


Figure 4.3: Spanning 2-trees of the graph. Chords and entering external momenta are labeled.

and two by  $(p_6 + p_7)^2 = 0$ :

$$\begin{aligned} \mathbf{A} = & p_6^2 (\alpha_1\alpha_2\alpha_3 + \alpha_1\alpha_2\alpha_4 + \alpha_1\alpha_2\alpha_5 + \alpha_1\alpha_3\alpha_4 \\ & + \alpha_1\alpha_3\alpha_5 + \alpha_2\alpha_3\alpha_4 + \alpha_2\alpha_4\alpha_5 + \alpha_3\alpha_4\alpha_5). \end{aligned} \quad (4.4)$$

Since a 2-tree is produced from a tree by removing a line, each term in **A** contains a product of  $L + 1$   $\alpha$ 's.

**Form B.** This expression involves a double summation. First, we sum over the internal lines of the graph. For the  $i$ -th line, we sum over the spanning trees containing that line. Each tree contributes a term which is a product of  $\alpha$ 's according to the chords, multiplied by a scalar product  $\xi_i p$ . Here  $\xi_i$  is the auxiliary vector, and  $p$  is the total momentum flowing (in the tree) through the  $i$ -th line along its direction. Fig. 4.4 presents two of the five contributions

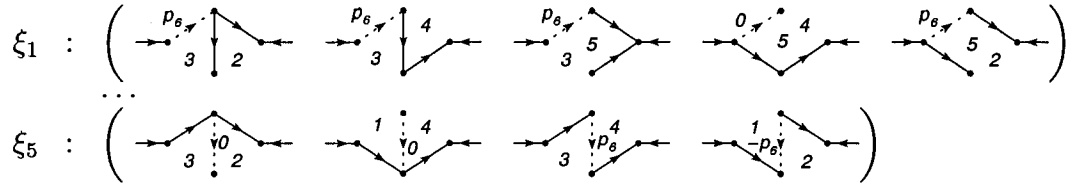


Figure 4.4: Example of trees corresponding to form **B**. Chords and momenta are labeled.

to **B**, which reads

$$\begin{aligned}
 \mathbf{B} = & (\xi_1 p_6) (\alpha_2 \alpha_3 + \alpha_2 \alpha_5 + \alpha_3 \alpha_4 + \alpha_3 \alpha_5) & (4.5) \\
 & + (\xi_2 p_6) (\alpha_1 \alpha_4 + \alpha_1 \alpha_5 + \alpha_3 \alpha_4 + \alpha_4 \alpha_5) \\
 & + (\xi_3 p_6) (\alpha_1 \alpha_2 + \alpha_1 \alpha_4 + \alpha_1 \alpha_5 + \alpha_4 \alpha_5) \\
 & + (\xi_4 p_6) (\alpha_1 \alpha_2 + \alpha_2 \alpha_3 + \alpha_2 \alpha_5 + \alpha_3 \alpha_5) \\
 & + (\xi_5 p_6) (\alpha_3 \alpha_4 - \alpha_1 \alpha_2) .
 \end{aligned}$$

**Form K.** Consider a spanning tree-with-a-cycle of the original graph. Having chosen a cycle direction, we compose a vector  $k$  as a sum of  $\xi$ 's with numbers corresponding to the cycle lines, taken with positive or negative sign depending on whether the line is directed along or against the cycle. Multiplying  $k^2$  by the the product of  $\alpha$ 's related to chords, and summing over all trees-with-a-cycle, we obtain **K**. According to Fig. 4.5, in our example we

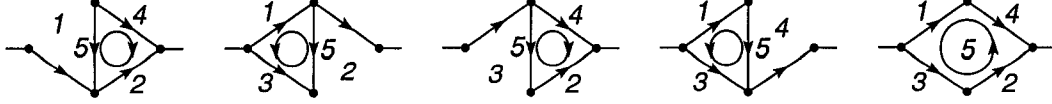


Figure 4.5: Trees-with-a-cycle contributing to  $\mathbf{K}$ . Cycle direction, cycle lines and chords are labeled.

have five such terms:

$$\begin{aligned} \mathbf{K} = & \alpha_1 (-\xi_2 + \xi_4 - \xi_5)^2 + \alpha_2 (-\xi_1 + \xi_3 - \xi_5)^2 \\ & + \alpha_3 (-\xi_2 + \xi_4 - \xi_5)^2 + \alpha_4 (-\xi_1 + \xi_3 - \xi_5)^2 + \alpha_5 (-\xi_1 + \xi_2 + \xi_3 - \xi_4)^2. \end{aligned} \quad (4.6)$$

The forms  $\mathbf{B}$  and  $\mathbf{K}$  vanish in the limit  $\xi_1, \dots, \xi_n = 0$ , so the numerator structure in Eq. 4.2 is some polynomial  $\mathbf{P}$  divided by an integer power of  $\mathbf{D}$ . For instance, a numerator product  $2p_6 p_1$  in our example is represented as

$$\begin{aligned} 2p_6^\mu \frac{1}{2i} \frac{\partial}{\partial \xi_1^\mu} e^{-i(\frac{2\mathbf{B}+\mathbf{K}}{\mathbf{D}})} \Big|_{\xi_i=0} &= -2p_6^2 \mathbf{P}/\mathbf{D}, \\ \mathbf{P} &= \alpha_2 \alpha_3 + \alpha_2 \alpha_5 + \alpha_3 \alpha_4 + \alpha_3 \alpha_5. \end{aligned} \quad (4.7)$$

Since every term in  $\mathbf{K}$  contains  $L - 1$   $\alpha$ 's, scalar products  $q_i q_j$  lead to a  $\mathbf{P}$  which is not of uniform degree in the  $\alpha$ 's. In general, terms in  $\mathbf{P}$  may have positive or negative signs due to dependence of terms in  $\mathbf{B}$  and  $\mathbf{K}$  on the directions of graph lines.

## Divergences in alpha-representation

Feynman integrals (Eq. 4.1) may diverge in the ultraviolet (UV) limit (associated with some loop momenta  $k_i \rightarrow \infty$ ), or in the infrared (IR) region (corresponding to  $k_i \rightarrow 0$  in some parameterization). In dimensional regularization, UV-divergent subgraphs yield at most a factor of  $1/\epsilon$ , and IR-divergent subgraphs may contribute  $1/\epsilon^2$  per loop in the Laurent expansion near  $\epsilon = 0$ .

The alpha-representation (Eq. 4.2) is a useful tool to analyze those singularities. According to Ref. [63], the overall UV divergence, if present, corresponds to the poles of the gamma-function in the numerator. UV-divergent subgraphs correspond to the divergent behavior of the integrand when some  $\alpha$ 's turn to zero. Apart from the obvious factors  $\alpha_i^{a_i-1}$  with  $a_i < 1$ , one should observe the

polynomial forms  $\mathbf{D}$  and  $\mathbf{F} \equiv [(\alpha_1 m_1^2 + \dots + \alpha_n m_n^2) \mathbf{D} + \mathbf{A}]$  raised to negative powers. Both are of uniform degree in the  $\alpha$ 's, and vanish when a subset of  $\alpha$ 's turns to zero (there may exist several such subsets for  $\mathbf{D}$  and  $\mathbf{F}$ ). The technique of the following section particularly well suits such situations.

All terms in  $\mathbf{D}$  being positive in the integration region, it has no other zeros. The polynomial  $\mathbf{F}$  is positive definite only in the Euclidean case: with all positive squared masses  $m_i^2$ , and all positive (space-like) kinematic invariants in  $\mathbf{A}$ . However, this situation is not physical: actual processes require negative values of kinematic invariants. The form  $\mathbf{F}$  then may vanish along some  $\vec{\alpha} \neq \vec{0}$ , which provides a necessary condition for an IR divergence.

A numerator structure  $Z$  at worst may lower the power of  $\mathbf{D}$ , thus contributing to the UV divergence. The IR behavior can only improve, which is obvious as we add powers of loop momenta in the numerator.

## Primary sectors

Before turning to the regularization schemes, let us first discuss the delta-function in Eq. 4.2. A numerical integrator works with a unit cube in an integer-dimensional space. The delta-function requires a change of variables before the actual integration. While a corresponding substitution is not too difficult to implement, an elegant method suggested in Ref. [64] allows to preserve most of the original structure of alpha-representation while avoiding bulky Jacobians. In what follows we present this “primary sector decomposition” in some detail, as very similar steps will be done in the next section.

Let us for a moment only consider numerator structures  $Z$  producing uniform expressions not scaling with  $\alpha$ 's, such as Eq. 4.7. (Otherwise, one may insert factors of  $\alpha_1 + \dots + \alpha_n = 1$  in the polynomial  $\mathbf{P}$  to achieve such scaling.)

The uniformity of  $\mathbf{D}$  and  $\mathbf{A}$  then allows one to easily establish the scaling

of the remaining integrand with  $\alpha$ 's in Eq. 4.2:

$$I(a_1, \dots, a_n) = \int_0^\infty d\alpha_1 \dots d\alpha_n \delta\left(1 - \sum \alpha_i\right) f(\alpha_1, \dots, \alpha_n), \quad (4.8)$$

$f$  scaling as

$$\begin{aligned} f(x\alpha_1, \dots, x\alpha_n) &= \frac{x^{\alpha_1-1} \dots x^{\alpha_n-1} (x^L)^{N_a - (L+1)D/2}}{(x^{L+1})^{N_a - LD/2}} f(\alpha_1, \dots, \alpha_n) \\ &= x^{-n} f(\alpha_1, \dots, \alpha_n). \end{aligned}$$

Now we separate the integration simplex into  $n$  regions where some  $\alpha_i$  is greater than all other  $\alpha$ 's:

$$\begin{aligned} &\int_0^\infty d\alpha_1 \dots d\alpha_n \delta\left(1 - \sum \alpha_i\right) f(\alpha_1, \dots, \alpha_n) \quad (4.9) \\ &= \left( \int_{\alpha_1 > \alpha_i, i \neq 1} + \dots + \int_{\alpha_n > \alpha_i, i \neq n} \right) d\alpha_1 \dots d\alpha_n \delta\left(1 - \sum \alpha_i\right) f(\alpha_1, \dots, \alpha_n). \end{aligned}$$

The first term after the substitution  $\alpha_i = \alpha_1 \beta_i$ ,  $i \neq 1$  becomes:

$$\begin{aligned} &\int_0^\infty d\alpha_1 \int_0^{\alpha_1} d\alpha_2 \dots d\alpha_n \delta\left(1 - \sum \alpha_i\right) f(\alpha_1, \dots, \alpha_n) \quad (4.10) \\ &= \int_0^1 d\alpha_1 \int_0^1 \alpha_1^{n-1} d\beta_2 \dots d\beta_n \delta\left(1 - \alpha_1 \left[1 + \sum \beta_i\right]\right) \alpha_1^{-n} f(1, \beta_2, \dots, \beta_n) \\ &= \int_0^1 d\beta_2 \dots d\beta_n f(1, \beta_2, \dots, \beta_n) \int_0^1 d\alpha_1 \frac{\delta\left(\alpha_1 - [1 + \sum \beta_i]^{-1}\right)}{\alpha_1 (1 + \sum \beta_i)} \\ &= \int_0^1 d\beta_2 \dots d\beta_n f(1, \beta_2, \dots, \beta_n). \end{aligned}$$

By similarly treating the other terms, and re-naming the  $\beta$ 's back to  $\alpha_1, \dots, \alpha_{n-1}$ , instead of an integral over a surface in  $n$  dimensions, we obtain an expression with  $n$  terms integrated over an  $(n-1)$ -dimensional unit cube.

Its form coincides with the following modification of Eq. 4.2:

$$\begin{aligned} I(a_1, \dots, a_n) &= \frac{\mathcal{F}^L \Gamma(N_a - LD/2)}{\Gamma^L(3 - D/2) \Gamma(a_1) \dots \Gamma(a_n)} \quad (4.11) \\ &\times \int_0^1 d\alpha_1 \dots d\alpha_n [\delta(\alpha_1 - 1) + \dots + \delta(\alpha_n - 1)] \alpha_1^{a_1-1} \dots \alpha_n^{a_n-1} \\ &\times \frac{\mathbf{D}^{N_a - (L+1)D/2} \left( Z \left( \frac{1}{2i} \frac{\partial}{\partial \xi_1}, \dots, \frac{1}{2i} \frac{\partial}{\partial \xi_n}, p_1, \dots, p_M \right) e^{-i \left( \frac{2\mathbf{B} + \mathbf{K}}{\mathbf{D}} \right)} \Big|_{\xi_j=0} \right)}{[(\alpha_1 m_1^2 + \dots + \alpha_n m_n^2) \mathbf{D} + \mathbf{A}]^{N_a - LD/2}}. \end{aligned}$$

The complexity of the integrand (involving the delta-function) has been removed at the expense of multiplying the number of terms. This strategy,

facilitated by computer-aided bookkeeping of the terms, is the basis for the sector decomposition method, for which Eq. 4.11 is an excellent starting point.

## 4.2 Sector decomposition

What obstacles would one encounter in trying to directly integrate Eq. 4.2 or Eq. 4.11?

First, integrating a function  $f(x_1, \dots, x_n)$  over an  $n$ -dimensional unit cube  $0 < x_i < 1$  is itself demanding even for moderately large  $n$ . For instance, a grid with only ten divisions per each  $x_i$  in 6-dimensional space requires a million evaluations of a function. Monte-Carlo methods are somewhat less sensitive to the dimensionality, but both deterministic and stochastic approaches fail if  $f$  is not “smooth” enough (even if it is finite and integrable). Adaptive algorithms (e.g., those collected in Ref. [65]) to a certain degree remedy the situation, but their performance relies on finding peaks in  $n$  dimensions and properly determining their shapes (both tasks heavily dependent on the dimensionality). All practically used algorithms are limited to either isolated peaks in a few variables or to simple regions inside the cube where the function can change fast. (In part, this limitation is due to the theoretical ambiguity in defining a consistent integral norm in more than one dimension.)

Second, as discussed above, the function  $f$  may not be even integrable in the limit  $\epsilon \rightarrow 0$ . However, we know the structure of  $f$ , and this knowledge can be used prior to integration to extract poles in  $\epsilon$  and to smooth the function enough for some adaptive scheme to produce stable numerical results. The advantage of sector decomposition is that it can be done completely automatically provided that the singularities only appear from polynomials raised to some ( $\epsilon$ -dependent) powers.

We start with a simple illustration. Let the function  $f(x, y)$  be finite over the square  $x, y \in [0, 1]$ . Consider an integral  $\int_0^1 dx dy f(x, y) (x + y)^{-2+\epsilon}$  that logarithmically diverges as  $\epsilon \rightarrow 0$  in the limit  $x, y \rightarrow 0$ . Splitting the

integration region into two triangular “sectors”  $x > y$  and  $x < y$  we have:

$$\int_0^1 \frac{dx dy f(x, y)}{(x + y)^{2-\epsilon}} = \left( \int_0^1 dx \int_0^x dy + \int_0^1 dy \int_0^y dx \right) \frac{f(x, y)}{(x + y)^{2-\epsilon}} \quad (4.12)$$

$$\left. \begin{array}{l} y \rightarrow xy' \\ x \rightarrow x'y \end{array} \right\} = \int_0^1 \frac{dx dy' f(x, xy')}{x^{1-\epsilon}(1+y')^{2-\epsilon}} + \int_0^1 \frac{dx' dy f(x'y, y)}{y^{1-\epsilon}(1+x')^{2-\epsilon}}.$$

Now the singularity is in a single variable (say,  $x$ ). With all factors that are regular at  $x = 0$  denoted by  $g(x)$ , the integral of interest is  $\int_0^1 g(x)x^{-1+\epsilon}dx$ . The transformation  $g(x) = g(0) + [g(x) - g(0)]$  and expansion of  $x^{-1+\epsilon}$  lead to

$$\int_0^1 \frac{g(x)dx}{x^{1-\epsilon}} = \frac{g(0)}{\epsilon} + \sum_{i=0}^{\infty} \int_0^1 \frac{(\epsilon \ln x)^i g(x) - g(0)}{i! x}. \quad (4.13)$$

After expanding  $g(x)$ , the  $x$ -dependent coefficients of each power of  $\epsilon$  can be safely integrated numerically.

## Multi-variate sector decomposition

Eqs. 4.12 and 4.13 can be generalized to the case of many dimensions. Consider an integral

$$\int_0^1 dx_1 \dots dx_n F_1^{a_1+b_1\epsilon} \dots F_k^{a_k+b_k\epsilon} \quad (4.14)$$

with integer (positive or negative)  $a_i$ . For each polynomial  $F_i$  and for each subset  $\{\tilde{x}\} = \{x_{i_1}, \dots, x_{i_m}\}$  ( $m \leq n$ ) of integration variables we define  $A(F_i|\{\tilde{x}\})$  as the minimal power of variables included in  $\{\tilde{x}\}$  among the terms of  $F_i$  (e.g.,  $A(xy^2 + xz|\{x, y\}) = 1$ ). Now we may formulate the criterion when sector decomposition is necessary:

*If for some subset  $\{\tilde{x}\}$  of  $m$  variables ( $2 \leq m \leq n$ ) it holds that  $A(F_1|\{\tilde{x}\})a_1 + \dots + A(F_k|\{\tilde{x}\})a_k + m \leq 0$ , then the integral of Eq. 4.14 diverges when the variables included in  $\{\tilde{x}\}$  simultaneously vanish.*

This clearly works for the example of Eq. 4.12:  $1 \cdot (-2) + 2 \leq 0$  for  $\{\tilde{x}\} = \{x, y\}$ . Re-numbering variables so that  $\{\tilde{x}\} = \{x_1, \dots, x_m\}$  is the smallest

suitable subset, we write the basic step of sector decomposition as follows:

$$\begin{aligned}
& \int_0^1 dx_1 \dots dx_m \prod_{q=m+1}^n dx_q \prod_{j=1}^k F_1^{a_1+b_1\epsilon}(x_1, \dots, x_n) \quad (4.15) \\
&= \sum_{i=1}^m \int_0^1 x_i^{m-1} dx'_1 \dots dx'_{i-1} dx_i dx'_{i+1} \dots dx'_m \prod_{q=m+1}^n dx_q \\
&\times x_i^{A(F_1|\{\tilde{x}\})(a_1+b_1\epsilon)+\dots+A(F_k|\{\tilde{x}\})(a_k+b_k\epsilon)} \\
&\times \prod_{j=1}^k \left( \frac{F_j(x_i x'_1, \dots, x_i x'_{i-1}, x_i, x_i x'_{i+1}, \dots, x_i x'_m, x_{m+1}, \dots, x_n)}{x_i^{A(F_j|\{x_1, \dots, x_m\})}} \right)^{a_j+b_j\epsilon}.
\end{aligned}$$

By construction, every expression in parentheses is a polynomial which is finite when all  $x'_1, \dots, x'_{i-1}, x_i, x'_i, \dots, x'_m = 0$ , and the divergence is moved to the power of  $x_i$ . For sector decomposition to be necessary, this power should be at most  $-1$ , which justifies the criterion above.

The proper selection of the subset  $\{\tilde{x}\}$  from all alternatives at each step is important for the convergence of the method and for keeping the size of the expression small. In the worst case, steps of Eq. 4.15 may fall into an infinite loop, but in many cases simple recursive descent from the smallest to larger sets  $\{\tilde{x}\}$  works fine. For complex problems, there exist more sophisticated strategies based on game theory, guaranteed to terminate in a finite number of steps [66], but those are out of the scope of this thesis.

When no more non-trivial subsets  $\{\tilde{x}\}$  remain, we need to regularize a single variable as in Eq. 4.13, with possibly a lower power of the pole than  $-1$ :

$$\begin{aligned}
\int_0^1 \frac{g(x) dx}{x^{a+b\epsilon}} &= \frac{g(0)}{1-a-b\epsilon} + \frac{g'(0)}{2-a-b\epsilon} + \dots + \frac{g^{(a-1)}(0)}{(a-1)!(-b\epsilon)} \quad (4.16) \\
&+ \int_0^1 dx \frac{g(x) - g(0) - xg'(0) - \dots - x^{a-1}g^{(a-1)}(0)/(a-1)!}{x^{a+b\epsilon}}.
\end{aligned}$$

Now we can expand the remaining expressions in  $\epsilon$ , and combining the powers of  $\epsilon$  together, we get lengthy but numerically stable integrands.

## Alpha-representation and sector decomposition

So far we only considered divergences occurring on the boundaries of integration space. When applied to the alpha-representation, this translates to



the requirement that the integral be IR-stable. For instance, we already have enough tools to obtain the massless integral in Fig. 4.1 with all exponents equal to one. From Eq. 4.11,

$$\begin{aligned} \text{N5c}(1, 1, 1, 1, 1) &= \int \frac{[d^D k][d^D l]}{k^2 l^2 (k+p)^2 (l+p)^2 (k+l+p)^2} & (4.17) \\ &= \mathcal{F}^2 \left( 1 + \frac{\pi^2}{6} \epsilon^2 - 2\zeta_3 \epsilon^3 + \frac{19\pi^4}{360} \epsilon^4 + \dots \right) \\ &\times \int_0^1 d\alpha_1 \dots d\alpha_5 \frac{[\delta(\alpha_1 - 1) + \dots + \delta(\alpha_5 - 1)]}{\mathbf{A}^{1+2\epsilon} \mathbf{D}^{1-3\epsilon}}, \end{aligned}$$

with  $\mathbf{D}$  and  $\mathbf{A}$  defined in Eq. 4.3 and Eq. 4.4 (where  $p_6 = p$ ). If we take a meaningful value of  $p^2 = -1$ , this sign factorizes and the expression can be sector decomposed and integrated with the result

$$\begin{aligned} \text{N5c}(1, 1, 1, 1, 1) &= -7.21 - \epsilon(24.16 + 45.31i) + \epsilon^2(74.21 - 151.83i) + \dots, & (4.18) \\ &\left( \text{exact answer being } -6\zeta_3 - \epsilon \left[ \frac{\pi^4}{10} + 12\zeta_3 + 12\zeta_3 \pi i \right] + \dots \right). \end{aligned}$$

However, important classes of integrals do not fall into this category. For instance, adding a unit mass to any line in Fig. 4.1 would introduce a non-trivial surface in the  $\alpha$ -space along which the denominator expression vanishes, thus rendering methods above not applicable.

A solution for such situations was suggested in Ref. [67]. First, we conduct the sector decomposition to isolate any divergences on the boundaries of the cube. Possible divergences at  $\alpha_i = 1$  (in the on-shell case) can be automatically taken care of if we initially split every side of the cube:

$$\int_0^1 dx f(x) = \frac{1}{2} \int_0^1 dx f(x/2) + \frac{1}{2} \int_0^1 dx f(1-x/2). \quad (4.19)$$

Every term now has a structure

$$\int_0^1 \prod dx_i x_i^{\alpha_i + b_i \epsilon} \frac{\mathbf{Q}(\vec{x}, \epsilon)}{\mathbf{F}^{c+d\epsilon}(\vec{x})}, \quad (4.20)$$

where  $\mathbf{Q}$  is some regular function, and the polynomial  $\mathbf{F}$  is non-zero at both  $\alpha_i = 0$  and 1 (but can turn to zero inside the cube).

To avoid the poles on the real axis, we deform the contour for each  $x$  as

$$z_i = x_i - i\lambda x_i(1-x_i) \frac{\partial \mathbf{F}}{\partial x_i}. \quad (4.21)$$

This introduces an imaginary contribution to  $\mathbf{F}$  that for small enough  $\lambda$  does not change the sign and turns to zero only if all partial derivatives vanish at the zero of  $\mathbf{F}$ , which becomes

$$\mathbf{F}(\vec{z}) = \mathbf{F}(\vec{x}) - i\lambda \sum_i x_i(1-x_i) \left( \frac{\partial \mathbf{F}}{\partial x_i} \right)^2 + \mathcal{O}(\lambda^2), \quad (4.22)$$

where the  $\mathcal{O}(\lambda^2)$  terms are purely real.

Denoting the corresponding Jacobian of the transformation as  $I(\vec{x} \rightarrow \vec{z})$ , our integral in Eq. 4.20 becomes

$$\int_0^1 \prod dx_i x_i^{a_i+b_i\epsilon} \left( \frac{z_i}{x_i} \right)^{a_i+b_i\epsilon} I(\vec{x} \rightarrow \vec{z}) \frac{\mathbf{Q}(\vec{z}, \epsilon)}{\mathbf{F}^{c+d\epsilon}(\vec{z})}. \quad (4.23)$$

Finally, we perform the expansion (Eq. 4.16), where derivatives are calculated for the whole non-singular expression including the Jacobian.

Such a transformation is powerful enough to handle many on-shell integrals (including massive cases of our two-loop example). The choice of deformation parameter  $\lambda$  requires some experimentation: the contour should lie sufficiently far from the pole, while  $\mathcal{O}(\lambda^3)$  corrections should not introduce new singularities on the contour. In addition,  $\lambda$  is naturally limited by the requirement that the contour should not cross any poles during the deformation from the real axis. In the case of two-loop on-shell topologies related to Fig. 4.1, the integration appears to be rather robust and values around  $\lambda \sim 0.5$  lead to stable and accurate results.

## Integration over phase space

Sector decomposition is not limited to the alpha-representation of loop integrals. Working with the complicated problem of real radiation, Ref. [68] suggested a fruitful idea of applying sector decomposition to integrals over phase space. Mapping the phase space volume available to some reaction to a unit hypercube is done in such a way that divergences in the matrix element and the volume element occur on the boundaries of the cube. Applying sector decomposition is then straightforward.

Eqs. A.9, A.10, and A.11 present correspondingly parameterized phase space volume applicable to the problems of semi-leptonic  $b$ -quark decay and the muon decay allowing for up to two gluons/photons in the final state.

One can easily see that these expressions and propagators only have singularities at the boundaries of the integration cube. Generally, this representation leads to very smooth integrands after the sector decomposition. Numerical integration then converges quickly even for the six-dimensional integral A.11.

Virtual corrections may produce imaginary contributions, complicating the analysis, but they can relatively easily be dealt with as suggested in Ref. [69]. Hyper-geometric functions are re-organized so that imaginary contributions can be integrated analytically before the numerical stage.

### 4.3 Mellin-Barnes transformation

Another powerful method of extracting the singularities into  $\epsilon$ -poles and smoothing the remaining integrand was first introduced in Ref. [70] and [71]. It is based on the following formula (Mellin-Barnes transformation):

$$\begin{aligned} \frac{1}{(X_1 + \dots + X_n)^\lambda} &= \frac{1}{\Gamma(\lambda)} \frac{1}{(2\pi i)^{n-1}} \int_{-i\infty}^{+i\infty} dz_1 \dots dz_{n-1} & (4.24) \\ &\times X_1^{z_1} \dots X_{n-1}^{z_{n-1}} X_n^{-\lambda - z_1 - \dots - z_{n-1}} \\ &\times \Gamma(-z_1) \dots \Gamma(-z_{n-1}) \Gamma(\lambda + z_1 + \dots + z_{n-1}). \end{aligned}$$

For every  $z_i$ , there are two series of poles on the imaginary plane. Eq. 4.24 is valid when the integration contour is located to the left from all poles of  $\Gamma(-z_i)$  (i.e. points  $z = 0, 1, 2, \dots$ ), and to the right from the poles of  $\Gamma(A + z_i)$  (points  $z = -A, -A - 1, -A - 2, \dots$ ). If  $A$  is such that this condition cannot be satisfied, one has to add the residues of poles appearing on the “wrong” side of the contour. The selection of the proper contour and accounting for residues can easily be automated [72, 73] for an arbitrary number of  $z$ 's.

Closing the contour to the right or to the left, we can switch from the integral in Eq. 4.24 to a sum of residues in each pole inside the contour (two possibilities in each case corresponding to the expansions with a different hierarchy of  $X_i$ ). This is the basis of analytical calculations of such integrals.

When analytical summation is difficult, numerical integration over complex  $z_i$  usually demonstrates good convergence due to fast decay of the gamma-functions far from the real axis.

To illustrate this method, we consider a generic two-loop integral of Fig. 4.1 with a single massive on-shell line. Rather than using the alpha-representation (which is also possible), in this case it is simpler to manually introduce Feynman parameters as this will lead to a smaller dimensionality of the resulting Mellin-Barnes integral.

Choosing denominator factors as  $D_1 = k^2$ ,  $D_2 = q^2$ ,  $D_3 = k^2 + 2kp$ ,  $D_4 = (q + p)^2$ ,  $D_5 = (k + q + p)^2$ , with  $p^2 = -1$ , we first use a Feynman parameter  $x$  for the factors  $D_1$  and  $D_5$ :

$$\begin{aligned} I(a_1, a_2, a_3, a_4, a_5) &= I = \int \frac{[d^D k][d^D q]}{D_1^{a_1} D_2^{a_2} D_3^{a_3} D_4^{a_4} D_5^{a_5}} \\ &= \int_0^1 \frac{dx x^{a_5-1} (1-x)^{a_1-1} \Gamma(a_{15})}{\Gamma(a_1) \Gamma(a_5)} \int \frac{[d^D k][d^D q]}{D_2^{a_2} D_3^{a_3} D_4^{a_4}} \\ &\quad \times \frac{1}{[(1-x)k^2 + x(k^2 + D_4 + 2k(q+p))]^{a_{15}}}, \end{aligned} \quad (4.25)$$

where we introduce a common notation  $a_{15} = a_1 + a_5$ .

We continue with another Feynman parameter  $y$ :

$$\begin{aligned} I &= \int_0^1 \frac{dx dy x^{a_5-1} (1-x)^{a_1-1} y^{a_{15}-1} (1-y)^{a_3-1} \Gamma(a_{135})}{\Gamma(a_1) \Gamma(a_3) \Gamma(a_5)} \\ &\quad \times \int \frac{[d^D k][d^D q]}{D_2^{a_2} D_4^{a_4} [(1-y)(k^2 + 2kp) + y(k^2 + xD_4 + 2xk(q+p))]^{a_{135}}} \end{aligned} \quad (4.26)$$

The expression in square brackets is the only piece depending on  $k$ . Completing the square and shifting  $k \rightarrow k'$ , it becomes  $k'^2 + D_4 xy(1-xy) + (1-y)^2 + (1-D_4 + D_2)xy(1-y)$ . Integrating over  $k'$  with Eq. A.1, we have:

$$\begin{aligned} I &= \frac{\mathcal{F}\Gamma(a_{135} - D/2)}{\Gamma(1+\epsilon)\Gamma(a_1)\Gamma(a_3)\Gamma(a_5)} \int_0^1 \frac{dx dy [d^D q]}{D_2^{a_2} D_4^{a_4}} \\ &\quad \times \frac{x^{a_5-1} (1-x)^{a_1-1} y^{a_{15}-1} (1-y)^{a_3-1}}{[D_2 xy(1-y) + D_4 xy^2(1-x) + (1-y)^2 + xy(1-y)]^{a_{135}-D/2}}. \end{aligned} \quad (4.27)$$

At this stage, to the four terms in square brackets we can apply the three-dimensional Mellin-Barnes transformation (Eq. 4.24), and integrate  $D_2$  and  $D_4$

with Eq. A.2. Powers of  $x$ ,  $y$ ,  $(1-x)$ ,  $(1-y)$  then lead to gamma-functions:

$$I = \frac{\mathcal{F}}{\Gamma(1+\epsilon)\Gamma(a_1)\Gamma(a_3)\Gamma(a_5)} \frac{1}{(2\pi i)^3} \int_{-i\infty}^{+i\infty} dz_1 dz_2 dz_3 \quad (4.28)$$

$$\begin{aligned} & \times \int_0^1 dx dy x^{a_5-1} (1-x)^{a_1-1} y^{a_{15}-1} (1-y)^{a_3-1} \int \frac{[d^D q]}{D_2^{a_2} D_4^{a_4}} \\ & \times [D_2 xy(1-y)]^{z_2} [D_4 xy^2(1-x)]^{z_1} [xy(1-y)]^{z_3} \\ & \times [1-y]^{2(-a_{135}+D/2-z_{123})} \Gamma(-z_1)\Gamma(-z_2)\Gamma(-z_3)\Gamma(a_{135}-D/2+z_{123}) \end{aligned} \quad (4.29)$$

$$\begin{aligned} & = \frac{\mathcal{F}}{\Gamma(1+\epsilon)\Gamma(a_1)\Gamma(a_3)\Gamma(a_5)} \frac{1}{(2\pi i)^3} \int_{-i\infty}^{+i\infty} dz_1 dz_2 dz_3 \int_0^1 dx dy \\ & \times x^{a_5-1+z_{123}} (1-x)^{a_1-1+z_1} y^{a_{15}-1+z_1+z_{123}} (1-y)^{a_3-1+z_{23}+2(-a_{135}+D/2-z_{123})} \\ & \times \int \frac{[d^D q]}{D_2^{a_2-z_2} D_4^{a_4-z_1}} \Gamma(-z_1)\Gamma(-z_2)\Gamma(-z_3)\Gamma(a_{135}-D/2+z_{123}) \\ & = \frac{\mathcal{F}^2}{\Gamma^2(1+\epsilon)\Gamma(a_1)\Gamma(a_3)\Gamma(a_5)} \frac{1}{(2\pi i)^3} \int_{-i\infty}^{+i\infty} dz_1 dz_2 dz_3 \quad (4.30) \\ & \times \frac{\Gamma(a_5+z_{123})\Gamma(a_1+z_1)\Gamma(a_{15}+z_1+z_{123})\Gamma(D-a_3-2a_{15}-2z_1-z_{23})}{\Gamma(a_{15}+z_1+z_{123})\Gamma(D-a_{135})} \\ & \times \frac{\Gamma(D/2-a_2+z_2)\Gamma(D/2-a_4+z_1)\Gamma(-D/2+a_{24}-z_{12})}{\Gamma(a_2-z_2)\Gamma(a_4-z_1)\Gamma(D-a_{24}+z_{12})} \\ & \times \Gamma(-z_1)\Gamma(-z_2)\Gamma(-z_3)\Gamma(a_{135}-D/2+z_{123})(-1)^{D/2-a_{24}+z_{12}}. \end{aligned}$$

The final expression is a three-dimensional integral which can be calculated numerically. However, we can further simplify it by applying to  $z_3$  the first Barnes lemma:

$$\begin{aligned} & \int_{-i\infty}^{+i\infty} \frac{dz}{2\pi i} \Gamma(\lambda_1+z)\Gamma(\lambda_2+z)\Gamma(\lambda_3-z)\Gamma(\lambda_4-z) \quad (4.31) \\ & = \Gamma(\lambda_{13})\Gamma(\lambda_{14})\Gamma(\lambda_{23})\Gamma(\lambda_{24})/\Gamma(\lambda_{1234}), \end{aligned}$$

and finally arrive at the two-dimensional Mellin-Barnes representation:

$$\begin{aligned} I & = \frac{\mathcal{F}^2}{\Gamma^2(1+\epsilon)\Gamma(a_1)\Gamma(a_3)\Gamma(a_5)\Gamma(D-a_{135})} \frac{1}{(2\pi i)^2} \int_{-i\infty}^{+i\infty} dz_1 dz_2 \quad (4.32) \\ & \times \frac{\Gamma(D/2-a_2+z_2)}{\Gamma(D/2-a_1+z_2)} \frac{\Gamma(a_5+z_{12})}{\Gamma(D-a_{24}+z_{12})} \frac{\Gamma(-z_1)}{\Gamma(a_4-z_1)} \frac{\Gamma(-z_2)}{\Gamma(a_2-z_2)} \\ & \times \Gamma(a_1+z_1)\Gamma(D/2-a_4+z_1)\Gamma(D/2-a_{15}-z_1)(-1)^{D/2-a_{24}+z_{12}} \\ & \times \Gamma(D-a_1-a_{135}-z_1)\Gamma(a_{135}-D/2+z_{12})\Gamma(a_{24}-D/2-z_{12}). \end{aligned}$$

Now the automated algorithm of Ref. [73] can be used to perform the integration for any values of indices  $a_1, \dots, a_5$ , including non-integer or  $\epsilon$ -dependent

exponents. It starts with choosing some (maybe non-zero) value of  $\epsilon$  and initial positions of the contours (straight lines parallel to the imaginary axis), satisfying the proper separation of poles: all poles from every factor  $\Gamma(\dots + z)$  to the left, all poles from  $\Gamma(\dots - z)$  to the right from the contour for variable  $z$ . ( $\Psi$  functions can be treated in the same way.) Next,  $\epsilon$  is shifted to zero while observing the behavior of poles. For “right” poles appearing to the left from the contour we subtract corresponding residues. If some pole ends up on the contour for  $\epsilon = 0$ , the contour is shifted and the procedure repeated.

Recursively applying this algorithm to all appearing Mellin-Barnes integrals, we arrive at a number of contributions of different dimensionality which can be integrated numerically.

Some attention should be given to the factor  $(-1)^{D/2 - a_{24} + z_{12}}$  (and in general, to the proper definition of any kinematic invariant like  $m^2$ ). As we have seen, the phase of negative unity is determined by the Feynman’s contour prescription. As the integration is done numerically, the deformation parameter should be small but non-zero,  $(-1 - i\delta)^{D/2 - a_{24} + z_{12}}$  to avoid ambiguity. This uniquely determines the analytical continuation of the logarithms that appear. In practice, with  $\delta$  smaller by several orders of magnitude than the expected numerical error, the results of integrating Eq. 4.32 are rather stable.

## Limitations of the method

The calculation above demonstrates the first shortcoming of the method: tedious manual calculations are required to produce the parameterization with the minimal dimensionality. If we started from the general alpha-parameterization for this integral, we would have to introduce seven parameters for  $\mathbf{D}$  (or four, using a smarter grouping of terms), a few more more for the factor  $\mathbf{F}$ . Possibly, using various reduction formulas, one could reduce that number by a few units, but eliminating all but two parameters would be very difficult. Automated algorithms, attempting to perform such reduction, do exist [74]; unfortunately, presently they are not capable of dealing with integrals needed for this thesis. Similarly, adding a non-unit mass to our example would introduce at least one additional integration parameter, so multi-scale problems

here are in general difficult.

An even more important problem is the numerical stability of on-shell integrals (and integrals with massive lines in general). While the two-loop integral of Eq. 4.32 converges quickly, we found that some non-planar three-loop topologies with two massive lines do not behave that well: growth and oscillations in the integrals are out of control for the available numerical schemes.

## 4.4 Conclusion

A huge progress has been made in the field of numerical methods in the last few years, facilitating many interesting physical and mathematical results. The method of sector decomposition was used in proving interesting relations between Feynman integrals and the so-called periodical numbers [75]. Reports of various improvements in the method are appearing often in the informal communication, although only a single public implementation is available so far [66]. In particular, various ideas have been suggested to reduce the number of terms appearing due to entangled numerator structures by smart bookkeeping techniques. Due to intrinsic parallelism of the procedure, one may expect it to benefit from the current trend of hardware development towards multi-core and multi-processor systems.

The Mellin-Barnes method was also extremely successful in obtaining many analytical and numerical results. Easy transition rules from contour integrals to multiple nested sums of various kinds and back were instrumental in proofs of certain summation formulas, as well as in extension of number theory through experimental mathematics [76]. Many tools have been developed to study the asymptotics and analytic properties of integrals using their Mellin-Barnes representation.

There is no doubt that numerical methods are rightfully becoming the mainstream of multi-loop calculations. Simpler to automate than analytical transformations, they ultimately may enter the experimental framework (e.g., as Monte-Carlo programs), allowing to routinely compute higher loop corrections to the quantities measured at colliders.

# Chapter 5

## Evaluation of integrals by differential equations

Analytical evaluation of Feynman integrals has always been an “art”: successful manipulations of complex relations between integrals, series and special functions require high skills and sometimes luck. Often, higher terms in the  $\epsilon$ -expansion of an integral could not be found using the methods that worked for the lower terms.

Recently, a combination of differential equations generated by recurrence relations [77, 78, 79, 80] and a new class of special functions – harmonic polylogarithms, or HPLs [81, 82, 83] – rendered a large class of calculations a “craft”. If this method works for the first terms in the expansion of an integral, it is only CPU resources that limit the accessible expansion depth. This breakthrough results from the very interesting properties of HPLs. Generalizing several kinds of “ordinary” special functions, HPLs are closed with respect to integration with certain weights – exactly the kind of functions appearing from the recurrence relations. That made possible the evaluation of the most difficult master integrals of this thesis.

This chapter starts with a one-loop calculation. Next, we briefly discuss the properties of harmonic polylogarithms, and illustrate them with a simple four-loop example. Finally, we demonstrate the practical difficulties in approaching the complicated four-loop topologies, and comment on ways to overcome them.



## 5.1 Simple one-loop example

Let us once again consider the topology in Fig. 2.1, this time allowing for arbitrary exponents of denominator factors. Normalizing the external momentum as  $p^2 = -m^2 = -1$ , and using  $x = m^2/M^2$ , the corresponding integral is

$$I(a, b; x) = \int \frac{[d^D k]}{(k^2)^a [(k+p)^2 + 1/x]^b}. \quad (5.1)$$

To demonstrate the method, let us reproduce several first terms in the on-shell result given by Eq. A.3:

$$\begin{aligned} I(1, 1; 1) &= \text{Onshell}(1, 1; 1) = \mathcal{F} \frac{1}{\epsilon(1-2\epsilon)} \\ &= \mathcal{F} \left( \frac{1}{\epsilon} + 2 + 4\epsilon + 8\epsilon^2 + \dots \right). \end{aligned} \quad (5.2)$$

As a by-product, we will also get the full  $x$  dependence at each order in  $\epsilon$ .

**Differential equation.** We start by applying the integration-by-parts relation Eq. 3.4 to an integral with indices  $a = b = 1$ :

$$(D-3)I(1, 1; x) - I(0, 2; x) + \frac{1-x}{x}I(1, 2; x) = 0. \quad (5.3)$$

Noticing from Eq. 5.1 that

$$\frac{d}{dx}I(1, 1; x) = \frac{1}{x^2}I(1, 2; x), \quad (5.4)$$

and substituting  $I(1, 2; x)$  in Eq. 5.3, we get the following differential equation:

$$\frac{d}{dx}I(1, 1; x) = \frac{1}{x^2} \frac{x}{1-x} [I(0, 2; x) - (1-2\epsilon)I(1, 1; x)]. \quad (5.5)$$

The function  $I(0, 2; x)$  in the RHS is a vacuum tadpole with a squared denominator, which can be calculated using Eq. A.1:

$$I(0, 2; x) = G_{m2}(0, 2; 1/x) = \frac{\mathcal{F} x^\epsilon}{\epsilon} = \mathcal{F} \left( \frac{1}{\epsilon} + \ln x + \epsilon \frac{\ln^2 x}{2} + \dots \right). \quad (5.6)$$

At this point it is convenient to expand the function. Since a one-loop integral cannot have a divergence more severe than  $\epsilon^{-1}$ , we write

$$I(1, 1; x) = \mathcal{F} \left( \frac{f_{-1}(x)}{\epsilon} + f_0(x) + \epsilon f_1(x) + \epsilon^2 f_2(x) + \dots \right). \quad (5.7)$$

Using Eq. 5.6, Eq. 5.5 turns into a chain of coupled linear, first order differential equations:

$$f'_{-1}(x) = -\frac{1}{x(1-x)}f_{-1}(x) + \frac{1}{x(1-x)}, \quad (5.8)$$

$$f'_0(x) = -\frac{1}{x(1-x)}f_0(x) + \frac{\ln x + 2f_{-1}(x)}{x(1-x)}, \quad (5.9)$$

$$f'_1(x) = -\frac{1}{x(1-x)}f_1(x) + \frac{(\ln^2 x)/2 + 2f_0(x)}{x(1-x)}, \quad (5.10)$$

...

**Solution.** The method of solving such equations is due to Euler. According to his formula, any equation

$$f'(x) + g(x)f(x) = R(x) \quad (5.11)$$

with a solution  $u(x)$  to the corresponding homogeneous equation

$$u'(x) + g(x)u(x) = 0, \quad (5.12)$$

has solutions of the form

$$f(x) = u(x) \left[ C + \int \frac{R(x)}{u(x)} dx \right], \quad (5.13)$$

with an integration constant  $C$  fixed by the boundary conditions.

Equations 5.8, 5.9, and 5.10 all have the same structure, differing only by the inhomogeneous part in the RHS. We start with finding the general solution to the common homogeneous differential equation

$$u'(x) = -\frac{1}{x(1-x)}u(x), \quad (5.14)$$

which in this case is easy to guess:  $u(x) = (1-x)/x$ .

With that, Eq. 5.8 has the solution

$$f_{-1}(x) = \frac{1-x}{x} \left[ C + \int \frac{1}{x(1-x)} \frac{x}{1-x} dx \right] = C \frac{1-x}{x} + \frac{1}{x}. \quad (5.15)$$

**Boundary conditions.** To fix the constant  $\mathbf{C}$  and constants appearing from further equations, we need to know the value of  $f(x)$  at some point. For that purpose we use the expansion obtained in Sec. 2.2 (Eq. 2.15), expanding the solutions as needed to match the terms in  $\epsilon$ - and  $x$ -expansions at  $x \rightarrow 0$ . At every order in  $\epsilon$ , we only need a single term in  $x$ -expansion. The remaining terms then serve as a useful cross-check of the solution.

**Solution (continued).** From Eq. 2.15,  $f_{-1}(x \rightarrow 0) = 1$ , so  $\mathbf{C} = -1$ , and  $f_{-1}(x) = 1$ . Note that requiring  $f_{-1}$  to be at most logarithmically divergent at  $x = 0$  (even not knowing the actual value) is sufficient to produce the answer.

At the next step, we use this result to solve Eq. 5.9:

$$\begin{aligned} f_0(x) &= \frac{1-x}{x} \left[ \mathbf{C} + \int \frac{\ln x + 2}{x(1-x)} \frac{x}{1-x} dx \right] \\ &= \mathbf{C} \frac{1-x}{x} + 2 + \ln x + \frac{1-x}{x} \ln(1-x). \end{aligned} \quad (5.16)$$

Since  $f_0(x \rightarrow 0) = 1 + \ln x + \frac{x}{2} + \dots$ , we find that  $\mathbf{C} = 0$ , and  $f_0(x) = 2 + \ln x + \ln(1-x)(1-x)/x$ .

At order  $\epsilon$ , the integration is non-trivial, involving powers of  $\ln x$ ,  $\ln(1-x)$ , finally leading to

$$\begin{aligned} f_1(x) &= 4 + 2 \ln x + \frac{\ln^2 x}{2} + \frac{1-x}{x} [2 \ln(1-x) \\ &+ \ln(1-x) \ln x - \ln^2(1-x) - \text{Li}_2(x)], \end{aligned} \quad (5.17)$$

where  $\text{Li}_2(x)$  is the polylogarithm – a special function defined as

$$\text{Li}_2(x) = - \int_0^1 \frac{\ln(1-xt)}{t} dt. \quad (5.18)$$

To continue the solution further, one has to integrate combinations of logarithms and polylogarithms, potentially producing other special functions. The approach suggested in Ref. [80] allows to avoid this by introducing a new class of functions – *harmonic polylogarithms* – such that sequential integrations of Eq. 5.13 at every step are expressible within that class using simple recursive formulas.

## 5.2 Harmonic polylogarithms

Let us define functions  $H(a_1, \dots, a_w; x)$ , with each index  $a_i$  taking values 1, -1, or 0. The number of indices  $w$  is called the weight of an HPL. They satisfy the following recursive relations.

At weight  $w = 1$ , there are three HPLs:

$$H(1; x) = -\ln(1-x), \quad H(0; x) = \ln x, \quad H(-1; x) = \ln(1+x), \quad (5.19)$$

with derivatives  $\frac{d}{dx}H(a; x) = f(a; x)$ , where

$$f(1; x) = \frac{1}{1-x}, \quad f(0; x) = \frac{1}{x}, \quad f(-1; x) = \frac{1}{1+x}. \quad (5.20)$$

At weights  $w > 1$ , definition is recursive. Isolating the case of all zero indices,

$$\begin{aligned} H(\underbrace{0, \dots, 0}_w; x) &= \frac{\ln^w x}{w!}, & (5.21) \\ H(a_1, \dots, a_w; x) &= \int_0^x f(a_1; y)H(a_2, \dots, a_w; y)dy \end{aligned}$$

where  $f(a; x)$  are defined in Eq. 5.20.

An important property of HPLs is the so-called shuffle algebra they satisfy,

$$H(a_1, \dots, a_w; x)H(b_1, \dots, b_m; x) = \sum_{\vec{r}=\vec{a} \uplus \vec{b}} H(r_1, \dots, r_{w+m}; x), \quad (5.22)$$

where the sum is taken over all mergers of vectors  $\vec{a} = (a_1, \dots, a_w)$  and  $\vec{b} = (b_1, \dots, b_m)$  into vectors  $\vec{r}$  preserving the relative order of components  $a_i$  and  $b_j$  (operation similar to shuffling two decks of cards, hence the name), e.g.

$$H(a; x)H(b, c; x) = H(a, b, c; x) + H(b, a, c; x) + H(b, c, a; x). \quad (5.23)$$

Using the definition of HPLs, Eq. 5.22, and integration by parts, any integral over  $x$  from 0 to  $y$  of a term like  $x^m(1-x)^n(1+x)^k H(a_1, \dots, a_w; x)$  with integer  $m$ ,  $n$ , and  $k$  can be expressed as a sum of functions of  $y$  having a similar structure. For instance, Eq. 5.17 becomes

$$\begin{aligned} f_1(x) &= 4 + H(0, 0; x) + 2H(0; x) - \frac{1-x}{x} [H(1, 0; x) \\ &+ 2H(1; x) + 2H(0, 1; x) + 2H(1, 1; x)], \end{aligned} \quad (5.24)$$

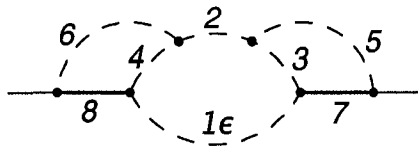


Figure 5.1: Generic topology T. Dashed lines represent massless, and solid lines – massive propagators. Index  $1\epsilon$  denotes the  $\epsilon$ -power of line 1.

and further terms can be obtained with an appropriate computer algebra implementation of HPLs, such as the Mathematica package HPL [84].

### 5.3 Simple four-loop example

The following example originated from computing mass-dependent corrections to semi-leptonic  $b$ -quark decay (discussed in Chapter 7). To obtain higher order terms in the asymptotic expansion of physical quantities, many master integrals had to be expanded to a higher power of  $\epsilon$ . The method of differential equations proved to be a reliable scheme applicable to most needed integrals.

We consider the topology in Fig. 5.1 with the external momentum  $p$ , internal mass  $1/x$  and denominator  $D_1$  raised to an  $\epsilon$ -dependent power:

$$\mathbb{T}(a_1, \dots, a_9) = \int \frac{[d^D k_1][d^D k_2][d^D k_3] D_9^{-a_9}}{D_1^{a_1+\epsilon} D_2^{a_2} D_3^{a_3} D_4^{a_4} D_5^{a_5} D_6^{a_6} D_7^{a_7} D_8^{a_8}}, \quad (5.25)$$

where  $D_1 = k_1^2$ ,  $D_2 = (k_1+p)^2$ ,  $D_3 = (k_1+k_2+p)^2$ ,  $D_4 = (k_1+k_3+p)^2$ ,  $D_5 = k_2^2$ ,  $D_6 = k_3^2$ ,  $D_7 = k_2^2 + 2k_2p - 1 + 1/x$ ,  $D_8 = k_3^2 + 2k_3p - 1 + 1/x$ ,  $D_9 = 2k_2k_3$ , and  $p^2 = -1$ . (It is classified as a four-loop integral since the  $\epsilon$ -power of  $D_1$  appeared due to integration of a massless sub-loop using Eq. A.2.)

**Differential equations.** The derivative of any master integral belonging to this topology,

$$\frac{d}{dx} \mathbb{T}(a_1, \dots, a_9) = \left( \frac{a_7}{x^2} \mathbf{7}^+ + \frac{a_8}{x^2} \mathbf{8}^+ \right) \mathbb{T}(a_1, \dots, a_9), \quad (5.26)$$

where we use the raising operators from Sec. 3.1, can be reduced (e.g. with Laporta algorithm) back to master integrals. Extending the reduction every time

new master integrals are found, we arrive at the closed system of equations:

$$V18' = \frac{x-2+\epsilon(4-3x)}{x(1-x)} V18 + \frac{3-5\epsilon}{1-x} V18a + \frac{2(\epsilon-1)}{1-x} V9, \quad (5.27)$$

$$V18a' = \frac{1-\epsilon}{x(1-x)} V18 + \frac{5\epsilon-3}{x(1-x)} V18a + \frac{2-\epsilon}{1-x} V9, \quad (5.28)$$

$$V9' = \frac{\epsilon-1}{1-x} V1 + \frac{3\epsilon-2}{x} V9 + \frac{3-4\epsilon}{1-x} V9a, \quad (5.29)$$

$$V9a' = \frac{1-\epsilon}{1-x} V1 + \frac{x-4+\epsilon(5-x)}{x(1-x)} V9a, \quad (5.30)$$

$$V1' = \frac{2(\epsilon-1)}{x} V1. \quad (5.31)$$

Here the master integrals are

$$V18 = T(0, 1, 1, 1, 0, 0, 1, 1, 0), \quad V18a = T(-1, 1, 1, 1, 0, 0, 1, 1, 0), \quad (5.32)$$

$$V9 = T(0, 1, 1, 0, 0, 0, 1, 1, 0), \quad V9a = T(-1, 1, 1, 0, 0, 0, 1, 1, 0),$$

$$V1 = T(0, 1, 0, 0, 0, 0, 1, 1, 0).$$

(Figures corresponding to the on-shell limit of  $V1$ ,  $V9$  and  $V18$  can be found in Eq. B.11, B.17, and B.25, respectively. Indices in those equations can be different due to the symmetries of this topology.) We will focus on the most non-trivial master integral  $V18$ , with the goal of establishing its on-shell value (at  $x = 1$ ). The semi-leptonic  $b$ -quark decay rate depends only on the imaginary part of this integral, and in what follows we discard the real contributions.

The system of Eqs. 5.27 - 5.31 has a few important features. First, each coefficient function has only powers of  $x$  and  $(1-x)$  in denominator, giving some hope that the corresponding solutions could be expressed with HPLs. Second, the system is clearly separated into an independent equation on  $V1$ , a closed system on  $V9$  and  $V9a$ , and a system on  $V18$  and  $V18a$ , which indicates that when finding solutions for the homogeneous equations, we will not have differential equations of order higher than two.

**Boundary conditions.** To find  $V18$  and other master integrals, it is necessary to be able to evaluate these functions (and their derivatives) at some point. We employed the technique of asymptotic expansion near  $x = 0$ , by

combining the contributions in the three regions (Fig. 5.2). Since for  $x \in [0, 1]$  the topology  $T$  does not develop cuts other than existing in the on-shell case, we only consider the regions with non-zero imaginary part. As in the previous examples, we evaluate as many terms in the  $x$ -expansion as was possible at every order in  $\epsilon$ , thus over-constraining the integration constants.

**Solution.** For the purpose of clarity we skip the evaluation of  $V1$ ,  $V9$ , and  $V9a$ . Integral  $V1$  can be found from Eqs. A.2 and A.1, and finding  $V9$  and  $V9a$  is similar to the calculation below, the latter being more instructive.

With simple integrals substituted in the RHS of Eqs. 5.27 and 5.28, we eliminate the derivatives of  $V18a$  from one of them. In the resulting second-order equation, we expand  $V18$  as

$$V18(\epsilon) = \mathcal{F}^4 \left( \frac{f_{-1}(x)}{\epsilon} + f_0(x) + f_1(x)\epsilon + \dots \right), \quad (5.33)$$

so that the equation for  $f_1$  becomes

$$f_{-1}'' - \frac{2x-5}{x(1-x)} f_{-1}' + \frac{4}{x^2(1-x)} f_{-1} = \frac{2}{1-x} + \frac{2}{x^2} + \frac{2}{x}. \quad (5.34)$$

For the generic second-order equation

$$f''(x) + g(x)f'(x) + h(x)f(x) = R(x), \quad (5.35)$$

Euler's formula becomes

$$f(x) = u_1(x) \left( \mathbf{A} - \int \frac{u_2(x)}{W(x)} R(x) dx \right) + u_2(x) \left( \mathbf{B} + \int \frac{u_1(x)}{W(x)} R(x) dx \right). \quad (5.36)$$

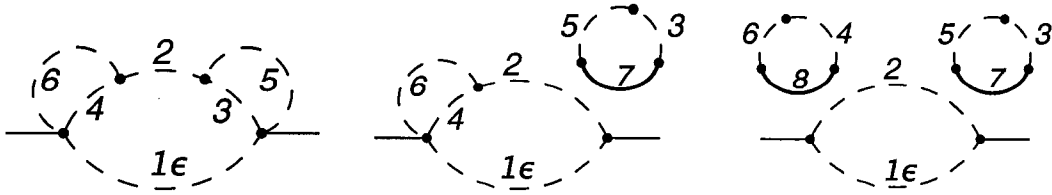


Figure 5.2: Three regions contributing to the imaginary part of topology  $T$  in the expansion about  $x = 0$ .

Here  $W = u_1 u_2' - u_1' u_2$  is the Wronskian of the two independent solutions  $u_1(x)$ ,  $u_2(x)$  of the homogeneous equation (with  $R(x) = 0$ ).

In our example,  $u_1 = (1 + 2x)/x^2$ ,  $u_2 = (x^2 - 7 - 2(1 + 2x) \ln x)/x^2$ , and the Wronskian  $W = -2(1 - x)^3/x^5$ . Using Eq. 5.36, the general solution is

$$f_{-1} = \frac{1}{2} + \mathbf{A} \frac{1 + 2x}{x^2} + \mathbf{B} \frac{x^2 - 7 - 2(1 + 2x)H(0; x)}{x^2}, \quad (5.37)$$

and the constants  $\mathbf{A}$  and  $\mathbf{B}$  are determined from the expansion near  $x = 0$ :  $f_{-1}(x \rightarrow 0) = 1/2$  (all terms singular in  $x$  vanish). Finally, we find

$$f_{-1}(x) = f_{-1}(1) = \frac{1}{2}, \quad (5.38)$$

and again the finiteness of  $f_{-1}$  at  $x = 0$  is sufficient to obtain the answer.

At the order  $\epsilon^0$ , we use  $f_{-1}$  and the RHS functions to find

$$R(x) = \frac{21x + 4xH(0; x) - 2(1 - x)H(1; x) - 2H(0, 1; x)}{x^3(1 - x)}. \quad (5.39)$$

(Of course, the homogeneous part is the same as in Eq. 5.34.) After the integration, the general solution is found to be

$$\begin{aligned} f_0 &= \frac{23}{4} + \frac{1}{x} + H(0; x) + \frac{x^2 - 1}{x^2} H(1; x) - \frac{2}{x} H(0, 1; x) \\ &+ \mathbf{A} \frac{1 + 2x}{x^2} + \mathbf{B} \frac{x^2 - 7 - 2(1 + 2x)H(0; x)}{x^2}. \end{aligned} \quad (5.40)$$

The boundary condition is  $f_0(x \rightarrow 0) = \ln x + \frac{13}{4} + \frac{x}{6} + \frac{x^2}{36} + \frac{x^3}{120} + \dots$ , and the final answer and its on-shell limit are

$$\begin{aligned} f_0(x) &= \frac{23}{4} + \frac{1}{x} + H(0; x) + \frac{x^2 - 1}{x^2} H(1; x) - \frac{2}{x} H(0, 1; x) \\ &\xrightarrow{x=1} \frac{27}{4} - \frac{\pi^2}{3}. \end{aligned} \quad (5.41)$$

Further application of the method (although taking significantly longer for each successive term in the  $\epsilon$ -expansion) is straightforward, leading to Eq. B.25.

## 5.4 The gory details of a four-loop calculation

The method above works if at every stage we deal with HPLs. In particular, solutions of the homogeneous differential equation should be expressible in



terms of the HPLs and rational functions of  $x$  such that denominators only contain  $x$  and  $(1 \pm x)$ . The inverse Wronskian of the solutions should also have this property. When the order of the equation is larger than two, the same condition applies also to the minors of the Wronski matrix.

In some cases, it takes several attempts to choose a suitable parameterization. For instance, the double-scale topologies in Fig. 5.3 (defined by analogy to the topology T above) have the same on-shell limit, differing only by the



Figure 5.3: Different topologies having the same on-shell ( $x = 1$ ) limit. Thin solid line represents mass 1, thick lines – squared mass  $1/x$ .

mass term in a single denominator factor ( $1/x$  in the left, and 1 in the right figure). However, the system of equations for the topology in the left leads to denominator factors  $(x + 3)$  appearing in addition to “normal” factors  $x$  and  $(1 \pm x)$  in the integrands, and the equations cannot be integrated in terms of ordinary HPLs. The topology on the right, although less symmetric and with more complicated boundary conditions, does not have this problem, and was used to evaluate the needed master integrals.

Another important question is the choice of integrals to solve for (e.g., the choice of  $V18$  rather than  $V18a$  in the above example). In some non-trivial cases (apparently related to one of the coefficient functions in the system vanishing in the limit  $\epsilon = 0$ ) such a change would lead to an equation not solvable in terms of HPLs, and some experimentation was needed to make the right choice.

The master integrals identified by the Laporta reduction may also be non-optimal for the solution. For example, a topology in Fig. 5.4 has the most

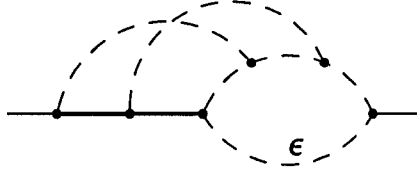


Figure 5.4: Topology leading to  $V30$  in the on-shell limit.

difficult master integral, in which all the lines are present with unit exponents, except for the exponent of the  $\epsilon$ -line, which is  $\epsilon$ . Without numerators, this integral in the on-shell limit should reproduce  $V30 = -\frac{4}{135}\pi^4 + \dots$  (Eq. B.32). However, the corresponding representation in terms of HPLs starts only at the order  $\epsilon$ , and diverges at  $x = 1$ . We introduced numerators to that integral to remove infra-red divergences, and reduced the new recurrence relations. After solving the new system,  $V30$  was found from the reduction at  $x = 1$ .

The final remark is about possible extensions of the class of integrated functions. In particular, Ref. [81] lists transformations useful for integration of  $H(\dots; \sqrt{x})$  and the related rational functions. Although restricted to certain HPL index vectors, such formulas were useful in dealing with topologies having more than two massive lines, leading to the results in Eqs. B.14, B.33, and B.34.

# Chapter 6

## Semi-leptonic $b$ -quark decay near maximum recoil

The second heaviest quark in the Standard Model – the bottom-quark – was discovered in 1977 at the Fermi National Accelerator Laboratory (Fermilab). Since its mass, close to the mass of a Helium atom, is large in comparison with the characteristic scale of non-perturbative QCD,  $b$ -quark decays can be reliably described using perturbation theory. Two prominent experiments, BELLE and BaBar, are using  $b$ -quarks to measure fundamental parameters of the Standard Model and search for possible manifestations of the New Physics. This necessitates multi-loop Standard Model calculations of  $b$ -quark decays. In the following two chapters we deal with the QCD corrections to the most frequent semi-leptonic  $b$ -quark decay. This chapter focuses on this process in a specific kinematic limit of zero invariant mass of lepton pair, whereas Chapter 7 is devoted to the total decay rate.

We start by discussing this kinematics, then briefly demonstrate the method of calculation using the examples of the tree-level decay rate and  $\mathcal{O}(\alpha_s)$  correction, and in Sec. 6.4 we present new  $\mathcal{O}(\alpha_s^2)$  analytic results [26].

### 6.1 Maximum recoil limit

The  $b$ -quark primarily decays into a  $c$ -quark and a virtual  $W$ -boson. If the  $W$  subsequently decays into leptons, such a process is called semi-leptonic. We denote the hadronic system by  $X$ ; in parton-level description it includes the

$c$ -quark and possibly gluons and light quarks. Neglecting the lepton mass, the amplitude can be written as

$$i\mathcal{M}(b \rightarrow X \ell \bar{\nu}_\ell) = \langle b | \mathcal{J}^\mu | X \rangle \frac{-i}{q^2 - M_W^2} \left( g_{\mu\alpha} - \frac{q_\mu q_\alpha}{M_W^2} \right) \frac{i g_w \bar{u} \gamma^\alpha (1 + \gamma^5) v}{2\sqrt{2}}. \quad (6.1)$$

Here  $\mathcal{J}^\mu$  is the quark current, including the QCD corrections,  $q$  is the momentum of a virtual  $W$ -boson, and  $M_W$  is the  $W$ -boson mass. For the decay rate, we need this amplitude squared,

$$\begin{aligned} |i\mathcal{M}(b \rightarrow X \ell \bar{\nu})|^2 &= \frac{g_w^2}{8} \frac{1}{(q^2 - M_W^2)^2} \left[ g_{\mu\alpha} - \frac{q_\mu q_\alpha}{M_W^2} \right] \left[ g_{\nu\beta} - \frac{q_\nu q_\beta}{M_W^2} \right] \\ &\times \langle b | \mathcal{J}^\mu | X \rangle \langle X | \mathcal{J}^{*\nu} | b \rangle \text{Tr} \left[ \hat{p}_\ell \gamma^\alpha (1 + \gamma^5) \hat{p}_\nu \gamma^\beta (1 + \gamma^5) \right], \end{aligned} \quad (6.2)$$

and the phase space element of the final particles  $d\Phi(b \rightarrow X \ell \bar{\nu})$  as in Eq. A.6:

$$\begin{aligned} d\Gamma(b \rightarrow X \ell \bar{\nu}_\ell) &= \frac{1}{2m_b} |i\mathcal{M}(b \rightarrow X \ell \bar{\nu}_\ell)|^2 d\Phi(b \rightarrow X \ell \bar{\nu}_\ell) \\ &= \frac{1}{2m_b} \frac{g_w^2}{8} \frac{\langle b | \mathcal{J}^\mu | X \rangle \langle X | \mathcal{J}^{*\nu} | b \rangle}{(q^2 - M_W^2)^2} \left[ g_{\mu\alpha} - \frac{q_\mu q_\alpha}{M_W^2} \right] \left[ g_{\nu\beta} - \frac{q_\nu q_\beta}{M_W^2} \right] \\ &\times 8 \left( p_\ell^\alpha p_\nu^\beta + p_\ell^\beta p_\nu^\alpha - g^{\alpha\beta} p_\ell p_\nu + \epsilon^{\alpha\beta\rho\sigma} p_\ell^\rho p_\nu^\sigma \right) \\ &\times \frac{dq^2}{2\pi} d\Phi(W^* \rightarrow \ell \bar{\nu}) d\Phi(b \rightarrow X W^*), \end{aligned} \quad (6.3)$$

where the phase space element was partitioned according to Eq. A.7.

The QCD corrections only involve hadrons, thus the integration over the phase space of the  $W^*$  decay products can be performed immediately, leading to

$$\begin{aligned} d\Gamma(b \rightarrow X \ell \bar{\nu}_\ell) &= \frac{1}{2m_b} d\Phi(b \rightarrow X W^*) \langle b | \mathcal{J}^\mu | X \rangle \langle X | \mathcal{J}^{*\nu} | b \rangle \\ &\times \frac{g_w^2}{48\pi^2} dq^2 \frac{q^2}{(q^2 - M_W^2)^2} \left( g_{\mu\nu} - \frac{q_\mu q_\nu}{q^2} \right). \end{aligned} \quad (6.4)$$

This expression can be compared in the limit  $q^2 \ll M_W^2$  to the decay rate of the  $b$ -quark to the same system  $X$  and a virtual  $W$ -boson with mass  $\sqrt{q^2}$ , where  $\mathcal{J}^\mu$ ,  $\mathcal{J}^\nu$  denote the same hadronic current as in the expressions above:

$$d\Gamma(b \rightarrow X W^*) = \frac{d\Phi(b \rightarrow X W^*) \langle b | \mathcal{J}^\mu | X \rangle \langle X | \mathcal{J}^{*\nu} | b \rangle}{2m_b} \left( g_{\mu\nu} - \frac{q^\mu q^\nu}{q^2} \right). \quad (6.5)$$

One can notice a simple relation between those rates:

$$d\Gamma(b \rightarrow X \ell \bar{\nu}_\ell) = \frac{g_w^2}{48\pi^2 M_W^4} \int dq^2 q^2 d\Gamma(b \rightarrow X W^*)|_{M_{W^*}=\sqrt{q^2}}. \quad (6.6)$$

The limit  $q^2 = 0$ , when the hadrons acquire the largest possible recoil momentum, can be studied experimentally (as the endpoint slope of the distribution over  $q^2$  of the semi-leptonic decay events). Perturbative calculations in this approximation are relatively simple, involving only two relevant scales:  $m_b$  and  $m_c$  (which is the mass of the  $c$ -quark). In what follows we focus on the QCD corrections to the decay width  $\Gamma(b \rightarrow cW^*)|_{M_{W^*}=0}$ .

## 6.2 Tree-level decay rate

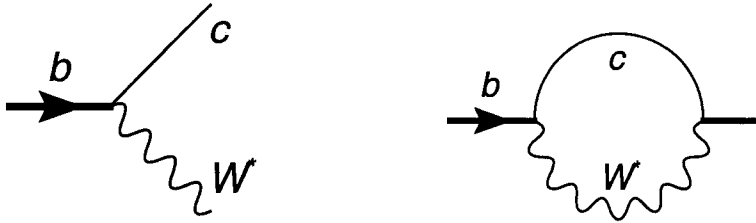


Figure 6.1: Tree-level decay  $b \rightarrow cW^*$       Figure 6.2: Self-energy diagram related to the tree-level decay  $b \rightarrow cW^*$

The integrated tree-level decay rate of the process in Fig. 6.1 is

$$\Gamma(b \rightarrow cW^*)|_{M_{W^*} \rightarrow 0} = \frac{G_F^* |V_{cb}|^2 m_b^3}{8\sqrt{2}\pi} \left[ 1 - \left( \frac{m_c}{m_b} \right)^2 \right]^3 \equiv \Gamma_0 (1 - \rho^2)^3, \quad (6.7)$$

where we used the notations  $\Gamma_0 = \frac{G_F^* |V_{cb}|^2 m_b^3}{8\sqrt{2}\pi}$ ,  $G_F^* = \frac{\sqrt{2}g_w^2}{8M_{W^*}^2}$  and  $\rho = \frac{m_c}{m_b}$ . The limit  $M_{W^*} \rightarrow 0$  is not physical – density matrix of real massless gauge bosons is not singular; hence the apparent divergence of  $G_F^*$ . It cancels in Eq. 6.6, describing a physical decay. The masses of quarks (depending on the definition) are  $m_b \approx 4.6$  GeV,  $m_c \approx 1.15$  GeV, and the value of  $\rho$  is around  $0.25 \dots 0.33$ , which explains the need for mass-dependent results.

With  $X_0 = (1 - \rho^2)^3$ , the QCD corrections to Eq. 6.7 are

$$\Gamma(b \rightarrow cW^*) = \Gamma_0 \left[ X_0 + \frac{\alpha_s}{\pi} X_1 + \left( \frac{\alpha_s}{\pi} \right)^2 X_2 + \mathcal{O}(\alpha_s^3) \right]. \quad (6.8)$$

For the purpose of calculating one- and two-gluon corrections  $X_1$  and  $X_2$  it is beneficial to use the optical theorem which connects the  $b$ -quark decay rate to the imaginary part of the  $b$ -quark self-energy operator. When computing the imaginary parts of corresponding integrals, infrared divergences arising from loop vertex corrections and real gluon emission cancel. At the tree level we consider the diagram on Fig. 6.2 with  $b$ -quark momentum  $p$  and  $W$ -boson momentum  $q$ :

$$\Gamma(b \rightarrow cW^*) = \frac{\text{Im } \Sigma(b \rightarrow [cW^*] \rightarrow b)}{m_b}, \quad (6.9)$$

$$\begin{aligned} i\Sigma &= \int \frac{d^D q}{(2\pi)^D} \bar{u}(p) \left( \frac{ig_w V_{cb}}{2\sqrt{2}} \gamma^\alpha (1 - \gamma_5) \right) \left( \frac{-i(\hat{q} + \hat{p} + m_c)}{(q+p)^2 - m_c^2 + i\delta} \right) \\ &\times \left( \frac{ig_w V_{cb}^*}{2\sqrt{2}} \gamma^\mu (1 - \gamma_5) \right) \left( \frac{i}{M_{W^*}^2} \frac{q_\alpha q_\mu}{q^2} \right) u(p). \end{aligned} \quad (6.10)$$

Averaging over the initial quark polarizations leads to

$$\frac{1}{2} \sum_{\sigma(b)} \bar{u}(p) \Gamma u(p) = \frac{1}{2} \text{Tr} [(\hat{p} - m_b) \Gamma], \quad (6.11)$$

where  $\Gamma$  stands for the combination of gamma-matrices in the numerator of Eq. 6.10.

One subtle point is the treatment of  $\gamma_5$  in dimensional regularization. Leaving more detailed discussion to the following chapter, we here notice that after taking the trace, the terms containing odd powers of  $\gamma_5$  give rise to the anti-symmetric tensor  $\epsilon^{\mu\nu\rho\sigma}$ . Contracted with the symmetric  $W$  polarization matrix  $T_{\mu\nu} \sim (q^2 g_{\mu\nu} - q_\mu q_\nu)$ , such contributions vanish.

An equivalent result is obtained by naively anti-commuting all  $\gamma_5$ 's to the left using the relations  $\gamma_5 \gamma_\mu = -\gamma_\mu \gamma_5$  and  $\gamma_5 \gamma_5 = 1$ , and then dropping all terms with  $\gamma_5$ . After that, trace can be safely calculated in  $D$  dimensions.

By taking the trace and Wick rotating, the diagram is expressed in terms of scalar double-scale one-loop integrals, which in principle can be exactly solved in terms of hyper-geometric functions. However, since the more complicated diagrams can only be treated by expansion, we here evaluate several first terms in the  $\rho$  powers by Taylor expanding the  $c$ -quark propagator:

$$\frac{1}{(q+p)^2 + m_c^2} = \frac{1}{(q+p)^2} \sum_{n=0}^{\infty} \left( -\frac{m_c^2}{(q+p)^2} \right)^n. \quad (6.12)$$

Now all that is left is evaluation of massless propagator-type one-loop topology (with various powers of denominators). Using Eq. A.2, we obtain:

$$\Gamma(b \rightarrow cW^*) = \Gamma_0 (1 - 3\rho^2 + 3\rho^4 - \rho^6), \quad (6.13)$$

consistent with Eq. 6.7 (terms with higher powers of  $\rho$  cancel).

### 6.3 One-gluon corrections

At this order we consider the imaginary part of three 2-loop diagrams (Fig. 6.3). Color structure provides a factor of  $C_F$  to each diagram. In addition, the left-most diagram requires a symmetry factor of 2. The corresponding scalar inte-

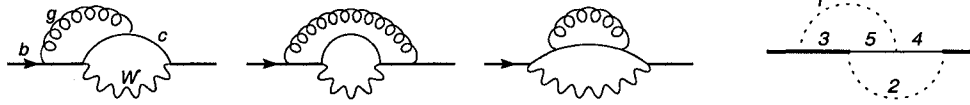


Figure 6.3: Diagrams contributing to  $\mathcal{O}(\alpha_s)$  corrections

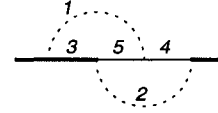
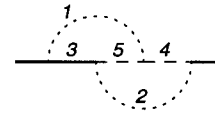


Figure 6.4: Common double-scale topology

grals belong to the double-scale topology in Fig. 6.4. We parameterize these integrals with external momentum  $p$  (with on-shell condition  $p^2 = -m_b^2$ ) and loop momenta  $k_1$  and  $k_2$ , so that the denominator factors are  $D_1 = (k_2 - k_1)^2$ ,  $D_2 = (k_1 - p)^2$ ,  $D_3 = (p + k_2 - k_1)^2 + m_b^2$ ,  $D_4 = k_1^2 + m_c^2$ , and  $D_5 = k_2^2 + m_c^2$ . There are four regions of virtualities of the loop momenta:

$\mathbf{k}_1, \mathbf{k}_2 \sim \mathbf{m}_b$ . In this region,  $D_4$  and  $D_5$  are Taylor expanded, and we arrive at the topology of Eq. 4.25:

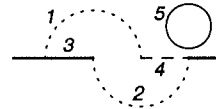
$$D_4 \rightarrow k_1^2, D_5 \rightarrow k_2^2$$



$\mathbf{k}_1 \sim \mathbf{m}_b, \mathbf{k}_2 \sim \mathbf{m}_c$ . After the expansion, the integral factorizes into massive vacuum bubbles (Eq. A.1), and a one-loop propagator-type topology. By par-

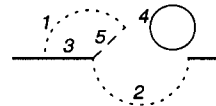
tial fraction decomposition, the latter separates into massless (Eq. A.2) and on-shell (Eq. A.3) contributions:

$$D_1 \rightarrow k_1^2, D_3 \rightarrow (p - k_1)^2 + m_b^2, D_4 \rightarrow k_1^2$$



$\mathbf{k}_1 \sim \mathbf{m}_c$ ,  $\mathbf{k}_2 \sim \mathbf{m}_b$ . As in the previous case, one-loop vacuum bubble factorizes, the rest becoming an on-shell topology:

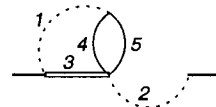
$$D_1 \rightarrow k_2^2, D_2 \rightarrow p^2, D_3 \rightarrow (p + k_2)^2 + m_b^2, D_5 \rightarrow k_2^2$$



However, this graph does not correspond to any allowed decay, since it cannot be cut through massless lines (line 2 is a point). Thus, the contribution of this region is purely real and can be neglected.

$\mathbf{k}_1, \mathbf{k}_2 \sim \mathbf{m}_c$ . In this region, the denominator factor  $D_3$  becomes linear in  $p$ , leading to the two-loop “eikonal” integrals:

$$D_2 \rightarrow p^2, D_3 \rightarrow 2p(k_2 - k_1) + i\delta$$



Those are real, and this region also produces no contribution to the decay rate.

Summing the contributions of non-zero regions of all diagrams, we automatically account for ultraviolet and infrared divergences in virtual and real emission contributions. However, the result still does not have a finite limit at  $D = 4$ , as the parameters used in calculation correspond to Lagrangian definition rather than to observable quantities. In order to properly account for the scale at which mass and charge are evaluated, we need to include two renormalization contributions (Fig. 6.5). Crossed circles on the picture repre-

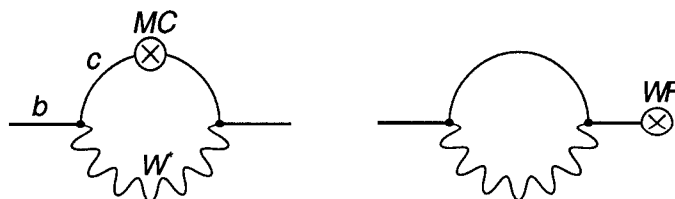


Figure 6.5:  $\mathcal{O}(\alpha_s)$  renormalization contributions



sent the insertion of renormalization constants. Wave function renormalization multiplies the tree-level diagram, while  $c$ -quark mass renormalization inserts an additional vertex in the  $c$ -quark propagator. These two diagrams can be computed by the same technique as the tree-level rate. In the on-shell scheme, the needed constants through  $\mathcal{O}(\epsilon)$  are

$$\begin{aligned} \text{WF} &= 1 - C_F \left( \frac{\alpha_s}{\pi} \frac{\mathcal{F}}{m_b^{2\epsilon}} \right) \left\{ \frac{3}{4\epsilon} + 1 + 2\epsilon \right\} + \dots, \\ \text{MC}_c &= im_c C_F \left( \frac{\alpha_s}{\pi} \frac{\mathcal{F}}{m_c^{2\epsilon}} \right) \left\{ \frac{3}{4\epsilon} + 1 + 2\epsilon \right\} + \dots. \end{aligned} \quad (6.14)$$

Finally, combining all contributions, the one-gluon correction of Eq. 6.8 becomes

$$\begin{aligned} X_1 &= C_F \left[ \left( \frac{5}{4} - \frac{\pi^2}{3} \right) + \left( \frac{\pi^2}{3} - 9 \ln \rho - \frac{11}{4} \right) \rho^2 \right. \\ &\quad + \left( \frac{\pi^2}{3} + 6 \ln \rho + \frac{1}{4} \right) \rho^4 + \left( \frac{\pi^2}{3} + 6 \ln \rho + \frac{1}{4} \right) \rho^4 \\ &\quad \left. + \left( \frac{5}{36} - \frac{\pi^2}{3} - \frac{5}{3} \ln \rho \right) \rho^6 + \left( \frac{65}{72} - \frac{5}{6} \ln \rho \right) \rho^8 + \mathcal{O}(\rho^{10}) \right]. \end{aligned} \quad (6.15)$$

## 6.4 Two-gluon corrections

The second order correction  $X_2$  may be written as a sum of finite, gauge-invariant combinations:

$$X_2 = C_F (T_R N_L X_L + T_R N_H X_H + T_R N_C X_C + C_F X_A + C_A X_{NA}). \quad (6.16)$$

$N_L$  represents the number of massless quarks (3 in this context), while  $N_H$  and  $N_C$  label the contributions of  $b$ - and  $c$ -quarks, respectively. The top quark contribution is suppressed by  $(m_b/m_t)^2$  and we neglect it. In  $SU(3)$ , the color factors are  $T_R = \frac{1}{2}$ ,  $C_F = \frac{4}{3}$ , and  $C_A = 3$ .

### Renormalization contributions

To obtain the  $\mathcal{O}(\alpha_s^2)$  corrections, we need to consider several insertions of constants into the tree-level and one-loop diagrams. First, we can apply  $\mathcal{O}(\alpha_s^2)$  renormalization constants to the tree-level diagram; next, we should consider  $\mathcal{O}(\alpha_s)$  renormalization of  $\mathcal{O}(\alpha_s)$  diagrams; and finally, we need to apply  $\mathcal{O}(\alpha_s)$

renormalization to  $\mathcal{O}(\alpha_s)$  renormalization of tree-level diagrams. Since  $\mathcal{O}(\alpha_s^2)$  renormalization includes diagrams with  $c$ -quark and  $b$ -quark loop insertions in the gluon propagator, the corresponding constants develop dependence on  $\rho$ . For mass and wave function renormalization, we use the  $\rho$ -expansion of the exact on-shell constants [85, 86, 87]. Extending Eq. 6.14, the  $b$ -quark wave function renormalization constant is

$$\begin{aligned}
\text{WF} &= 1 - C_F \left( \frac{\alpha_s}{\pi} \frac{\mathcal{F}}{m_b^{2\epsilon}} \right) \left\{ \frac{3}{4\epsilon} + 1 + 2\epsilon \right\} + C_F \left( \frac{\alpha_s}{\pi} \frac{\mathcal{F}}{m_b^{2\epsilon}} \right)^2 \times \\
&\times \left\{ C_F \left( \frac{9}{32\epsilon^2} + \frac{51}{64\epsilon} - \frac{13\pi^2}{16} + \frac{433}{128} - \frac{3\zeta_3}{2} + \pi^2 \ln 2 \right) \right. \\
&+ C_A \left( -\frac{11}{32\epsilon^2} - \frac{101}{64\epsilon} + \frac{5\pi^2}{16} - \frac{803}{128} + \frac{3\zeta_3}{4} - \frac{\pi^2 \ln 2}{2} \right) \\
&+ T_{RN_L} \left( \frac{1}{8\epsilon^2} + \frac{9}{16\epsilon} + \frac{\pi^2}{12} + \frac{59}{32} \right) + T_{RN_H} \left( \frac{1}{4\epsilon^2} + \frac{19}{48\epsilon} - \frac{\pi^2}{3} + \frac{1139}{288} \right) \\
&+ T_{RN_C} \left( \frac{1}{4\epsilon^2} + \frac{19}{48\epsilon} - \frac{1}{2\epsilon} \ln \rho + \frac{635}{288} + \frac{\pi^2}{12} + \frac{2}{3} \ln \rho + \ln^2 \rho \right. \\
&\quad \left. - \frac{3\pi^2}{8} \rho + 3\rho^2 - \frac{5\pi^2}{8} \rho^3 + \left[ \frac{125}{48} + \frac{\pi^2}{4} - \frac{11}{4} \ln \rho + \frac{3}{2} \ln^2 \rho \right] \rho^4 \right. \\
&\quad \left. + \left[ \frac{8}{15} \ln \rho - \frac{11}{25} \right] \rho^6 + \left[ \frac{9}{56} \ln \rho - \frac{1137}{15680} \right] \rho^8 + \mathcal{O}(\rho^{10}) \right\}, \tag{6.17}
\end{aligned}$$

the  $c$ -quark mass renormalization constant

$$\begin{aligned}
\text{MC}_c &= im_c C_F \left( \frac{\alpha_s}{\pi} \frac{\mathcal{F}}{m_c^{2\epsilon}} \right) \left\{ \frac{3}{4\epsilon} + 1 + 2\epsilon \right\} - im_c C_F \times \\
&\times \left( \frac{\alpha_s}{\pi} \frac{\mathcal{F}}{m_c^{2\epsilon}} \right)^2 \left\{ C_F \left( \frac{9}{32\epsilon^2} + \frac{45}{64\epsilon} + \frac{199}{128} - \frac{3\zeta_3}{4} + \frac{\pi^2 \ln 2}{2} - \frac{5\pi^2}{16} \right) \right. \\
&+ C_A \left( -\frac{11}{32\epsilon^2} - \frac{91}{64\epsilon} - \frac{605}{128} + \frac{3\zeta_3}{8} - \frac{\pi^2 \ln 2}{4} + \frac{\pi^2}{12} \right) \\
&+ T_{RN_L} \left( \frac{1}{8\epsilon^2} + \frac{7}{16\epsilon} + \frac{45}{32} + \frac{\pi^2}{12} \right) + T_{RN_C} \left( \frac{1}{8\epsilon^2} + \frac{7}{16\epsilon} + \frac{69}{32} - \frac{\pi^2}{6} \right) \\
&+ T_{RN_H} \left( \frac{1}{8\epsilon^2} + \frac{7}{16\epsilon} + \frac{103}{288} + \frac{13}{12} \ln \rho - \frac{1}{2} \ln^2 \rho \right. \\
&\quad \left. + \left[ \frac{19}{150} - \frac{2}{15} \ln \rho \right] \rho^2 + \left[ \frac{1389}{78400} - \frac{9}{280} \ln \rho \right] \rho^4 \right. \\
&\quad \left. + \left[ \frac{997}{198450} - \frac{4}{315} \ln \rho \right] \rho^6 + \left[ \frac{1229}{627264} - \frac{5}{792} \ln \rho \right] \rho^8 + \mathcal{O}(\rho^{10}) \right\}, \tag{6.18}
\end{aligned}$$

and the  $b$ -quark mass renormalization constant

$$\begin{aligned}
\text{MC}_b &= im_b C_F \left( \frac{\alpha_s \mathcal{F}}{\pi m_b^{2\epsilon}} \right) \left\{ \frac{3}{4\epsilon} + 1 + 2\epsilon \right\} - im_b C_F \times \\
&\times \left( \frac{\alpha_s \mathcal{F}}{\pi m_b^{2\epsilon}} \right)^2 \left\{ C_F \left( \frac{9}{32\epsilon^2} + \frac{45}{64\epsilon} + \frac{199}{128} - \frac{3\zeta_3}{4} + \frac{\pi^2 \ln 2}{2} - \frac{5\pi^2}{16} \right) \right. \\
&+ C_A \left( -\frac{11}{32\epsilon^2} - \frac{91}{64\epsilon} - \frac{605}{128} + \frac{3\zeta_3}{8} - \frac{\pi^2 \ln 2}{4} + \frac{\pi^2}{12} \right) \\
&+ T_{RN_L} \left( \frac{1}{8\epsilon^2} + \frac{7}{16\epsilon} + \frac{45}{32} + \frac{\pi^2}{12} \right) + T_{RN_H} \left( \frac{1}{8\epsilon^2} + \frac{7}{16\epsilon} + \frac{69}{32} - \frac{\pi^2}{6} \right) \\
&+ T_{RN_C} \left( \frac{1}{8\epsilon^2} + \frac{7}{16\epsilon} + \frac{45}{32} + \frac{\pi^2}{12} - \frac{\pi^2}{4} \rho + \frac{3}{2} \rho^2 - \frac{\pi^2}{4} \rho^3 \right. \\
&+ \left[ \frac{151}{144} + \frac{\pi^2}{12} - \frac{13}{12} \ln \rho + \frac{1}{2} \ln^2 \rho \right] \rho^4 + \left[ \frac{2}{15} \ln \rho - \frac{19}{150} \right] \rho^6 \\
&\left. + \left[ \frac{9}{280} \ln \rho - \frac{1389}{78400} \right] \rho^8 + \mathcal{O}(\rho^{10}) \right\}. \tag{6.19}
\end{aligned}$$

Finally, the charge renormalization constant (calculated in  $\overline{\text{MS}}$  scheme with five quark flavours) is

$$\text{PH} = 1 + \left( \frac{\alpha_s \mathcal{F}}{\pi m_b^{2\epsilon}} \right) \frac{1}{3\epsilon} \left\{ T_R(N_L + N_H + N_C) - \frac{11}{4} C_A \right\}. \tag{6.20}$$

## Quark loop contribution

The three diagrams in Fig. 6.6 with different quarks  $q$  in the loop represent relatively “simple” gauge-invariant quark-loop contributions. Integration over the momentum of  $q$  can be simplified by averaging in a  $(D - 1)$ -dimensional subspace orthogonal to gluon momentum. In addition, integrals proportional to the gauge parameter (for general gluon gauge) are simplified by cancellations between the numerator and denominator factors.

First, we consider the case when  $q$  represents massless quarks ( $u, d$ , and  $s$ ). Contributing regions in this case are determined in the same fashion as for the one-gluon correction. It is also possible to “promote” the corresponding two-scale topology to one of the more complicated topologies, corresponding to the “true” three-loop diagrams. This is done by inserting missing lines (with zero exponents) into 4-leg vertices and similar transformations. The simplicity of this particular type of integrals then provides useful cross-checks.

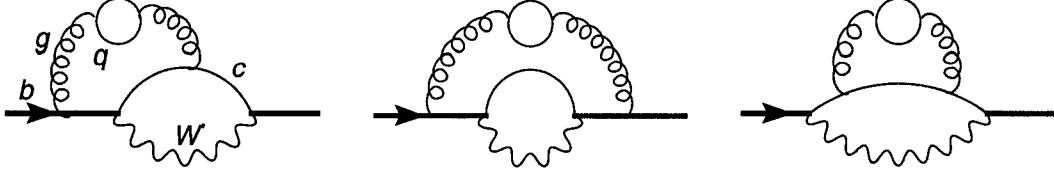


Figure 6.6: Quark loop contribution to  $b$ -decay at  $\mathcal{O}(\alpha_s^2)$

Combining the diagrams with the proper symmetry factors and renormalization contributions, the light quark contribution is

$$\begin{aligned}
X_L &= \zeta_3 + \frac{23\pi^2}{108} - \frac{4}{9} \\
&+ \left[ \frac{28}{9} - \zeta_3 - \frac{101\pi^2}{108} + \frac{13}{2} \ln \rho - 3 \ln^2 \rho \right] \rho^2 \\
&+ \left[ \frac{40}{9} - \zeta_3 + \frac{61\pi^2}{108} - \frac{47}{6} \ln \rho + 6 \ln^2 \rho \right] \rho^4 \\
&+ \left[ \zeta_3 - \frac{11\pi^2}{108} - \frac{1663}{324} + \frac{170}{27} \ln \rho - 3 \ln^2 \rho \right] \rho^6 \\
&+ \left[ \frac{4903}{5184} - \frac{5\pi^2}{108} - \frac{145}{216} \ln \rho \right] \rho^8 + \mathcal{O}(\rho^{10}).
\end{aligned} \tag{6.21}$$

Next, we evaluate diagrams in Fig. 6.6 with  $q$  being the  $b$ -quark. This case being significantly more complex, the result becomes

$$\begin{aligned}
X_H &= \frac{12991}{1296} - \frac{\zeta_3}{3} - \frac{53\pi^2}{54} \\
&+ \left[ \frac{\zeta_3}{3} + \frac{167\pi^2}{54} - \frac{205397}{6480} + \frac{13}{2} \ln \rho - 3 \ln^2 \rho \right] \rho^2 \\
&+ \left[ \frac{43334359}{1270080} + \frac{\zeta_3}{3} - \frac{175\pi^2}{54} - \frac{2323}{168} \ln \rho + 6 \ln^2 \rho \right] \rho^4 \\
&+ \left[ \frac{61\pi^2}{54} - \frac{\zeta_3}{3} - \frac{750684173}{57153600} + \frac{36079}{4536} \ln \rho - 3 \ln^2 \rho \right] \rho^6 \\
&+ \left[ \frac{54853471}{89812800} - \frac{3283}{6480} \ln \rho \right] \rho^8 + \mathcal{O}(\rho^{10}).
\end{aligned} \tag{6.22}$$

Finally, we evaluate the case with  $q$  being  $c$ -quarks. Four  $c$ -quark propagators result in up to seven contributing regions, some involving eikonal propagators.

These regions give rise to the terms with odd powers of  $\rho$ :

$$\begin{aligned}
 X_C = & \zeta_3 + \frac{23\pi^2}{108} - \frac{4}{9} - \frac{3}{4}\pi^2\rho & (6.23) \\
 & + \left[ \frac{65}{18} - \zeta_3 + \frac{133\pi^2}{108} + \frac{13}{2}\ln\rho - 3\ln^2\rho \right] \rho^2 - \frac{25}{18}\pi^2\rho^3 \\
 & + \left[ \frac{401}{72} - \zeta_3 - \frac{371\pi^2}{108} - \frac{101}{6}\ln\rho + 9\ln^2\rho \right] \rho^4 + \frac{59}{9}\pi^2\rho^5 \\
 & + \left[ \frac{97\pi^2}{108} - \frac{5941}{324} + \zeta_3 + \frac{707}{54}\ln\rho - 9\ln^2\rho \right] \rho^6 - \frac{107}{18}\pi^2\rho^7 \\
 & + \left[ \frac{116869}{8100} + \frac{229\pi^2}{108} + \frac{4379}{1080}\ln\rho - 7\ln^2\rho \right] \rho^8 + \frac{55}{36}\pi^2\rho^9 + \mathcal{O}(\rho^{10}).
 \end{aligned}$$

### Abelian contribution

The abelian diagrams (Fig. 6.7), proportional to the factor  $C_F^2$ , are the most difficult part of this calculation. Although some regions and topologies can be

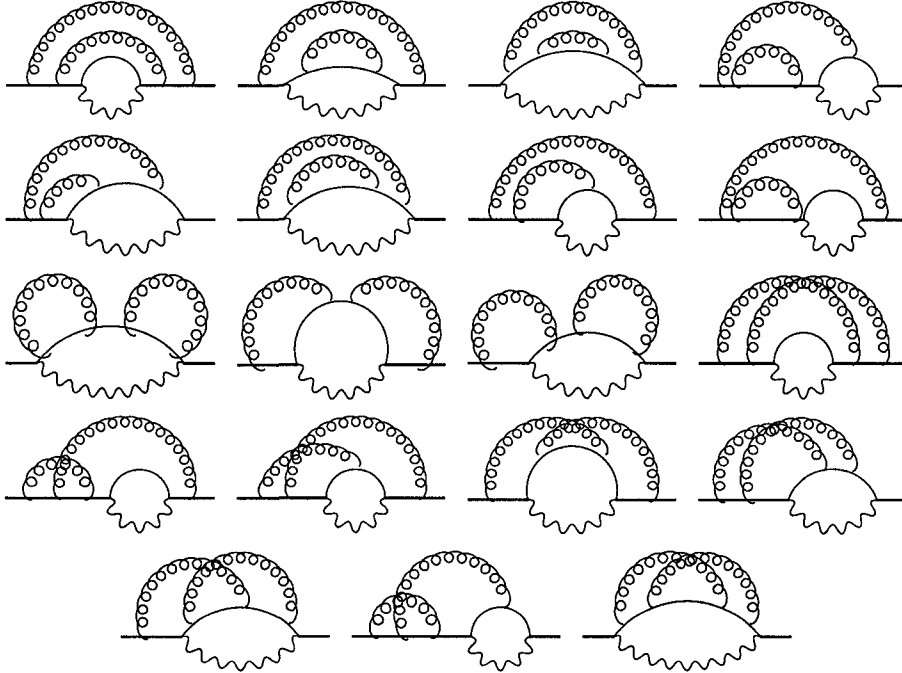


Figure 6.7: Abelian contributions to  $b$ -decay at  $\mathcal{O}(\alpha_s^2)$

used to evaluate quark loop contributions and thus be tested against alternative methods, the most difficult regions have no cross-checks, except for gauge invariance and cancellation of poles to all available orders.

Through expansions and tensor reduction all diagrams are expressed in terms of topologies for which the general solutions have been developed in Ref. [28]. In addition, for the most difficult three-loop non-planar topologies Laporta tables proved necessary to reduce the computation time. Also, one master integral (Eq. B.1) had to be evaluated in addition to those found in Ref. [28]. Finally, we obtain one of the most significant results of this thesis:

$$\begin{aligned}
X_A = & 5 - \frac{53\zeta_3}{8} - \frac{119\pi^2}{48} + \frac{19\pi^2 \ln 2}{4} - \frac{11\pi^4}{720} & (6.24) \\
& + \left[ \frac{37\pi^4}{360} + \left( \pi^2 - \frac{75}{8} \right) \ln \rho - \frac{27}{2} \ln^2 \rho + \frac{151\zeta_3}{8} \right. \\
& \quad \left. - \frac{315}{8} + \frac{497\pi^2}{48} - \frac{57\pi^2 \ln 2}{4} \right] \rho^2 - \frac{4}{3} \pi^2 \rho^3 \\
& + \left[ \frac{653}{12} + \left( \frac{161\pi^2}{24} - \frac{49}{2} \right) \ln \rho + 18 \ln^2 \rho - \frac{\zeta_3}{8} \right. \\
& \quad \left. - \frac{281\pi^2}{32} + \frac{57\pi^2 \ln 2}{4} - \frac{97\pi^4}{720} \right] \rho^4 - \frac{12}{5} \pi^2 \rho^5 \\
& + \left[ \frac{269\pi^2}{108} - \frac{41827}{2400} + \left( \frac{5929}{360} - \frac{277\pi^2}{72} \right) \ln \rho - \frac{151}{18} \ln^2 \rho \right. \\
& \quad \left. - \frac{191\zeta_3}{24} - \frac{19\pi^2 \ln 2}{4} - \frac{91\pi^4}{360} \right] \rho^6 + \frac{224}{45} \pi^2 \rho^7 \\
& + \left[ \frac{25\zeta_3}{12} - \frac{5666953}{25401600} \left( \frac{3\pi^2}{8} - \frac{29411}{7560} \right) \ln \rho - \frac{5}{8} \ln^2 \rho - \frac{43\pi^2}{54} \right] \rho^8 \\
& + \frac{32}{75} \pi^2 \rho^9 + \mathcal{O}(\rho^{10}).
\end{aligned}$$

## Non-abelian contribution

The last class is pure QCD contributions, proportional to  $C_F C_A$ : diagrams, involving triple-gluon vertices and ghost loops. Although some new topologies have to be considered, the most complicated integrals are already solved in

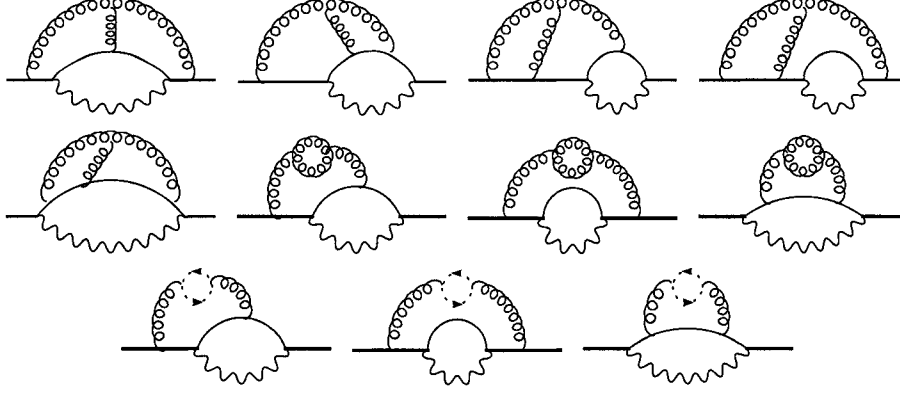


Figure 6.8: Non-abelian contributions to  $b$ -decay at  $\mathcal{O}(\alpha_s^2)$

the abelian contribution, and the result is

$$\begin{aligned}
X_{NA} = & \frac{521}{576} + \frac{9\zeta_3}{16} + \frac{505\pi^2}{864} - \frac{19\pi^2 \ln 2}{8} + \frac{11\pi^4}{1440} \\
& + \left[ \frac{57\pi^2 \ln 2}{8} - \frac{2315}{576} - \frac{185}{8} \ln \rho + \frac{33}{4} \ln^2 \rho - \frac{107\zeta_3}{16} \right. \\
& \quad \left. - \frac{2119\pi^2}{864} - \frac{\pi^4}{144} \right] \rho^2 + \frac{2}{3} \pi^2 \rho^3 \\
& + \left[ \frac{9\pi^4}{160} - \frac{18461}{576} + \left( \frac{1589}{48} - \frac{43\pi^2}{16} \right) \ln \rho - \frac{33}{2} \ln^2 \rho \right. \\
& \quad \left. + \frac{45\zeta_3}{16} + \frac{7399\pi^2}{1728} - \frac{57\pi^2 \ln 2}{8} \right] \rho^4 + \frac{6}{5} \pi^2 \rho^5 \\
& + \left[ \frac{136319}{8100} + \left( \frac{253\pi^2}{144} - \frac{35207}{2160} \right) \ln \rho + \frac{71}{12} \ln^2 \rho + \frac{59\zeta_3}{48} \right. \\
& \quad \left. - \frac{697\pi^2}{432} + \frac{19\pi^2 \ln 2}{8} + \frac{67\pi^4}{720} \right] \rho^6 - \frac{112}{45} \pi^2 \rho^7 \\
& + \left[ \left( \frac{48023}{20160} - \frac{13\pi^2}{48} \right) \ln \rho - \frac{19}{36} \ln^2 \rho - \frac{25\zeta_3}{24} \right. \\
& \quad \left. + \frac{547\pi^2}{864} - \frac{53113447}{50803200} \right] \rho^8 - \frac{16}{75} \pi^2 \rho^9 + \mathcal{O}(\rho^{10}).
\end{aligned} \tag{6.25}$$

## 6.5 Applications of the result

Fig. 6.9 illustrates the existing second-order QCD corrections [88, 89, 90] to semi-leptonic quark decays in various kinematic configurations. The dashed arrow shows the expansion presented in this chapter. Previously published expansions are indicated with solid arrows. The integral over the dotted line

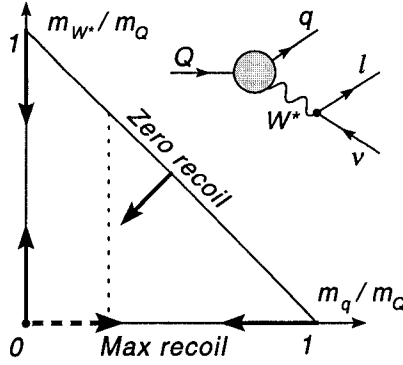


Figure 6.9:  $\mathcal{O}(\alpha_s^2)$  mass expansions of the semi-leptonic heavy quark decay rate  $\Gamma(Q \rightarrow q\ell\bar{\nu})$  in various kinematic limits. Allowed kinematic configurations are inside the triangle. On the lower side, recoil momentum of  $q$  is the largest.

(equivalent to integration over the leptonic phase space in the decay  $b \rightarrow c\ell\bar{\nu}_\ell$ ) corresponds to the complete semi-leptonic result of the following chapter. Analytic expressions are known along the zero recoil line and in all the corners of the triangle.

Our results may be directly compared to the expansions around  $\rho = 1$  [88] as follows ( $\Delta_{L,H,F,A}$  are defined in that reference, and  $\delta = 1 - \rho$ ):

$$\begin{aligned} X_{L,C,A}(\rho) &\leftrightarrow \delta^3 \Delta_{L,C,F}(\delta), \quad X_H(\rho) \leftrightarrow \delta^3 [\Delta_H(\delta) - \Delta_C(\delta)], \quad (6.26) \\ X_{NA}(\rho) &\leftrightarrow \delta^3 [\Delta_A(\delta) - \Delta_F(\delta)/2]. \end{aligned}$$

Here we use the unpublished result of Ref. [88], which in that reference was lumped together with  $\Delta_H$ :

$$\begin{aligned} \Delta_C &= \frac{230}{9} - \frac{8\pi^2}{3} + \left[ \frac{22\pi^2}{3} - 69 \right] \delta + \left[ \frac{15005}{162} - \frac{262\pi^2}{27} \right] \delta^2 \quad (6.27) \\ &+ \left[ \frac{695\pi^2}{108} - \frac{91051}{1620} - \frac{32}{9} \ln 2\delta \right] \delta^3 + \left[ \frac{1517}{405} - \frac{77\pi^2}{135} \right] \delta^4 \\ &+ \left[ \frac{1002319}{56700} - \frac{3751\pi^2}{2160} - \frac{88}{135} \ln 2\delta \right] \delta^5 + \left[ \frac{13033\pi^2}{15120} - \frac{60481}{7560} \right. \\ &\quad \left. - \frac{88}{135} \ln 2\delta \right] \delta^6 + \left[ \frac{2773441}{1587600} - \frac{493\pi^2}{3780} - \frac{586}{945} \ln 2\delta \right] \delta^7 \\ &+ \left[ \frac{140572}{297675} - \frac{2\pi^2}{405} - \frac{556}{945} \ln 2\delta \right] \delta^8 + \mathcal{O}(\delta^9). \end{aligned}$$



The plots in Fig. 6.10 present  $X_L$ ,  $X_H$ ,  $X_C$ ,  $X_A$ , and  $X_{NA}$  calculated to  $\mathcal{O}(\rho^{10})$ , and the expansions of the corresponding functions from Ref. [88] (Eq. (A1) of that work), according to Eq. 6.26, calculated through  $\mathcal{O}((1-\rho)^{21})$ . To better illustrate the behaviour of these corrections near  $\rho = 1$ , where the decay is suppressed by the phase space volume, we normalize all plots by  $(1-\rho)^3$ . As expected, the  $c$ -quark contribution  $X_C$  interpolates between heavy ( $X_H$ ) and light ( $X_L$ ) quark contributions.

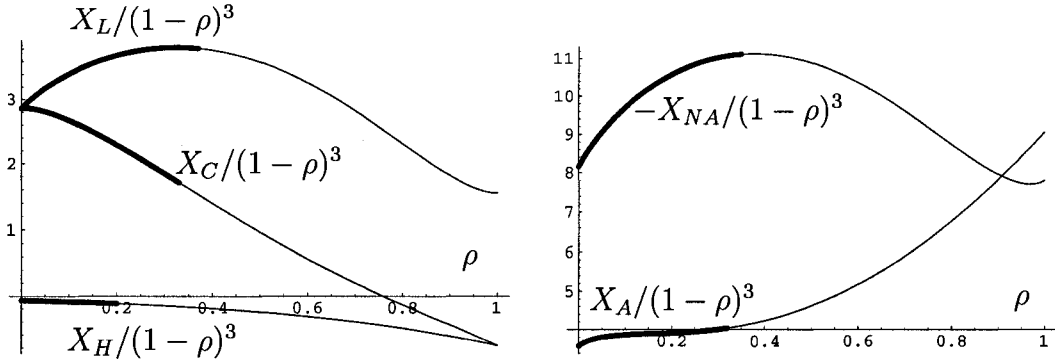


Figure 6.10: Matching of expansions around  $\rho = 0$  (thick line) and  $\rho = 1$  (thin line) for maximum quark recoil,  $M_{W^*} = 0$ . Matching point corresponds to the smallest difference between the two approximations.

For convenience we present results for a numerical fit providing accuracy better than 0.01 for  $X_L$ ,  $X_C$ ,  $X_A$ , and  $X_{NA}$ , and better than  $10^{-5}$  for  $X_H$  for  $0 \leq \rho \leq 1$  (terms proportional to  $\sqrt{\rho}$  are introduced for shorter expressions):

$$X_A/(1-\rho)^3 \approx 3.531 + 1.305\sqrt{\rho} + 0.1496\rho - 13.76\rho^2 + 49.64\rho^3 - 57.77\rho^4 + 33.69\rho^5 - 7.746\rho^6, \quad (6.28)$$

$$X_{NA}/(1-\rho)^3 \approx -8.090 - 1.696\sqrt{\rho} - 12.77\rho + 20.35\rho^2 + 8.257\rho^3 - 43.23\rho^4 + 58.52\rho^5 - 29.09\rho^6,$$

$$X_L/(1-\rho)^3 \approx 2.872 + 6.849\rho - 17.00\rho^2 + 22.56\rho^3 - 26.92\rho^4 + 13.16\rho^6,$$

$$X_H/(1-\rho)^3 \approx -0.06361 - 0.1902\rho - 0.2378\rho^2 - 0.1733\rho^3 - 0.09828\rho^4,$$

$$X_C/(1-\rho)^3 \approx 2.882 - 0.9432\rho - 14.31\rho^2 + 25.00\rho^3 - 18.49\rho^4 + 5.113\rho^5.$$

Together with zero-recoil [91, 92] and intermediate-recoil results [93], the

presented maximum-recoil corrections can be used to evaluate the integral over the dotted line in Fig. 6.9. The original attempt to perform this integration based on polynomial extrapolation [93], unfortunately, was prone to errors (see, e.g., Ref. [94]), but later calculations [95] demonstrate an excellent agreement with the results of the following chapter.

The importance of this calculation is not limited to this particular kinematic configuration. The techniques developed in this project (in addition to those described in Ref. [28]) have made possible the challenging calculation of the following chapter – the total semi-leptonic  $b$ -quark decay rate. In particular, the good convergence of the series in Eqs. (6.21-6.25) justified the moderate (but still very challenging) expansion of the total semi-leptonic rate through  $\mathcal{O}((m_c/m_b)^7)$ . As in this calculation, this allows to reach the relative accuracy of 1% for the realistic value of  $m_c/m_b \approx 1/3$ .

# Chapter 7

## Semi-leptonic $b$ -quark decay and muon decay

Decays of heavy fermions are an abundant source of information about fundamental interactions. In particular, muon decay, insensitive to strong interactions, can be very precisely described by the electroweak model. The experiment MuLan at the Paul Scherrer Institute will likely measure the rate of the muon decay with an uncertainty better than 1 ppm and thus improve the determination of the Fermi constant  $G_F$  that describes the strength of the charged-current weak interaction [96]. Along with the fine structure constant  $\alpha$  and the  $Z$ -boson mass,  $G_F$  is one of the three pillars of electroweak Standard Model tests [97].

To match this experimental progress, both the rate [98] and the energy distribution [69] have been calculated in QED with  $\mathcal{O}(\alpha^2)$  accuracy. In the decay rate studies, the electron mass  $m_e$  was assumed negligible in the already small  $\mathcal{O}(\alpha^2)$  effects.

In this chapter, we show that the finite  $m_e$  effect decreases the muon decay rate by about half ppm, exceeding previous estimates [99] and approaching the expected MuLan precision.

The final-state fermion mass effects are much larger in the already discussed decay  $b \rightarrow c\ell\bar{\nu}$ . Studied in  $B$ -factories and the Tevatron, this process provides information about the Cabibbo-Kobayashi-Maskawa matrix element  $V_{cb}$ , as well as about parameters governing heavy-quark dynamics [100]. Also in this case, theoretical studies at  $\mathcal{O}(\alpha_s^2)$  are complete only for a massless final-state

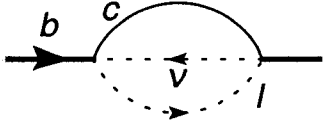


Figure 7.1: Diagram corresponding to the tree-level decay rate

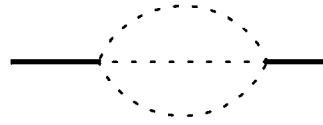


Figure 7.2: Region 1:  $q \sim m_b \gg m_c$

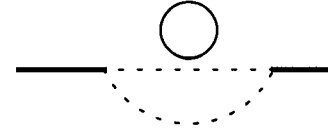


Figure 7.3: Region 2:  $q \sim m_c$

quark [101].

For the actual massive  $c$ -quark, the  $\mathcal{O}(\alpha_s^2)$  effects are known in some special cases of kinematics, as described in the end of the Chapter 6. The so-called Brodsky-Lepage-Mackenzie (BLM) corrections [102] (associated with the numerically large  $\beta_0$  value) have been obtained for the width [103], moments of the energy spectrum [104, 105], and triple differential distributions [106]. Also some logarithms of the mass  $m_c$  have been determined to all orders in  $\alpha_s$  [107]. Most recently, Melnikov calculated numerically the  $m_c$  effects for the width and the first two moments of the energy distribution of hadrons and of the charged lepton produced in this decay [94]. In this chapter we present the calculation of corresponding analytical results obtained (similarly to the previous chapter) as an expansion in powers and logarithms of  $\rho \equiv m_c/m_b$ .

This chapter starts with a brief description of the leading order and one-loop calculations. It continues with the discussion of the details of the two-loop calculation, and ends with presentation and a discussion of the new results [27].

## 7.1 Tree-level decay rate and first-order correction

The tree-level decay rate can be found by analogy with Eq. 6.13 as an imaginary part of a self-energy diagram in Fig. 7.1. Denominators of scalar integrals after the tensor reduction are  $D_1 = q^2 + m_c^2$ ,  $D_2 = l^2$ , and  $D_3 = (q + l + p)^2$ , where  $p$  is the incoming  $b$ -quark momentum ( $p^2 = -m_b^2$ ).

Expansion of the massive  $c$ -quark propagator  $D_1$  in small mass  $m_c$  as in Eq. 6.12 produces integrals such as in Fig. 7.2. Integration is then performed

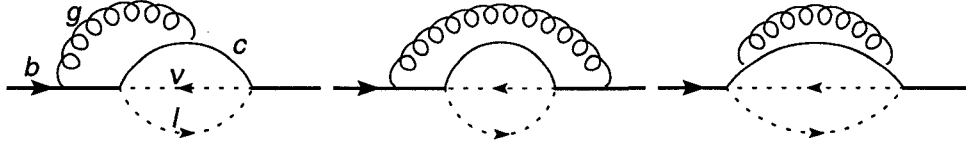


Figure 7.4: One-gluon corrections to the semi-leptonic decay rate

by successive application of Eq. A.2.

There is an additional contributing kinematic configuration. Setting the scale of loop momentum  $q \sim m_c$ , we expand  $D_3$ , obtaining the topology in Fig. 7.3. Eqs. A.1 and A.2 then lead to the result, which in combination with the first region reads

$$\begin{aligned} \Gamma^{(0)}(b \rightarrow cl\bar{\nu}) &= \Gamma_0 X_0, & \Gamma_0 &= \frac{G_F^2 |V_{cb}|^2 m_b^5}{192\pi^3}, \\ X_0 &= 1 - 8\rho^2 - 24\rho^4 \ln \rho + 8\rho^6 - \rho^8, \end{aligned} \quad (7.1)$$

and further QCD corrections can be parameterized as

$$\Gamma(b \rightarrow cl\bar{\nu}) = \Gamma_0 \left[ X_0 + C_F \frac{\alpha_s}{\pi} X_1 + C_F \left( \frac{\alpha_s}{\pi} \right)^2 X_2 + \dots \right]. \quad (7.2)$$

The one-gluon correction  $X_1$  corresponds to the three diagrams in Fig. 7.4. Belonging to the topology in Fig. 2.4 (with substitution of  $m_b$  and  $m_c$  instead of  $M$  and  $m$ ), they are treated according to the procedure outlined for the example of Eq. 2.19. Complete with the mass and wave function counter-terms as in Fig. 7.5 (with constants defined in Eq. 6.14), the first-order correction is

$$\begin{aligned} X_1 &= \frac{25}{8} - \frac{\pi^2}{2} - (34 + 24 \ln \rho) \rho^2 + 16\pi^2 \rho^3 \\ &\quad - \left( \frac{273}{2} - 36 \ln \rho + 72 \ln^2 \rho + 8\pi^2 \right) \rho^4 + 16\pi^2 \rho^5 \\ &\quad - \left( \frac{526}{9} - \frac{152}{3} \ln \rho \right) \rho^6 + \dots \end{aligned} \quad (7.3)$$

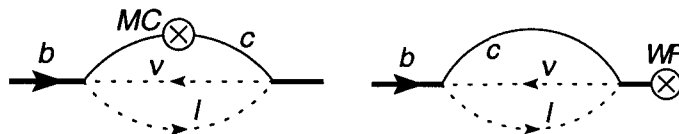


Figure 7.5: Wave function and mass renormalization contributions

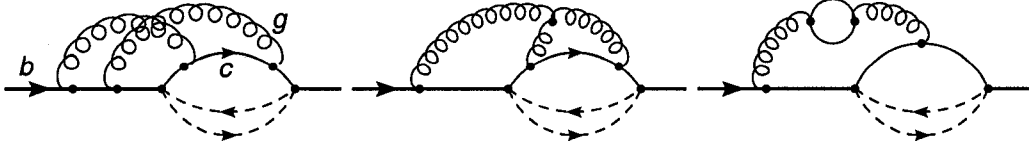


Figure 7.6: Examples of  $\mathcal{O}(\alpha_s^2)$  diagrams

Similarly to Eq. 6.16, the two-loop correction splits into independent parts:

$$X_2 = T_R N_L X_L + T_R N_H X_H + T_R N_C X_C + C_F X_A + C_A X_{NA}. \quad (7.4)$$

## 7.2 Calculation of two-loop corrections

Renormalization at the two-loop level is done similarly to the maximum-recoil case. The 39 diagrams (analogous to those in Figs. 6.6, 6.7, and 6.8), some of which are shown in Fig. 7.6, belong to ten independent double-scale topologies. Each topology is expanded in all asymptotic regions (an example of such expansions is shown in Fig. 7.7), and the results are added together to produce the finite corrections. The  $m_c = 0$  expressions for all diagrams were obtained in Refs. [99, 101], allowing the direct cross-check of the most difficult “hard” regions (such as Fig. 7.7(b)). Expanded in  $\rho$ , those regions required weeks

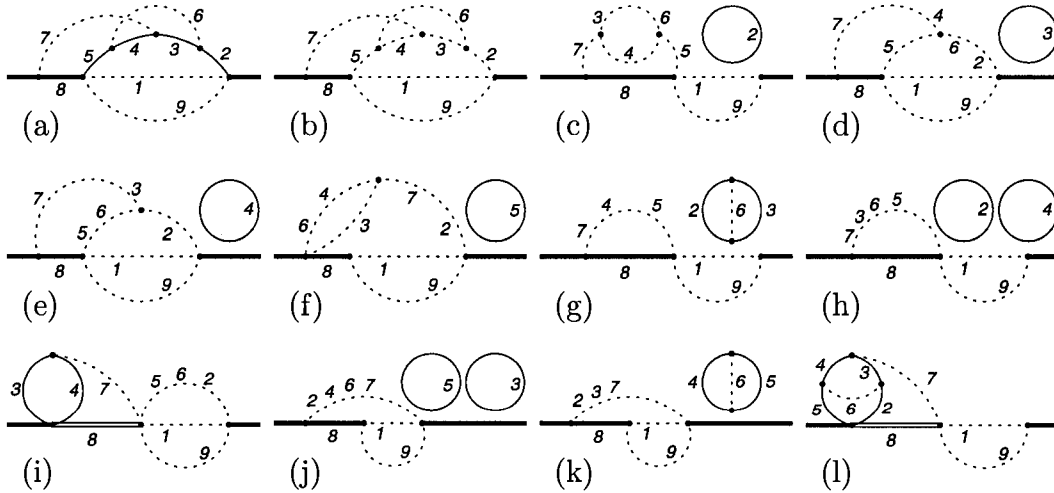


Figure 7.7: Expansion of a double-scale topology (a) in all contributing asymptotic regions (b-l). Thick lines represent mass  $m_b$ , thin – mass  $m_c$ , dashed lines are massless, double lines correspond to eikonal propagators.

of Laporta reduction to obtain terms through  $\mathcal{O}(\rho^6)$ . Eikonal regions (such as Fig. 7.7(i,l)), contributing to odd powers of the  $\rho$ -expansion, were evaluated through  $\mathcal{O}(\rho^7)$ , resulting in better than one percent accuracy near the physical value of  $\rho \sim 0.3$ . Three-loop eikonal integrals of topologies Eqs. B.44 and B.45 (e.g., Fig. 7.7(1)) were also reduced with Laporta technique, and the corresponding master integrals were found in Refs. [62, 108, 109].

One technical difficulty appearing in the factorized regions is complicated tensor reduction in the four-loop case. Consider the topology in Fig. 7.7, and its expansion in the case when  $p_3$  and  $p_7$  (momenta flowing through lines 3 and 7) are both “soft” (at the scale  $m_c$ ), as in Fig. 7.7(i). To disentangle the products of loop momenta  $p_3, p_7$  with the remaining loop momenta  $p_1, p_9$  one needs to average over the directions of a *pair* of momenta preserving their relative angle in the subspace orthogonal to the third. Such reduction can be performed by the general formula [110] applied, e.g., to the pair of  $p_3$  and  $p_7$  in  $(D-1)$ -dimensional subspace orthogonal to  $p_0$  (the external momentum). However, the complexity of this operation grows fast due to multiple nested expansions in terms of traceless tensors and Gegenbauer polynomials, considerably limiting the available  $\rho$ -expansion depth.

Instead, in every such case it was possible to average in sequence over the directions of a *single* momentum in a  $(D-1)$ -dimensional subspace. For the example of Fig. 7.7(i), we first average  $p_3$  in the subspace orthogonal to  $p_7$ ; after that,  $p_7$  is averaged in subspace orthogonal to  $p_0$  but in such a way that the powers of product  $p_3 p_7$  are not effected. Being somewhat less computationally intensive, this procedure allowed to extend the expansion through  $\mathcal{O}(\rho^7)$ .

The computational resources used by the steps above are considerable but not at the limit of present capacity: Laporta reduction required two weeks of parallel computations on a cluster with Opteron processors, occupying at most 10 GB of RAM at each machine, and FORM [111] manipulations with Feynman diagrams (taking a few days) were limited by the available disk space, with temporary files growing as large as 200 GB at intermediate stages.

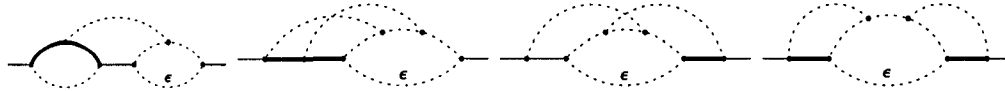


Figure 7.8: Double-scale topologies with artificial large mass  $1/x$  (thick lines), unit mass (thin solid lines), and massless propagators (dashed lines).  $\epsilon$  denotes non-integer propagator power from integration of a massless sub-loop.

### 7.3 Evaluation of master integrals

The integrals appearing in the “hard” regions belong to the topologies in Eqs. B.2–B.10. Their master integrals, identified through Laporta reduction, are closely related to those in Ref. [99]. In addition to  $\mathcal{O}(\rho^0)$  answer calculated in that reference, the expressions presented there are sufficient to obtain the  $\mathcal{O}(\rho^2)$  terms, but the following  $\mathcal{O}(\rho^4)$  contribution required further terms in  $\epsilon$ -expansion of the most difficult integrals.

To calculate the needed terms, the differential equations method was applied to the four double-scale topologies in Fig. 7.8, where the thick line corresponds to artificial large mass  $1/x$  introduced in such a way that differential equations on  $x$  could be solved in terms of harmonic polylogarithms. The treatment of the rightmost topology was discussed in detail in Section 5.3.

As a result of solving the system of equations, all master integrals of those topologies were found as explicit functions of  $x$ . As a boundary condition, asymptotic expansions of integrals near  $x \rightarrow 0$  were used, and the needed on-shell expressions were found in the limit  $x \rightarrow 1$ . These results are presented in Appendix B to the order needed for the calculation.

### 7.4 Integrated decay rate

The (rather lengthy) expressions for  $X_L$ ,  $X_H$ ,  $X_C$ ,  $X_A$ , and  $X_N$  are presented in Eqs. C.1–C.5 and plotted in Fig. 7.9 as functions of  $\rho$ . Gauge-independence of these results is ensured by the cancellation of the general gauge parameter in the final expressions.

The definitive cross-check can be made with the results of Ref. [94], where



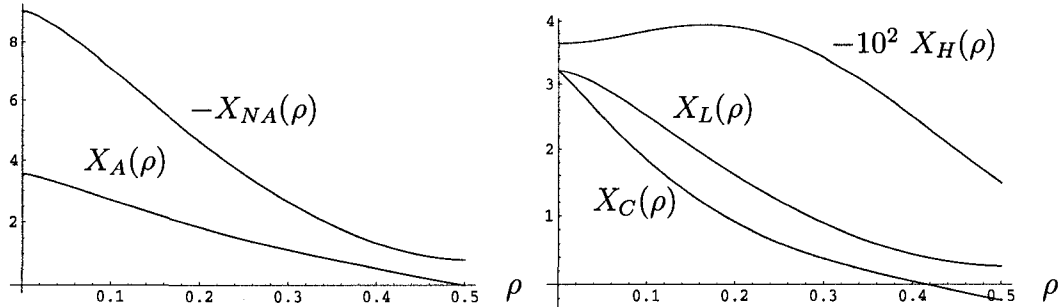


Figure 7.9: Mass-dependent corrections to  $X_2$  of Eq. 7.4.

$X_2$  was computed for  $\rho = 0.25$  by the method of sector decomposition. Numerically, the agreement is at the level 0.1%, which is well within the accuracy of both results.

Further, Ref. [107] presents a renormalization group analysis of the structure of some logarithmic terms, re-summed to all orders on  $\alpha_s$ . At the order  $\mathcal{O}(\alpha_s^2)$ , this reference predicted the coefficients in  $X_2$  of terms  $\rho^2 \ln^2 \rho$ ,  $\rho^4 \ln^3 \rho$ , and  $\rho^3 \ln \rho$ . The logarithms in  $\rho^2$  term were shown to appear from the running of the  $c$ -quark mass, and those in  $\rho^4$  term – from a mixture of dimension seven operators. Our results completely agree with those predictions.

However, we find a different origin of the  $\rho^3$  term. In [107], it was attributed to the running of  $m_c$ , with the resulting coefficient different from ours. To understand the origin of this difference, let us consider the four-quark operator  $\mathcal{O} = \bar{h}_b h_b \bar{c} \Gamma c$ . In the context of the Operator Product Expansion framework used in Ref. [107], it connects the  $c$ -quark field with  $h_b$ , a static field of a slow-moving quark (an eikonal line in the language of asymptotic expansions).

In the toy model with a *vector* weak coupling of quarks ( $\sim \gamma_\mu$ ), this operator

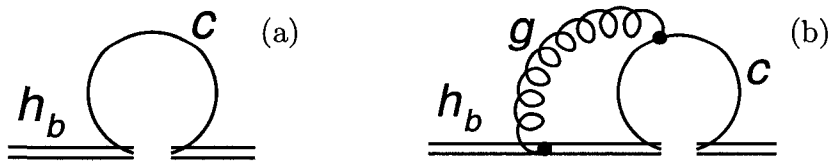


Figure 7.10: Tree-level and  $\mathcal{O}(\alpha_s)$  matrix elements of the four-quark operator

has  $\Gamma = 1$ , and its tree-level matrix element in Fig. 7.10(a) gives rise to the  $\rho^3$  terms in the tree-level width (Eq. C.31).

In the physical case of *chiral* weak couplings ( $\sim \gamma_\mu(1 - \gamma_5)$ ), the insertion in  $\mathcal{O}$  becomes  $\Gamma = \gamma_\mu v^\mu$  (where  $v^\mu$  is the velocity of the  $b$ -quark), and the matrix element in Fig. 7.10(a) vanishes. This explains the absence of cubic terms in Eq. 7.1. Due to this fact, Ref. [107] neglects the evolution of the operator  $\mathcal{O}$ .

However, at the order  $\mathcal{O}(\alpha_s)$  there is a non-zero matrix element shown in Fig. 7.10(b), and it leads to the  $\rho^3$  term in Eq. 7.3. The anomalous dimension of this operator and running of the coupling constant then generate the contribution in  $X_2$  proportional to  $\rho^3 \ln \rho$  which agrees with our result.

The linear term  $-\frac{5}{4}\pi^2\rho$  in Eq. C.2, related to diagrams such as the right-most graph in Fig. 7.6, is noteworthy. It originates from the region where the momenta in the  $c$ -quark loop are at the scale  $m_c$ , and the heavy propagator becomes eikonal. Obviously, this perturbative description becomes invalid for  $m_c \leq \Lambda_{QCD}$ , and such effects have to be included in the definition of the  $b$ -quark mass. Indeed, when a short-distance mass definition (e.g.,  $\overline{\text{MS}}$ ) is adopted instead of the pole mass scheme (which has to be done before application to phenomenology), that term gets absorbed into the tree-level rate.

Finally, the results can be transformed into QED. By substitutions  $\alpha_s = \alpha$ ,  $C_F = |V_{cb}| = T_R = N_H = N_C = 1$ ,  $C_A = N_L = 0$ , and  $m_b = m_\mu$ ,  $m_c = m_e$ , the expressions describe electron mass effects on  $\mathcal{O}(\alpha^2)$  corrections to the muon decay rate,  $\Gamma(\mu \rightarrow e\nu\bar{\nu})$ . In QED, the perturbative expansion is valid at any scale, and pole masses are traditionally used, thus the mass definition need not be changed. Together with the large logarithms, the above mentioned linear term then leads to a 0.43 ppm correction to the muon lifetime, which is in contrast to the previous estimate of those effects as  $(\frac{\alpha}{\pi})^2 \left(\frac{m_e}{m_\mu}\right)^2 \ln^2\left(\frac{m_e}{m_\mu}\right)^2 \sim 10^{-8}$  given in Ref. [99]. Since modern experiments, such as MuLan [96], expect an accuracy below 1 ppm in measuring the muon lifetime, this correction may influence the measured value of the Fermi constant  $G_F$ .

## 7.5 Moments of distributions and axial current

In addition to the integrated decay rate, precision fits to experimental data are done for the moments of the lepton energy  $E_l$  and the hadronic system energy  $E_h$  distributions in the rest frame of the  $b$ -quark, with the goal of accurately measuring many parameters such as  $|V_{cb}|$ ,  $m_b$ , and the Wilson coefficients of non-perturbative operators. Through  $\mathcal{O}(\alpha_s^2)$ , the corrections to those quantities are

$$\int (E_l/m_b)^n d\Gamma = \Gamma_0 \left( L_0^{(n)} + C_F \left( \frac{\alpha_s}{\pi} \right) L_1^{(n)} + C_F \left( \frac{\alpha_s}{\pi} \right)^2 L_2^{(n)} \right), \quad (7.5)$$

and similarly for the moments of  $E_h$ , described by coefficients  $H_j^{(n)}$ . The average is taken over the whole phase space of decay products.

In addition to generally larger expressions and longer computation times, one complication arising in evaluating the moments is the proper treatment of  $\gamma_5$ . With the introduction of powers of  $E_l = p_l p_l / m_b$  in Eq. 6.3, the integration over the lepton phase space produces a tensor  $T^{\mu\nu}$  which is no longer symmetric as in Eq. 6.4. Traces with  $\gamma_5$  then produce antisymmetric tensors that contribute to the result, invalidating the simple recipe of Sec. 6.2.

A self-consistent treatment of anti-symmetric objects in non-integer number of dimensions has been suggested by Larin [112]. According to his prescription,  $\gamma_5$  in  $D$  dimensions has to be defined as

$$\gamma_5 = \frac{i}{4!} \epsilon^{\mu\nu\rho\sigma} \gamma_\mu \gamma_\nu \gamma_\rho \gamma_\sigma. \quad (7.6)$$

The four-dimensional Levi-Civita tensor  $\epsilon^{\mu\nu\rho\sigma}$  is then formally kept outside the regularized expression. Indices of gamma-matrices are assumed  $D$ -dimensional in the traces for the purpose of divergence cancellations, and contract with  $\epsilon$ -tensor after the limit  $D \rightarrow 4$  is taken.

Due to that definition,  $\gamma_5$  no longer anti-commutes with  $\gamma_\mu$ , and the axial current has to be anti-symmetrized explicitly as

$$J_A^\mu = \frac{1}{2} \bar{\psi} (\gamma^\mu \gamma_5 - \gamma_5 \gamma^\mu) \psi = \frac{i}{6} \epsilon^{\mu\nu\rho\sigma} \bar{\psi} \gamma_\nu \gamma_\rho \gamma_\sigma \psi. \quad (7.7)$$

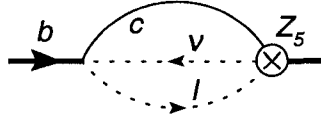


Figure 7.11: Renormalization contribution of the axial current

To restore the Ward identities which depend on anti-commutativity of  $\gamma_5$ ,  $J_A$  has to be renormalized. The corresponding constant in  $\overline{\text{MS}}$  scheme is

$$Z_A = 1 + C_F \left( \frac{\alpha_s}{\pi} \frac{\mathcal{F}}{m_b^{2\epsilon}} \right)^2 \frac{1}{\epsilon} \left\{ \frac{11}{24} C_A - \frac{1}{6} T_R (N_L + N_H + N_C) \right\} + \dots \quad (7.8)$$

Finally, to restore the renormalization scale independence of this current,  $J_A$  has to be supplemented with a finite renormalization constant

$$Z_5 = 1 - C_F \left( \frac{\alpha_s}{\pi} \frac{\mathcal{F}}{m_b^{2\epsilon}} \right) + C_F \left( \frac{\alpha_s}{\pi} \frac{\mathcal{F}}{m_b^{2\epsilon}} \right)^2 \times \left\{ \frac{11}{8} C_F - \frac{107}{144} C_A + \frac{1}{36} T_R (N_L + N_H + N_C) \right\} + \dots, \quad (7.9)$$

and the renormalized axial current becomes  $J_A^{\mu (R)} = Z_5 Z_A J_A$ , where  $J_A$  of Eq. 7.7 is calculated with bare quark field  $\psi$ .

According to this prescription, the one-gluon correction should include an additional renormalization term due to  $Z_5$  as in Fig. 7.11, where the blob denotes a four-point interaction of the axial current  $J_A$  with a regular ( $V - A$ ) lepton current. Combining all parts together, we reproduce the decay rate Eq. 7.3, and obtain moments  $L_{0,1}^{(1,2)}$  and  $H_{0,1}^{(1,2)}$  of Eqs. C.7 and C.19. The latter, of course, reproduce the expansion moments of the exactly known spectra at  $\mathcal{O}(\alpha_s)$  [113].

The second-order corrections need both  $Z_5$  and  $Z_A$ , inserted in four-fermion vertices of one-loop and two-loop diagrams, as well as in mass and wave function counter-terms. The resulting expressions for  $L_2^{(1,2)}$  and  $H_2^{(1,2)}$  are presented in Appendix C and are plotted in Fig. 7.12. They also very well agree with the numerical results of Ref. [94].

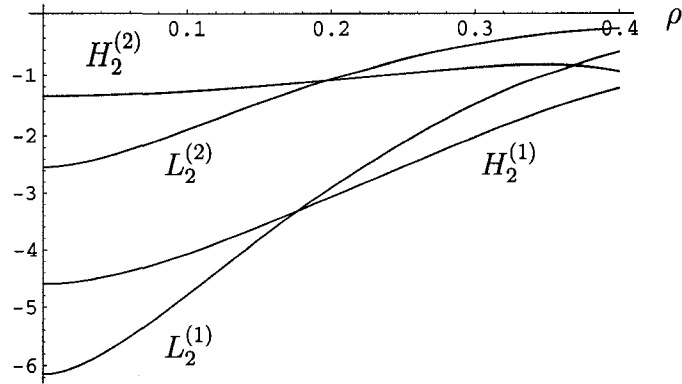


Figure 7.12: First two moments of lepton and hadron energy distributions

## 7.6 Charm mass in $b \rightarrow u$ decays and vector couplings

The calculational setup developed for this problem was used also for the two simpler, related calculations. In the first one, the left-handed coupling of quarks to a  $W$ -boson was substituted by a pure vector ( $\sim \gamma^\mu$ ) coupling. This is a useful toy model for the studies of angular distributions of the final particles [113] and the behavior of logarithms [107]. The results, parameterized similarly to  $X_2$ , are presented in Section C.4.

The second calculation is related to  $c$ -quark mass effects in the decay to massless quarks,  $b \rightarrow u\ell\bar{\nu}$ . A typical diagram describing such effects is shown in Fig. 7.13. The result, needed e.g. in  $b \rightarrow X_s\gamma$  studies [114], is presented in Section C.5.

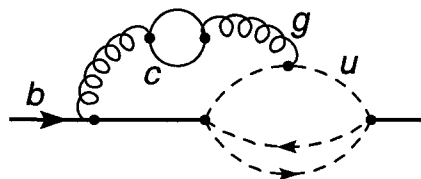


Figure 7.13: Charm contributions to semi-leptonic decay  $b \rightarrow u$

## 7.7 Conclusion: semi-leptonic results

The importance of the calculation in this chapter is twofold. First, there are direct phenomenological applications. In the determination of the Fermi constant  $G_F$  from the muon life time the correction found here amounts to about half a ppm shift. Another application is the determination of the CKM matrix element  $V_{cb}$  from a variety of measurements at the B-factories.

Previously, the fits used a combination of the BLM approximation [102] with a polynomial estimate of the remaining non-BLM corrections. Our results disagree with those predictions, which is due to a mistake in the extrapolating procedure as explained in [95]. Updating the fits may result in a shift of order one percent in the central value of  $|V_{cb}|$  found from inclusive decays  $B \rightarrow X_c \ell \bar{\nu}$ . With this correction, the value (presently  $|V_{cb}|^{incl} = (41.88 \pm 0.81) \cdot 10^{-3}$ , [115]) will move closer to the value measured in exclusive decays, such as  $B^- \rightarrow D^{*0} e^- \bar{\nu}_e$ , which is  $|V_{cb}|^{excl} = (39.0 \pm 0.6 \pm 2.0) \cdot 10^{-3}$  [116].

Second, the tools developed during this work and the better understanding of the subtleties of higher-order calculations may allow the pursuit of more challenging and urgent goals. Of particular importance are the four-loop self-energy functions, needed for mass renormalization constants at NNNLO.

# Chapter 8

## Conclusion

In this thesis, we demonstrated several contemporary calculational techniques in Quantum Field Theory and their application to outstanding physical problems. After the introduction and motivation for this work in Chapter 1, in Chapter 2 we described the framework of effective field theories. A powerful leverage in problems with multiple energy scales, in loop calculations it is supplemented by the asymptotic expansion method (described further in that chapter) which allows to reduce the problem to single-scale integrals. Chapter 3 was devoted to recurrence relations between integrals. After showing a practical method capable of handling very large problems, alternative ideas were presented. Two numerical techniques to compute integrals after the reduction, sector decomposition and Mellin-Barnes transformation, were discussed in Chapter 4. The relatively novel method of differential equations, capable of producing analytical results, was the focus of Chapter 5.

These methods were applied to the two challenging problems, providing accurate analytic solutions which improved upon the existing answers or corrected errors in them.

Chapter 6 presented the two-gluon corrections to general weak decay of a heavy to a light quark in the limit of the maximum allowed recoil momentum of the light quark. Applicable to the experimentally well-studied decay of a  $b$ -quark to a  $c$ -quark, this result complements and constrains the results of other calculations, improving also the knowledge of top quark decays and muon decays.

Developing further the tools created for that calculation and introducing new ones, the research project presented in Chapter 7 accomplished the challenging task of evaluating the second-order QCD corrections to the semi-leptonic decays, integrated over the phase space of leptons. Important for the precision measurements of fundamental constants, this result also gives an insight into the structure of certain terms to all orders in perturbation theory. The integrals solved during that project and the computer programs created will be useful for future calculations, including such distant areas as atomic physics and positronium spectra.

Future advances in calculations may come from various sources. At the implementation level, borrowing successful ideas from computer science already proved useful. Efficient use of parallel environments benefits computer algebra systems, such as ParFORM, TFORM, Mathematica, while novel fast polynomial algorithms leverage the Laporta method and Gröbner basis techniques. However, there is still a lot to borrow, e.g. the MapReduce paradigm in application to very large distributed calculations [117] (with a possible caveat that tuning the software built for very distant purposes may be a non-trivial task).

Opening the code to the public and collective work on core platforms (such as GiNaC [118]) may also provide the basis for general quality improvement of the calculational tools. Finally, automation of algorithms (such as asymptotic expansion [119]) may allow theorists to attack problems which are presently out of grasp due to very large number of diagrams and topologies.

To summarize, as we are becoming aware of the theoretical challenges the LHC era brings, we are also witnessing an exciting progress in precision calculations, giving hope that theory will pass this test.



# Bibliography

- [1] G. V. Chibisov, *Sov. Phys. Usp.* **19**, 624 (1976).
- [2] E. Adelberger, G. Dvali, and A. Gruzinov, *Phys. Rev. Lett.* **98**, 010402 (2007), hep-ph/0306245.
- [3] M. Gell-Mann, *Phys. Lett.* **8**, 214 (1964).
- [4] G. Zweig, *An  $SU(3)$  model for strong interaction symmetry and its breaking (2)*, CERN-TH-412 (1964).
- [5] D. J. Gross and F. Wilczek, *Phys. Rev. Lett.* **30**, 1343 (1973).
- [6] H. D. Politzer, *Phys. Rev. Lett.* **30**, 1346 (1973).
- [7] D. J. Gross and F. Wilczek, *Phys. Rev.* **D8**, 3633 (1973).
- [8] H. Fritzsche, M. Gell-Mann, and H. Leutwyler, *Phys. Lett.* **B47**, 365 (1973).
- [9] H. Fritzsche and P. Minkowski, *Ann. Phys.* **93**, 193 (1975).
- [10] E. D. Bloom *et al.*, *Phys. Rev. Lett.* **23**, 930 (1969).
- [11] M. Breidenbach *et al.*, *Phys. Rev. Lett.* **23**, 935 (1969).
- [12] G. Unal *et al.*, *Nucl. Phys. Proc. Suppl.* **39BC**, 343 (1995).
- [13] T. D. Lee and C.-N. Yang, *Phys. Rev.* **104**, 254 (1956).
- [14] C.-S. Wu, E. Ambler, R. W. Hayward, D. D. Hoppes, and R. P. Hudson, *Phys. Rev.* **105**, 1413 (1957).
- [15] S. L. Glashow, *Nucl. Phys.* **22**, 579 (1961).
- [16] S. Weinberg, *Phys. Rev. Lett.* **19**, 1264 (1967).
- [17] G. Arnison *et al.*, *Phys. Lett.* **B126**, 398 (1983).
- [18] K. Kodama *et al.*, *Phys. Lett.* **B504**, 218 (2001), hep-ex/0012035.
- [19] D. Hanneke, S. Fogwell, and G. Gabrielse, *Phys. Rev. Lett.* **100**, 120801 (2008), arXiv:0801.1134.

- [20] G. W. Bennett *et al.*, Phys. Rev. Lett. **92**, 161802 (2004), hep-ex/0401008.
- [21] T. P. Cheng and L. F. Li, *Gauge Theory of Elementary Particle Physics* (Clarendon, Oxford, UK, 1984).
- [22] M. E. Peskin and D. V. Schroeder, *An Introduction to quantum field theory* (Addison-Wesley, Reading, USA, 1995).
- [23] N. Cabibbo, Phys. Rev. Lett. **10**, 531 (1963).
- [24] M. Kobayashi and T. Maskawa, Prog. Theor. Phys. **49**, 652 (1973).
- [25] C. Amsler *et al.*, Phys. Lett. **B667**, 1 (2008).
- [26] A. Pak, I. Blokland, and A. Czarnecki, Phys. Rev. **D73**, 114009 (2006), hep-ph/0604233.
- [27] A. Pak and A. Czarnecki, Phys. Rev. Lett. **100**, 241807 (2008), arXiv:0803.0960.
- [28] I. Blokland, Ph.D. thesis, University of Alberta, 2004, UMI-NQ-95909.
- [29] J. Polchinski, *Effective field theory and the Fermi surface*, lectures given at TASI, 1992, hep-th/9210046.
- [30] D. B. Kaplan, *Effective field theories*, lectures given at 7th Summer School in Nuclear Physics Symmetries, 1995, nucl-th/9506035.
- [31] K. G. Wilson, Phys. Rev. **B4**, 3174 (1971).
- [32] V. A. Smirnov, Commun. Math. Phys. **134**, 109 (1990).
- [33] V. A. Smirnov, *Renormalization and asymptotic expansions* (Birkhaeuser, Basel, Switzerland, 1991), pp. 1–380.
- [34] K. G. Chetyrkin, Theor. Math. Phys. **75**, 346 (1988).
- [35] K. G. Chetyrkin, Theor. Math. Phys. **76**, 809 (1988).
- [36] F. V. Tkachov, Int. J. Mod. Phys. **A8**, 2047 (1993).
- [37] F. Tkachov, Sov. J. Part. Nucl. **25**, 649 (1994).
- [38] K. G. Chetyrkin and F. V. Tkachov, Phys. Lett. **B114**, 340 (1982).
- [39] K. G. Chetyrkin and V. A. Smirnov, Phys. Lett. **B144**, 419 (1984).
- [40] S. G. Gorishnii, S. A. Larin, F. V. Tkachov, and K. G. Chetyrkin, Phys. Lett. **B132**, 351 (1983).
- [41] H. Kleinert, J. Neu, V. Schulte-Frohlinde, K. G. Chetyrkin, and S. A. Larin, Phys. Lett. **B272**, 39 (1991), [Erratum-ibid. **B319** (1993) 545].
- [42] K. G. Chetyrkin, Phys. Lett. **B126**, 371 (1983).

- [43] V. A. Smirnov, Springer Tracts Mod. Phys. **177**, 1 (2002).
- [44] A. Czarnecki, A. Pak, and M. Slusarczyk, Acta Phys. Polon. **B36**, 3265 (2005).
- [45] A. Czarnecki and V. A. Smirnov, Phys. Lett. **B394**, 211 (1997), hep-ph/9608407.
- [46] Y. Nir, Phys. Lett. **B221**, 184 (1989).
- [47] G. 't Hooft and M. J. G. Veltman, Nucl. Phys. **B44**, 189 (1972).
- [48] F. V. Tkachov, Phys. Lett. **B100**, 65 (1981).
- [49] K. G. Chetyrkin and F. V. Tkachov, Nucl. Phys. **B192**, 159 (1981).
- [50] S. Laporta, Int. J. Mod. Phys. **A15**, 5087 (2000), hep-ph/0102033.
- [51] C. Anastasiou and A. Lazopoulos, JHEP **07**, 046 (2004).
- [52] A. V. Smirnov, *Algorithm FIRE – Feynman Integral REduction*, 2008, arXiv:0807.3243.
- [53] R. H. Lewis, *Fermat's User Guide*, <http://home.bway.net/lewis/>.
- [54] T. Gehrmann and E. Remiddi, Nucl. Phys. Proc. Suppl. **89**, 251 (2000).
- [55] C. Anastasiou, J. B. Tausk, and M. E. Tejeda-Yeomans, Nucl. Phys. Proc. Suppl. **89**, 262 (2000).
- [56] E. W. N. Glover and M. E. Tejeda-Yeomans, Nucl. Phys. Proc. Suppl. **89**, 196 (2000).
- [57] K. G. Chetyrkin, M. Faisst, C. Sturm, and M. Tentyukov, Nucl. Phys. **B742**, 208 (2006), hep-ph/0601165.
- [58] V. P. Gerdt, Nucl. Phys. Proc. Suppl. **135**, 232 (2004), hep-ph/0501053.
- [59] O. V. Tarasov, Acta Phys. Polon. **B29**, 2655 (1998), hep-ph/9812250.
- [60] B. Buchberger and F. Winkler, *Groebner bases and applications* (Cambridge University Press, Cambridge, UK, 1998).
- [61] A. V. Smirnov and V. A. Smirnov, *On the reduction of Feynman integrals to master integrals*, 2007, arXiv:0707.3993.
- [62] A. G. Grozin, A. V. Smirnov, and V. A. Smirnov, JHEP **11**, 022 (2006), hep-ph/0609280.
- [63] N. N. Bogolyubov and D. V. Shirkov, *Introduction to the theory of quantized fields*, Vol. 3 of *Intersci. Monogr. Phys. Astron.* (Interscience, New York, USA, 1959), pp. 1–720.
- [64] T. Binoth and G. Heinrich, Nucl. Phys. **B585**, 741 (2000), hep-ph/0004013.

- [65] T. Hahn, Nucl. Instr. Meth. **A559**, 273 (2006), hep-ph/0509016.
- [66] C. Bogner and S. Weinzierl, Comput. Phys. Commun. **178**, 596 (2008), arXiv:0709.4092.
- [67] C. Anastasiou, S. Beerli, and A. Daleo, JHEP **05**, 071 (2007), hep-ph/0703282.
- [68] C. Anastasiou, K. Melnikov, and F. Petriello, Phys. Rev. **D69**, 076010 (2004), hep-ph/0311311.
- [69] C. Anastasiou, K. Melnikov, and F. Petriello, JHEP **09**, 014 (2007), hep-ph/0505069.
- [70] V. A. Smirnov, Phys. Lett. **B460**, 397 (1999), hep-ph/9905323.
- [71] J. B. Tausk, Phys. Lett. **B469**, 225 (1999), hep-ph/9909506.
- [72] C. Anastasiou and A. Daleo, JHEP **10**, 031 (2006), hep-ph/0511176.
- [73] M. Czakon, Comput. Phys. Commun. **175**, 559 (2006), hep-ph/0511200.
- [74] J. Gluza, K. Kajda, and T. Riemann, Comput. Phys. Commun. **177**, 879 (2007), arXiv:0704.2423.
- [75] C. Bogner and S. Weinzierl, *Periods and Feynman integrals*, 2007, arXiv:0711.4863.
- [76] V. A. Smirnov, *Feynman integral calculus* (Springer, Berlin, Germany, 2006), pp. 1–283.
- [77] Z. Bern, L. J. Dixon, and D. A. Kosower, Phys. Lett. **B302**, 299 (1993), [Erratum-ibid. **B318**, 649 (1993)].
- [78] Z. Bern, L. J. Dixon, and D. A. Kosower, Nucl. Phys. **B412**, 751 (1994).
- [79] A. V. Kotikov, Phys. Lett. **B267**, 123 (1991).
- [80] E. Remiddi, Nuovo Cim. **A110**, 1435 (1997), hep-th/9711188.
- [81] E. Remiddi and J. A. M. Vermaseren, Int. J. Mod. Phys. **A15**, 725 (2000), hep-ph/9905237.
- [82] T. Gehrmann and E. Remiddi, Comput. Phys. Commun. **141**, 296 (2001), hep-ph/0107173.
- [83] T. Gehrmann and E. Remiddi, Comput. Phys. Commun. **144**, 200 (2002), hep-ph/0111255.
- [84] D. Maitre, Comput. Phys. Commun. **174**, 222 (2006), hep-ph/0507152.
- [85] D. J. Broadhurst, N. Gray, and K. Schilcher, Z. Phys. **C52**, 111 (1991).
- [86] K. Melnikov and T. van Ritbergen, Nucl. Phys. **B591**, 515 (2000), hep-ph/0005131.

- [87] T. van Ritbergen, J. A. M. Vermaseren, and S. A. Larin, Phys. Lett. **B400**, 379 (1997), hep-ph/9701390.
- [88] A. Czarnecki and K. Melnikov, Phys. Rev. **D56**, 7216 (1997), hep-ph/9706227.
- [89] I. Blokland, A. Czarnecki, M. Slusarczyk, and F. Tkachov, Phys. Rev. **D71**, 054004 (2005), hep-ph/0503039.
- [90] A. Czarnecki and K. Melnikov, Phys. Rev. Lett. **88**, 131801 (2002), hep-ph/0112264.
- [91] A. Czarnecki, Phys. Rev. Lett. **76**, 4124 (1996), hep-ph/9603261.
- [92] A. Czarnecki and K. Melnikov, Nucl. Phys. **B505**, 65 (1997), hep-ph/9703277.
- [93] A. Czarnecki and K. Melnikov, Phys. Rev. **D59**, 014036 (1999), hep-ph/9804215.
- [94] K. Melnikov,  *$O(\alpha_s^2)$  corrections to semileptonic decay  $b \rightarrow cl\bar{\nu}_l$* , 2008, arXiv:0803.0951.
- [95] M. Dowling, Master's thesis, University of Alberta, 2008, ALBERTA THY 09-08.
- [96] D. B. Chitwood *et al.*, Phys. Rev. Lett. **99**, 032001 (2007), arXiv:0704.1981.
- [97] W. J. Marciano, Phys. Rev. **D60**, 093006 (1999), hep-ph/9903451.
- [98] T. van Ritbergen and R. G. Stuart, Phys. Rev. Lett. **82**, 488 (1999), hep-ph/9808283.
- [99] T. van Ritbergen and R. G. Stuart, Nucl. Phys. **B564**, 343 (2000), hep-ph/9904240.
- [100] M. Neubert, *QCD Calculations of Decays of Heavy Flavor Hadrons*, 2008, arXiv:0801.0675.
- [101] T. van Ritbergen, Phys. Lett. **B454**, 353 (1999), hep-ph/9903226.
- [102] S. J. Brodsky, G. P. Lepage, and P. B. Mackenzie, Phys. Rev. **D28**, 228 (1983).
- [103] M. E. Luke, M. J. Savage, and M. B. Wise, Phys. Lett. **B343**, 329 (1995), hep-ph/9409287.
- [104] A. F. Falk and M. E. Luke, Phys. Rev. **D57**, 424 (1998), hep-ph/9708327.
- [105] P. Gambino and N. Uraltsev, Eur. Phys. J. **C34**, 181 (2004), hep-ph/0401063.
- [106] V. Aquila, P. Gambino, G. Ridolfi, and N. Uraltsev, Nucl. Phys. **B719**, 77 (2005), hep-ph/0503083.

- [107] C. W. Bauer, A. F. Falk, and M. E. Luke, Phys. Rev. **D54**, 2097 (1996), hep-ph/9604290.
- [108] A. G. Grozin, T. Huber, and D. Maitre, JHEP **07**, 033 (2007), arXiv:0705.2609.
- [109] V. A. Smirnov, private communication.
- [110] A. I. Davydychev and J. B. Tausk, Nucl. Phys. **B465**, 507 (1996), hep-ph/9511261.
- [111] J. A. M. Vermaseren, *New features of FORM*, 2000, math-ph/0010025.
- [112] S. A. Larin, Phys. Lett. **B303**, 113 (1993), hep-ph/9302240.
- [113] A. Czarnecki, M. Jezabek, and J. H. Kuhn, Nucl. Phys. **B351**, 70 (1991).
- [114] M. Misiak, talk at 2nd Workshop on Flavor Dynamics, Albufeira, Portugal, November 2007.
- [115] B. Aubert *et al.*, *Measurement of Moments of the Hadronic-Mass and -Energy Spectrum in Inclusive Semileptonic  $\bar{B} \rightarrow X_c \ell^- \bar{\nu}$  Decays*, 2007, arXiv:0707.2670.
- [116] B. Aubert *et al.*, Phys. Rev. Lett. **100**, 231803 (2008), arXiv:0712.3493.
- [117] H.-C. Yang, A. Dasdan, R.-L. Hsiao, and D. Stott Parker, in *SIGMOD '07: Proceedings of the 2007 ACM SIGMOD international conference on Management of data* (ACM, New York, NY, USA, 2007), pp. 1029–1040.
- [118] J. Vollinga, Nucl. Instr. Meth. **A559**, 282 (2006), hep-ph/0510057.
- [119] T. Seidensticker, *Automatic application of successive asymptotic expansions of Feynman diagrams*, 1999, hep-ph/9905298.

# Appendix A

## Selected integration formulas

### A.1 Exactly known integrals

Here we list several integrals used throughout this thesis. Dimension  $D = 4 - 2\epsilon$ , integration measure is  $[d^D p] \equiv \frac{d^D p}{(2\pi)^D}$ , and the loop factor is  $\mathcal{F} = \frac{\Gamma(1+\epsilon)}{(4\pi)^{2-\epsilon}}$ . All integrations are done in the Euclidean metric.

$$\begin{aligned} G_{m2}(a, b; m^2) &= \int \frac{[d^D k]}{(k^2)^a (k^2 + m^2)^b} & (A.1) \\ &= \mathcal{F} (m^2)^{2-\epsilon-a-b} \frac{\Gamma(a+b-2+\epsilon)\Gamma(2-\epsilon-a)}{\Gamma(1+\epsilon)\Gamma(b)\Gamma(2-\epsilon)} \end{aligned}$$

$$\begin{aligned} \text{One}(a, b; q^2) &= \int \frac{[d^D k]}{(k^2)^a [(k+q)^2]^b} & (A.2) \\ &= \mathcal{F} (q^2)^{2-\epsilon-a-b} \frac{\Gamma(2-\epsilon-a)\Gamma(2-\epsilon-b)\Gamma(a+b-2+\epsilon)}{\Gamma(1+\epsilon)\Gamma(a)\Gamma(b)\Gamma(4-2\epsilon-a-b)} \end{aligned}$$

$$\begin{aligned} \text{Onshell}(a, b; q^2) &= \int \frac{[d^D k]}{(k^2)^a (k^2 + 2kq)^b} & (A.3) \\ &= \mathcal{F} (-q^2)^{2-\epsilon-a-b} \frac{\Gamma(a+b-2+\epsilon)\Gamma(4-2\epsilon-2a-b)}{\Gamma(1+\epsilon)\Gamma(b)\Gamma(4-2\epsilon-a-b)} \end{aligned}$$

$$\begin{aligned} G_{m3}(a, b, c; m^2) &= \int \frac{[d^D k][d^D q]}{(k^2 + m^2)^a [(q+k)^2]^b (q^2 + m^2)^c} & (A.4) \\ &= \mathcal{F}^2 (m^2)^{4-2\epsilon-a-b-c} \frac{\Gamma(a+b+c-4+2\epsilon)}{\Gamma(1+\epsilon)^2 \Gamma(a)\Gamma(c)\Gamma(2-\epsilon)} \\ &\times \frac{\Gamma(a+b-2+\epsilon)\Gamma(b+c-2+\epsilon)\Gamma(2-\epsilon-b)}{\Gamma(a+2b+c-4+2\epsilon)} \end{aligned}$$

A tensor structure in the numerator of  $G_{m2}$ -type integral allows angular

averaging:

$$\int \frac{[d^D k] k^{\alpha_1} \dots k^{\alpha_{2n}}}{(k^2)^a (k^2 + m^2)^b} = \frac{g_s^{\alpha_1 \dots \alpha_{2n}} \Gamma(2 - \epsilon)}{2^n \Gamma(n + 2 - \epsilon)} G_{m^2}(a - n, b; m^2), \quad (\text{A.5})$$

where  $g_s$  is the symmeterized product of metric tensors,  $g_s^{\alpha_1 \dots \alpha_{2n}} = g^{\alpha_1 \alpha_2} g^{\alpha_3 \alpha_4} \dots \cdot g^{\alpha_{2n-1} \alpha_{2n}} +$  all distinct permutations of indices  $\alpha_i$ ,  $(2n - 1)!!$  terms in total. Integrals with odd powers of  $k$  in the numerator vanish.

## A.2 Phase space parameterizations

A phase space element of a particle with momentum  $P_0$  decaying to particles with momenta  $P_1, \dots, P_N$  in  $D$  dimensions is defined as

$$d\Phi(P_0 \rightarrow P_1, \dots, P_N) = (2\pi)^D \delta^{(D)}(P_0 - P_1 - \dots - P_N) \prod_{i=1}^N \frac{d^{D-1} \vec{q}_i}{(2\pi)^{D-1} 2E_i}, \quad (\text{A.6})$$

where a Minkowski vector  $P_i = (E_i, \vec{q}_i)$  is defined in  $D = 4 - 2\epsilon$  dimensions so that  $P_i^2 = E_i^2 - |\vec{q}_i|^2 = m_i^2$  where  $\vec{q}_i$  is a  $(D - 1)$ -dimensional spatial momentum and  $E_i$  is the energy. Integration over all directions of a Euclidean vector in  $D$  dimensions is proportional to the surface area of a unit sphere,  $\Omega_D = \frac{2\pi^{D/2}}{\Gamma(D/2)}$ .  $D$ -dimensional delta-function splits as  $\delta^{(D)}(P_k) = \delta(E_k) \delta^{(D-1)}(\vec{q}_k)$ . The phase space above can be partitioned as

$$\begin{aligned} d\Phi(P_0 \rightarrow P_1, \dots, P_N) &= \int \frac{dP_{(1\dots K)}^2}{2\pi} d\Phi(P_{(1\dots K)} \rightarrow P_1, \dots, P_K) \\ &\times d\Phi(P_0 \rightarrow P_{(1\dots K)}, P_{K+1}, \dots, P_N), \end{aligned} \quad (\text{A.7})$$

where  $P_{(1\dots K)}$  is the total momentum of particles  $1\dots K$ , and the integration is done over the kinematically allowed range of  $P_{(1\dots K)}^2$ .

### Two-body phase space

A particle with mass  $M$  and momentum  $P_0 = (M, \vec{0})$  decays into two particles with masses  $m_{1,2}$  and momenta  $P_{1,2} = (E_{1,2}, \vec{q}_{1,2})$ . The corresponding phase



space (integrated over the directions of final particles) is

$$\begin{aligned} \int d\Phi(P_0 \rightarrow P_1, P_2) &= \frac{2\pi^{3/2} \mathcal{F}}{\Gamma(1+\epsilon)\Gamma(3/2-\epsilon)} \frac{q_1^{1-2\epsilon}}{M} & (\text{A.8}) \\ \text{limit } D=4: &\longrightarrow \frac{q_1}{4\pi M} \\ \text{case } m_1 = m_2 = 0: &\longrightarrow \frac{2^{2\epsilon}\pi^{3/2} \mathcal{F} M^{-2\epsilon}}{\Gamma(1+\epsilon)\Gamma(3/2-\epsilon)}, \end{aligned}$$

where  $q_1 = (2M)^{-1} \sqrt{(M^2 - (m_1 + m_2)^2)(M^2 - (m_1 - m_2)^2)}$  is the magnitude of  $\vec{q}_1 = -\vec{q}_2$ . Energies of the particles are  $E_{1,2} = (2M)^{-1}(M^2 \pm m_1^2 \mp m_2^2)$ .

### Three-body phase space with one mass

A particle with mass  $M$  and momentum  $P_0 = (M, \vec{0})$  (a “muon”) decays into a particle with mass  $m = \delta M$  and momentum  $P_1 = (E_1, \vec{q}_1)$  (an “electron”), and two massless particles with momenta  $P_{2,3} = (q_{2,3}, \vec{q}_{2,3})$  (“neutrinos”) whose directions can be integrated over. Denoting as  $P_w = P_2 + P_3 = (E_w, \vec{q}_w)$  the combined momentum of massless particles, the parameterization convenient for the sector decomposition is:

$$\begin{aligned} \int d\Phi(P_0 \rightarrow P_1, P_2, P_3) &= \frac{\mathcal{F}^2 2^{4\epsilon-1} \pi^2 M^{2-4\epsilon} (1-\delta)^{3-4\epsilon}}{\Gamma(1+\epsilon)^2 \Gamma(3/2-\epsilon)^2} & (\text{A.9}) \\ &\times \int_0^1 dy y^{1/2-\epsilon} (1-y)^{-\epsilon} (4\delta + y(1-\delta)^2)^{1/2-\epsilon}. \end{aligned}$$

The parameter  $y$  is chosen so that

$$\begin{aligned} E_1 &= (M/2)(2\delta + y(1-\delta)^2), \quad q_1^2 = yM^2(4\delta + y(1-\delta)^2), \\ P_w^2 &= M^2(1-y)(1-\delta)^2. \end{aligned}$$

### Four-body phase space with one mass

In addition to the particles in the previous case, the decay produces a massless particle with momentum  $P_4 = (q_4, \vec{q}_4)$  (a “photon”). We have:

$$\begin{aligned} \int d\Phi(P_0 \rightarrow P_1, P_2, P_3, P_4) &= \frac{\mathcal{F}^3 2^{4\epsilon-1} \pi^2 M^{4-6\epsilon} (1-\delta)^{5-6\epsilon}}{\Gamma(1+\epsilon)^3 \Gamma(3/2-\epsilon)^2 \Gamma(1-\epsilon)} & (\text{A.10}) \\ &\times \int_0^1 dy d\lambda_1 d\lambda_2 S^{-2+2\epsilon} Y^{1-2\epsilon} (1-y)^{2-3\epsilon} \lambda_1^{-\epsilon} (1-\lambda_1)^{1-2\epsilon} \lambda_2^{-\epsilon} (1-\lambda_2)^{-\epsilon}, \end{aligned}$$

$$Y = \sqrt{y(4\delta + y(1-\delta)^2)}, \quad S = 1 - \frac{y}{2}(1-\delta) + \left(\lambda_2 - \frac{1}{2}\right)Y.$$

Parameterized quantities are

$$\begin{aligned} E_1 &= (M/2)(2\delta + y(1-\delta)^2), \quad P_w^2 = M^2(1-\delta)^2\lambda_1(1-y), \\ q_1 &= (M/2)(1-\delta)Y, \quad q_4 = (M/2)(1-\delta)(1-\lambda_1)(1-y)/S, \\ 2P_1P_4 &= M^2(1-\delta)(1-y)(1-\lambda_1)(1-(1-\delta)S)/S. \end{aligned}$$

## Five-body phase space with one mass

To the previous case, we add an additional massless particle (the second ‘‘photon’’) with momentum  $P_5 = (q_5, \vec{q}_5)$ :

$$\begin{aligned} \int d\Phi(P_0 \rightarrow P_1, P_2, P_3, P_4, P_5) &= \frac{\mathcal{F}^4 2^{2\epsilon-1} \pi^{3/2} M^{6-8\epsilon} (1-\delta)^{7-8\epsilon}}{\Gamma^4(1+\epsilon) \Gamma^2(\frac{3}{2}-\epsilon) \Gamma(1-\epsilon) \Gamma(\frac{1}{2}-\epsilon)} \quad (\text{A.11}) \\ &\times \int_0^1 dy d\lambda_1 d\lambda_2 d\lambda_3 d\lambda_4 d\lambda_5 Y^{1-2\epsilon} W^{-2+2\epsilon} (1-y)^{4-5\epsilon} \lambda_1^{-\epsilon} (1-\lambda_1)^{3-4\epsilon} \\ &\times [\lambda_2(1-\lambda_2)]^{1-2\epsilon} [\lambda_3(1-\lambda_3)\lambda_4(1-\lambda_4)]^{-\epsilon} [\lambda_5(1-\lambda_5)]^{-\epsilon-1/2}, \end{aligned}$$

$$\begin{aligned} Y &= \sqrt{y(4\delta + y(1-\delta)^2)}, \quad S_{1,2} = 1 - \frac{y}{2}(1-\delta) + \left(\lambda_{3,4} - \frac{1}{2}\right)Y, \\ W &= S_1 S_2 - \frac{1}{2}\lambda_2(1-\lambda_1)(1-y)(1-\vec{n}_1\vec{n}_2), \\ \vec{n}_1\vec{n}_2 &= (2\lambda_3-1)(2\lambda_4-1) + 4(2\lambda_5-1)\sqrt{\lambda_3\lambda_4(1-\lambda_3)(1-\lambda_4)}. \end{aligned}$$

Then, kinematic variables become

$$\begin{aligned} P_w^2 &= M^2\lambda_1(1-y)(1-\delta)^2, \quad E_1 = (M/2)(2\delta + y(1-\delta)^2), \\ q_1 &= (M/2)(1-\delta)Y, \quad q_4 = (M/2)(1-\delta)(1-y)\lambda_2(1-\lambda_1)/S_1, \\ q_5 &= (M/2)(1-\delta)(1-y)(1-\lambda_1)(1-\lambda_2)S_1/W, \\ 2P_4P_5 &= (M^2/2)(1-\delta)^2(1-y)^2(1-\lambda_1)^2\lambda_2(1-\lambda_2)(1-\vec{n}_1\vec{n}_2)/W, \\ 2P_1P_4 &= (M^2/2)(1-\delta)(1-y)(1-\lambda_1)\lambda_2(1-(1-\delta)S_1)/S_1, \\ 2P_1P_5 &= (M^2/2)(1-\delta)(1-y)(1-\lambda_1)(1-\lambda_2)(1-(1-\delta)S_2)S_1/W. \end{aligned}$$

# Appendix B

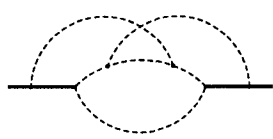
## Topologies and master integrals

In this section we use the common notations  $\mathcal{F} = \frac{\Gamma(1+\epsilon)}{(4\pi)^{D/2}}$ ,  $D = 4 - 2\epsilon$ ,  $A_4 = \text{Li}_4\frac{1}{2}$ ,  $A_5 = \text{Li}_5\frac{1}{2}$ , and  $H_6 = \zeta_{-5,-1} + \zeta_6 = 0.98744142\dots$ . Constants  $X_{45}$  and  $X_{55}$  do not propagate to the physical results. All integrals are defined in Euclidean space with on-shell external momentum,  $p^2 = -1$ . In the sketches, dashed lines represent massless, solid lines – massive, and double lines – eikonal (static) propagators. Notation  $1\epsilon$  designates a propagator raised to power  $a_1 + \epsilon$ . In four-loop topologies, integer exponents  $a_1, \dots, a_8$  can be positive or negative, while  $a_9$  is non-positive.

Four-loop master integrals are presented to the order in  $\epsilon$  required for the semi-leptonic  $b$ -quark decay calculation (in most cases higher than in Ref. [99]). The eikonal topologies  $E3$  and  $E4$  were considered in Ref. [62] (we correct here some misprints).  $\mathcal{O}(\epsilon)$  and  $\mathcal{O}(\epsilon^2)$  terms of  $U6$  were presented in Ref. [108]. Also,  $\mathcal{O}(\epsilon)$  term of  $U9$  was privately communicated by V.A. Smirnov.

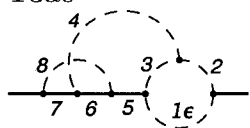
### B.1 Three-loop on-shell master integral

A self-energy integral calculated in addition to those in Ref. [89] is

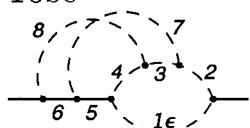


$$\begin{aligned}
 & \text{Im} \int \frac{[d^D k_1][d^D k_2][d^D k_3]}{(k_2^2 + 2k_2 p)(k_3^2 + 2k_3 p)(p + k_1 + k_2)^2} & (B.1) \\
 & \times \frac{1}{k_1^2 k_2^2 k_3^2 (p + k_1 + k_3)^2 (p + k_1 + k_2 + k_3)^2} \\
 & = \mathcal{F}^3 \pi \left[ \frac{61\pi^4}{360} + \mathcal{O}(\epsilon) \right].
 \end{aligned}$$

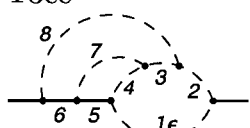
## B.2 Four-loop on-shell topologies

T3ae  
$$\int \frac{[d^D k_1][d^D k_4][d^D k_8] (2k_1 k_8)^{-a_9}}{(k_1 + p)^{2a_2} (k_1 + k_4 + p)^{2a_3} k_4^{2a_4} (k_4^2 + 2k_4 p)^{a_5}} \quad (\text{B.2})$$

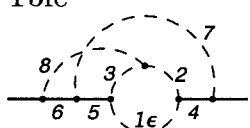
$$\times \frac{1}{k_1^{2a_1+2\epsilon} [(k_4 + k_8 + p)^2 + 1]^{a_6} (k_8^2 + 2k_8 p)^{a_7} k_8^{2a_8}}$$

T3be  
$$\int \frac{[d^D k_1][d^D k_7][d^D k_8] (2k_7 p)^{-a_9}}{(k_1 + p)^{2a_2} (k_1 + k_7 + p)^{2a_3} (k_1 + k_7 + k_8 + p)^{2a_4}} \quad (\text{B.3})$$

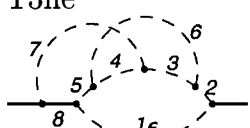
$$\times \frac{1}{k_1^{2a_1+2\epsilon} [(k_7 + k_8 + p)^2 + 1]^{a_5} (k_8^2 + 2k_8 p)^{a_6} k_7^{2a_7} k_8^{2a_8}}$$

T3ce  
$$\int \frac{[d^D k_1][d^D k_7][d^D k_8] (2k_7 p)^{-a_9}}{(k_1 + p)^{2a_2} (k_1 + k_8 + p)^{2a_3} (k_1 + k_7 + k_8 + p)^{2a_4}} \quad (\text{B.4})$$

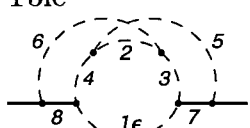
$$\times \frac{1}{k_1^{2a_1+2\epsilon} [(k_7 + k_8 + p)^2 + 1]^{a_5} (k_8^2 + 2k_8 p)^{a_6} k_7^{2a_7} k_8^{2a_8}}$$

T3fe  
$$\int \frac{[d^D k_1][d^D k_7][d^D k_8] (2k_1 p)^{-a_9}}{(k_1 + k_7 + p)^{2a_2} (k_1 + k_7 + k_8 + p)^{2a_3} k_7^{2a_7} k_8^{2a_8}} \quad (\text{B.5})$$

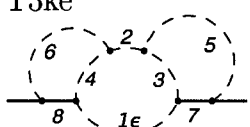
$$\times \frac{1}{k_1^{2a_1+2\epsilon} [(k_7 + k_8 + p)^2 + 1]^{a_5} (k_8^2 + 2k_8 p)^{a_6} (k_7^2 + 2k_7 p)^{a_4}}$$

T3he  
$$\int \frac{[d^D k_1][d^D k_6][d^D k_7] (2k_6 p)^{-a_9}}{(k_1 + p)^{2a_2} (k_1 + k_6 + p)^{2a_3} (k_1 + k_6 + k_7 + p)^{2a_4}} \quad (\text{B.6})$$

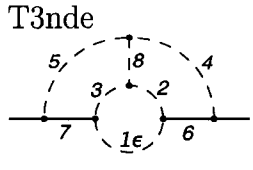
$$\times \frac{1}{k_1^{2a_1+2\epsilon} (k_1 + k_7 + p)^{2a_5} k_6^{2a_6} k_7^{2a_7} (k_7^2 + 2k_7 p)^{a_8}}$$

T3ie  
$$\int \frac{[d^D k_1][d^D k_5][d^D k_6] (2k_1 p)^{-a_9}}{k_1^{2a_1+2\epsilon} (k_1 + k_5 + k_6 + p)^{2a_2} (k_1 + k_5 + p)^{2a_3}} \quad (\text{B.7})$$

$$\times \frac{1}{(k_1 + k_6 + p)^{2a_4} k_5^{2a_5} k_6^{2a_6} (k_5^2 + 2k_5 p)^{a_7} (k_6^2 + 2k_6 p)^{a_8}}$$

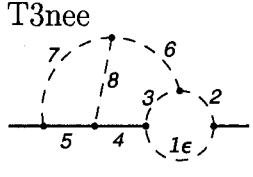
T3ke  
$$\int \frac{[d^D k_1][d^D k_5][d^D k_6] (2k_5 k_6)^{-a_9}}{(k_1 + p)^{2a_2} (k_1 + k_5 + p)^{2a_3} (k_1 + k_6 + p)^{2a_4}} \quad (\text{B.8})$$

$$\times \frac{1}{k_1^{2a_1+2\epsilon} k_5^{2a_5} k_6^{2a_6} (k_5^2 + 2k_5 p)^{a_7} (k_6^2 + 2k_6 p)^{a_8}}$$

T3nde 

$$\int \frac{[d^D k_1][d^D k_4][d^D k_5] (2k_1 p)^{-a_9}}{k_1^{2a_1+2\epsilon}(k_1+k_4+p)^{2a_2}(k_1+k_5+p)^{2a_3}k_4^{2a_4}} \quad (\text{B.9})$$

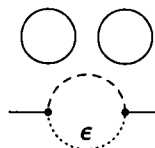
$$\times \frac{1}{k_5^{2a_5}(k_4^2+2k_4 p)^{2a_6}(k_5^2+2k_5 p)^{a_7}(k_4-k_5)^{2a_8}}$$

T3nee 

$$\int \frac{[d^D k_1][d^D k_6][d^D k_7] (2k_1 k_7)^{-a_9}}{(k_1+p)^{2a_2}(k_1+k_6+p)^{2a_3}(k_6^2+2k_6 p)^{a_4}} \quad (\text{B.10})$$

$$\times \frac{1}{k_1^{2a_1+2\epsilon}(k_7^2+2k_7 p)^{a_5}k_6^{2a_6}k_7^{2a_7}(k_6-k_7)^{2a_8}}$$

### B.3 Four-loop master integrals

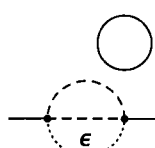
V1 

$$\text{Im T3ke}(0, 1, 0, 0, 0, 0, 1, 1, 0) / (\pi \mathcal{F}^4) \quad (\text{B.11})$$

$$= \frac{1}{2\epsilon} + \frac{13}{4} + \left( \frac{111}{8} - \frac{5\pi^2}{12} \right) \epsilon + \left( \frac{797}{16} - \frac{65\pi^2}{24} - 4\zeta_3 \right) \epsilon^2$$

$$+ \left( \frac{5255}{32} - \frac{185\pi^2}{16} + \frac{43\pi^4}{720} - 26\zeta_3 \right) \epsilon^3$$

$$+ \left( \frac{33141}{64} - \frac{3985\pi^2}{96} + \frac{559\pi^4}{1440} - 111\zeta_3 + \frac{10\pi^2\zeta_3}{3} - 24\zeta_5 \right) \epsilon^4$$

V2 

$$\text{Im T3ke}(0, 0, 1, 0, 1, 0, 0, 1, 0) / (\pi \mathcal{F}^4) \quad (\text{B.12})$$

$$= -\frac{1}{12} - \frac{65}{72}\epsilon + \left( \frac{11\pi^2}{72} - \frac{2653}{432} \right) \epsilon^2 + \left( \frac{715\pi^2}{432} - \frac{87941}{2592} \right.$$

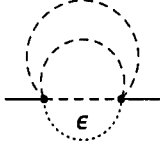
$$\left. + \frac{13\zeta_3}{6} \right) \epsilon^3 + \left( \frac{29183\pi^2}{2592} - \frac{2601277}{15552} - \frac{283\pi^4}{4320} + \frac{845\zeta_3}{36} \right) \epsilon^4$$

$$+ \left( \frac{967351\pi^2}{15552} - \frac{71855525}{93312} - \frac{3679\pi^4}{5184} + \frac{34489\zeta_3}{216} \right.$$

$$\left. - \frac{143\pi^2\zeta_3}{36} + \frac{41\zeta_5}{2} \right) \epsilon^5$$

$$\text{Im } T_{3ce}(0, 0, 0, 1, 0, 0, 1, 1, 0) / (\pi \mathcal{F}^4) \quad (\text{B.13})$$

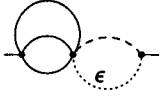
V3



$$\begin{aligned} &= \frac{1}{144}\epsilon + \frac{7}{64}\epsilon^2 + \left( \frac{21703}{20736} - \frac{19\pi^2}{864} \right) \epsilon^3 \\ &+ \left( \frac{219385}{27648} - \frac{133\pi^2}{384} - \frac{29\zeta_3}{72} \right) \epsilon^4 \\ &+ \left( \frac{157267231}{2985984} - \frac{412357\pi^2}{124416} + \frac{313\pi^4}{17280} - \frac{203\zeta_3}{32} \right) \epsilon^5 \\ &+ \left( \frac{1280594921}{3981312} - \frac{4168315\pi^2}{165888} + \frac{2191\pi^4}{7680} - \frac{629387\zeta_3}{10368} \right. \\ &\quad \left. + \frac{551\pi^2\zeta_3}{432} - \frac{137\zeta_5}{24} \right) \epsilon^6 \end{aligned}$$

$$\text{Im } T_{3ae}(0, 1, 0, 0, 1, 1, 1, 0, 0) / (\pi \mathcal{F}^4) \quad (\text{B.14})$$

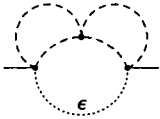
V4



$$\begin{aligned} &= -\frac{3}{4\epsilon} - \frac{11}{2} + \left( \frac{5\pi^2}{8} - \frac{401}{16} \right) \epsilon + \left( \frac{47\pi^2}{12} - \frac{1441}{16} + 6\zeta_3 \right) \epsilon^2 \\ &+ \left( 30\zeta_3 - \frac{17603}{64} + \frac{1301\pi^2}{96} + 4\pi^2 \ln 2 - \frac{43\pi^4}{480} \right) \epsilon^3 \\ &+ \left( \frac{2485\pi^2}{96} - \frac{2899}{4} - 96A_4 - 4\ln^4 2 + 44\pi^2 \ln 2 \right. \\ &\quad \left. - 8\pi^2 \ln^2 2 + \frac{47\pi^4}{80} + \frac{93\zeta_3}{2} - 5\pi^2\zeta_3 + 36\zeta_5 \right) \epsilon^4 \end{aligned}$$

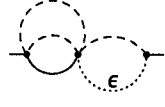
$$\text{Im } T_{3ke}(0, 0, 1, 1, 1, 1, 0, 0, 0) / (\pi \mathcal{F}^4) \quad (\text{B.15})$$

V6



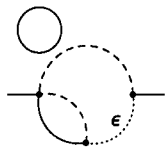
$$\begin{aligned} &= \frac{1}{6} + \frac{85}{36}\epsilon + \left( \frac{4495}{216} - \frac{19\pi^2}{36} \right) \epsilon^2 + \left( \frac{191641}{1296} - \frac{1615\pi^2}{216} \right. \\ &\quad \left. - \frac{26\zeta_3}{3} \right) \epsilon^3 + \left( \frac{7250503}{7776} - \frac{85405\pi^2}{1296} + \frac{65\pi^4}{144} - \frac{1105\zeta_3}{9} \right) \epsilon^4 \\ &+ \left( \frac{255112969}{46656} - \frac{3641179\pi^2}{7776} + \frac{5525\pi^4}{864} - \frac{58435\zeta_3}{54} \right. \\ &\quad \left. + \frac{247\pi^2\zeta_3}{9} - 130\zeta_5 \right) \epsilon^5 \end{aligned}$$

**V8**



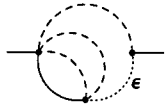
$$\begin{aligned}
& \text{Im } T_{3ae}(0, 1, 0, 1, 0, 1, 0, 1, 0) / (\pi \mathcal{F}^4) & (B.16) \\
& = -\frac{1}{4\epsilon} - \frac{7}{4} + \left( \frac{\pi^2}{24} - \frac{119}{16} \right) \epsilon + \left( \frac{7\pi^2}{24} - \frac{191}{8} \right) \epsilon^2 \\
& + \left( \frac{119\pi^2}{96} - \frac{3785}{64} - \frac{11\pi^4}{160} \right) \epsilon^3 \\
& + \left( \frac{191\pi^2}{48} - \frac{5869}{64} - \frac{77\pi^4}{160} - 24\zeta_5 \right) \epsilon^4
\end{aligned}$$

**V9**



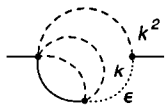
$$\begin{aligned}
& \text{Im } T_{3ke}(0, 1, 0, 1, 0, 0, 1, 1, 0) / (\pi \mathcal{F}^4) & (B.17) \\
& = -\frac{1}{2\epsilon} - 5 + \frac{\pi^2}{6} + \left( \frac{5\pi^2}{4} - \frac{65}{2} + 8\zeta_3 \right) \epsilon \\
& + \left( 7\pi^2 - 175 + \frac{59\pi^4}{180} + 44\zeta_3 \right) \epsilon^2 \\
& + \left( \frac{141\pi^2}{4} - \frac{1701}{2} + \frac{379\pi^4}{240} + 176\zeta_3 - \frac{22\pi^2\zeta_3}{3} + 186\zeta_5 \right) \epsilon^3 \\
& + \left( \frac{502\pi^2}{3} - 3885 + \frac{199\pi^4}{40} + 652\zeta_3 - 40\pi^2\zeta_3 \right. \\
& \quad \left. + \frac{2519\pi^6}{5040} - 48\zeta_3^2 + 954\zeta_5 \right) \epsilon^4
\end{aligned}$$

**V13**



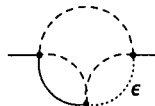
$$\begin{aligned}
& \text{Im } T_{3ce}(0, 1, 0, 1, 0, 1, 1, 0, 0) / (\pi \mathcal{F}^4) & (B.18) \\
& = -\frac{1}{4\epsilon} - \frac{11}{6} - \left( \frac{1031}{144} + \frac{\pi^2}{24} \right) \epsilon - \left( \frac{2285}{216} + \frac{29\pi^2}{72} + 7\zeta_3 \right) \epsilon^2 \\
& + \left( \frac{513913}{5184} - \frac{2263\pi^2}{864} - \frac{187\pi^4}{288} - \frac{343\zeta_3}{6} \right) \epsilon^3 + \left( \frac{9583921}{7776} \right. \\
& \quad \left. - \frac{38549\pi^2}{2592} - \frac{31\pi^4}{6} - \frac{10297\zeta_3}{36} + \frac{13\pi^2\zeta_3}{6} - 385\zeta_5 \right) \epsilon^4
\end{aligned}$$

**V13a**



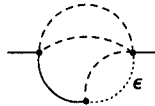
$$\begin{aligned}
& \text{Im } T_{3ce}(-1, 1, 0, 1, 0, 1, 1, 0, 0) / (\pi \mathcal{F}^4) & (B.19) \\
& = \frac{1}{12\epsilon} + \frac{29}{48} + \left( \frac{4513}{1728} - \frac{24\pi^2}{1728} \right) \epsilon + \left( \frac{52949}{6912} - \frac{29\pi^2}{288} \right. \\
& \quad \left. + \frac{2\zeta_3}{3} \right) \epsilon^2 + \left( \frac{1923793}{248832} - \frac{4513\pi^2}{10368} + \frac{29\pi^4}{288} + \frac{29\zeta_3}{6} \right) \epsilon^3 \\
& + \left( \frac{4513\zeta_3}{216} - \frac{100182571}{995328} - \frac{52949\pi^2}{41472} + \frac{841\pi^4}{1152} \right. \\
& \quad \left. - \frac{\pi^2\zeta_3}{9} + 60\zeta_5 \right) \epsilon^4
\end{aligned}$$

**V14**



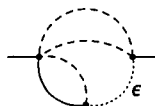
$$\begin{aligned}
& \text{Im T3ce}(0, 0, 1, 0, 1, 0, 1, 1, 0) / (\pi \mathcal{F}^4) & (\text{B.20}) \\
& = \frac{1}{12} + \frac{67}{72}\epsilon + \left( \frac{2677}{432} - \frac{\pi^2}{8} \right) \epsilon^2 + \left( \frac{81175}{2592} - \frac{199\pi^2}{144} \right. \\
& \quad \left. - \frac{2\zeta_3}{3} \right) \epsilon^3 + \left( \frac{1980661}{15552} - \frac{7783\pi^2}{864} + \frac{161\pi^4}{1440} - \frac{241\zeta_3}{36} \right) \epsilon^4 \\
& + \left( \frac{36787207}{93312} - \frac{225835\pi^2}{5184} + \frac{10987\pi^4}{8640} - \frac{920\zeta_3}{27} \right. \\
& \quad \left. + \frac{\pi^2\zeta_3}{3} + 26\zeta_5 \right) \epsilon^5
\end{aligned}$$

**V15**



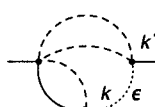
$$\begin{aligned}
& \text{Im T3ce}(0, 0, 0, 1, 1, 0, 1, 1, 0) / (\pi \mathcal{F}^4) & (\text{B.21}) \\
& = \left( \frac{5}{6} - \frac{\pi^2}{12} \right) \epsilon + \left( \frac{1979}{144} - \frac{13\zeta_3}{2} - \frac{7\pi^2}{12} \right) \epsilon^2 \\
& + \left( \frac{117755}{864} - \frac{737\pi^2}{144} - \frac{11\pi^4}{36} - \frac{91\zeta_3}{2} \right) \epsilon^3 + \left( \frac{2750503}{2592} \right. \\
& \quad \left. - \frac{44477\pi^2}{864} - \frac{77\pi^4}{36} - \frac{5801\zeta_3}{24} + \frac{247\pi^2\zeta_3}{12} - \frac{563\zeta_5}{2} \right) \epsilon^4
\end{aligned}$$

**V16**




$$\begin{aligned}
& \text{Im T3ke}(0, 0, 1, 1, 0, 1, 1, 0, 0) / (\pi \mathcal{F}^4) & (\text{B.22}) \\
& = \frac{1}{12} + \left( \frac{23}{9} - \frac{\pi^2}{6} \right) \epsilon + \left( \frac{14809}{432} - \frac{25\zeta_3}{2} - \frac{53\pi^2}{36} \right) \epsilon^2 \\
& + \left( \frac{26108}{81} - \frac{2351\pi^2}{216} - \frac{289\pi^4}{360} - \frac{605\zeta_3}{6} \right) \epsilon^3 + \left( \frac{38678449}{15552} \right. \\
& \quad \left. - \frac{107579\pi^2}{1296} - \frac{9013\pi^4}{1440} - \frac{37951\zeta_3}{72} + \frac{259\pi^2\zeta_3}{12} - \frac{1243\zeta_5}{2} \right) \epsilon^4
\end{aligned}$$

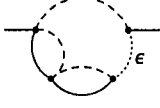
**V16a**




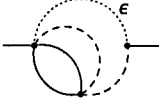
$$\begin{aligned}
& \text{Im T3ke}(-1, 0, 1, 1, 0, 1, 1, 0, 0) / (\pi \mathcal{F}^4) & (\text{B.23}) \\
& = -\frac{1}{72} + \left( \frac{\pi^2}{36} - \frac{41}{96} \right) \epsilon + \left( \frac{13\zeta_3}{6} - \frac{58531}{10368} + \frac{49\pi^2}{216} \right) \epsilon^2 \\
& + \left( \frac{2143\pi^2}{1296} - \frac{240527}{4608} + \frac{77\pi^4}{540} + \frac{1157\zeta_3}{72} \right) \epsilon^3 + \left( \frac{6271\pi^2}{486} \right. \\
& \quad \left. - \frac{591750475}{1492992} + \frac{26513\pi^4}{25920} + \frac{68263\zeta_3}{864} - \frac{15\pi^2\zeta_3}{4} + \frac{217\zeta_5}{2} \right) \epsilon^4
\end{aligned}$$

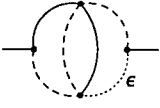


$$\begin{aligned}
& \text{Im T3ce}(0, 1, 0, 1, 1, 0, 1, 1, 0) / (\pi \mathcal{F}^4) & (B.24) \\
\mathbf{V17} & = \frac{1}{4\epsilon} + \frac{29}{8} - \frac{\pi^2}{6} + \left( \frac{533}{16} - 13\zeta_3 - \frac{7\pi^2}{8} \right) \epsilon \\
& + \left( \frac{7945}{32} - \frac{35\pi^2}{16} - \frac{109\pi^4}{90} - 65\zeta_3 \right) \epsilon^2 \\
& + \left( \frac{105021}{64} - \frac{217\pi^2}{96} - \frac{9053\pi^4}{1440} - \frac{247\zeta_3}{2} + \frac{7\pi^2\zeta_3}{6} - 759\zeta_5 \right) \epsilon^3
\end{aligned}$$


$$\begin{aligned}
& \text{Im T3ke}(0, 1, 1, 1, 0, 0, 1, 1, 0) / (\pi \mathcal{F}^4) & (B.25) \\
\mathbf{V18} & = \frac{1}{2\epsilon} + \frac{27}{4} - \frac{\pi^2}{3} + \left( \frac{467}{8} - 22\zeta_3 - \frac{25\pi^2}{12} \right) \epsilon \\
& + \left( \frac{6615}{16} - \frac{271\pi^2}{24} - \frac{14\pi^4}{9} - 105\zeta_3 \right) \epsilon^2 \\
& + \left( \frac{83811}{32} - \frac{3119\pi^2}{48} - \frac{917\pi^4}{144} - \frac{697\zeta_3}{2} + \frac{59\pi^2\zeta_3}{3} - 1092\zeta_5 \right) \epsilon^3
\end{aligned}$$


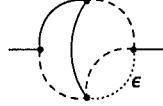
$$\begin{aligned}
& \text{Im T3fe}(0, 1, 1, 0, 1, 1, 1, 0, 0) / (\pi \mathcal{F}^4) & (B.26) \\
\mathbf{V19} & = \left( \frac{7}{4} - \frac{\pi^2}{6} \right) \epsilon + \left( \frac{259}{8} - 15\zeta_3 - \frac{4\pi^2}{3} \right) \epsilon^2 + \left( \frac{5699}{16} - \frac{209\pi^2}{24} \right. \\
& - \left. \frac{67\pi^4}{60} - 129\zeta_3 \right) \epsilon^3 + \left( \frac{97375}{32} - \frac{3161\pi^2}{48} - \frac{203\pi^4}{20} \right. \\
& - \left. 673\zeta_3 - 814\zeta_5 + \frac{137\pi^2\zeta_3}{6} \right) \epsilon^4
\end{aligned}$$


$$\begin{aligned}
& \text{Im T3ae}(0, 1, 1, 0, 0, 1, 1, 0, 0) / (\pi \mathcal{F}^4) & (B.27) \\
\mathbf{V20} & = -\frac{1}{2\epsilon} - \frac{15}{4} + \left( \frac{5\pi^2}{12} - \frac{145}{8} \right) \epsilon + \left( \frac{25\pi^2}{8} - \frac{1155}{16} + 4\zeta_3 \right) \epsilon^2 \\
& + \left( \frac{725\pi^2}{48} - \frac{8281}{32} - \frac{43\pi^4}{720} + 30\zeta_3 \right) \epsilon^3 \\
& + \left( \frac{1925\pi^2}{32} - \frac{55755}{64} - \frac{43\pi^4}{96} + 145\zeta_3 - \frac{10\pi^2\zeta_3}{3} + 24\zeta_5 \right) \epsilon^4
\end{aligned}$$


$$\begin{aligned}
& \text{Im T3ae}(0, 1, 1, 0, 0, 1, 1, 1, 0) / (\pi \mathcal{F}^4) & (B.28) \\
\mathbf{V21} & = \frac{1}{4\epsilon} + \frac{19}{8} + \left( \frac{251}{16} - \frac{13\pi^2}{24} \right) \epsilon + \left( \frac{3071}{32} - 14\zeta_3 \right. \\
& - \left. \frac{235\pi^2}{48} \right) \epsilon^2 + \left( \frac{38027}{64} - \frac{889\pi^2}{32} - \frac{1261\pi^4}{1440} - 133\zeta_3 \right) \epsilon^3
\end{aligned}$$


$$\text{Im } T3ae(0, 0, 1, 1, 0, 1, 1, 1, 0) / (\pi \mathcal{F}^4) \quad (\text{B.29})$$

V22

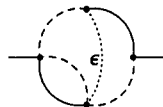
$$= \frac{3}{16} \epsilon + \left( \frac{61}{16} - \zeta_3 - \frac{\pi^2}{48} \right) \epsilon^2$$


$$+ \left( \frac{2927}{64} - \frac{71\pi^2}{96} - \frac{67\pi^4}{720} - \frac{93\zeta_3}{8} \right) \epsilon^3$$

$$+ \left( \frac{27069}{64} - \frac{2171\pi^2}{192} - \frac{1457\pi^4}{1440} - 97\zeta_3 + \frac{31\pi^2\zeta_3}{12} - 58\zeta_5 \right) \epsilon^4$$

$$\text{Im } T3fe(0, 1, 1, 1, 0, 1, 1, 0, 0) / (\pi \mathcal{F}^4) \quad (\text{B.30})$$

V24

$$= \frac{1}{4} + \left( \frac{17}{8} + \frac{\pi^2}{12} \right) \epsilon + \left( \frac{73}{16} + \frac{11\zeta_3}{2} + \frac{7\pi^2}{12} \right) \epsilon^2 + \left( \frac{35\pi^2}{8} - \frac{2419}{32} \right.$$


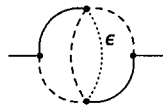
$$+ \frac{43\pi^4}{180} + \frac{243\zeta_3}{4} \Big) \epsilon^3 + \left( \frac{725\pi^2}{16} - \frac{75023}{64} + \frac{4367\pi^4}{1440} + \frac{3747\zeta_3}{8} \right.$$

$$\left. - \frac{55\pi^2\zeta_3}{4} + \frac{407\zeta_5}{2} \right) \epsilon^4 + \left( \frac{43307\pi^2}{96} - \frac{1390475}{128} + \frac{22229\pi^4}{960} \right.$$

$$\left. + \frac{10943\pi^6}{30240} + \frac{51503\zeta_3}{16} - \frac{3737\pi^2\zeta_3}{24} - \frac{367\zeta_3^2}{2} + \frac{9545\zeta_5}{4} \right) \epsilon^5$$

$$\text{Im } T3fe(0, 0, 1, 1, 0, 1, 1, 1, 0) / (\pi \mathcal{F}^4) \quad (\text{B.31})$$

V25

$$= \left( \frac{\pi^2}{24} - \frac{5}{16} \right) \epsilon + \left( \frac{11\zeta_3}{4} - \frac{95}{16} + \frac{7\pi^2}{16} \right) \epsilon^2 + \left( \frac{63\pi^2}{16} - \frac{4313}{64} \right.$$


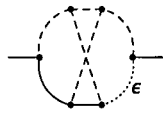
$$+ \frac{59\pi^4}{720} + \frac{231\zeta_3}{8} \Big) \epsilon^3 + \left( \frac{6739\pi^2}{192} - \frac{38127}{64} + \frac{413\pi^4}{480} + \frac{403\zeta_5}{4} \right.$$

$$+ \frac{3403\zeta_3}{16} - \frac{235\pi^2\zeta_3}{24} \Big) \epsilon^4 + \left( \frac{18825\pi^2}{64} - \frac{1160841}{256} + \frac{28699\pi^4}{5760} \right.$$

$$\left. + \frac{10219\pi^6}{181440} + \frac{45439\zeta_3}{32} - \frac{1645\pi^2\zeta_3}{16} - \frac{231\zeta_3^2}{2} + \frac{8463\zeta_5}{8} \right) \epsilon^5$$

V30

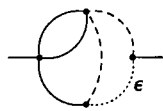
$$\text{Im } T3be(0, 1, 1, 1, 1, 1, 1, 1, 0) / (\pi \mathcal{F}^4) \quad (\text{B.32})$$



$$= -\frac{4\pi^4}{135} - \left( \frac{95\zeta_5}{6} + \frac{13\pi^2\zeta_3}{18} + \frac{8\pi^4}{135} \right) \epsilon$$

V35

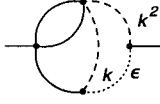
$$\text{Im } T3ae(0, 1, 1, 0, 1, 1, 1, 0, 0) / (\pi \mathcal{F}^4) \quad (\text{B.33})$$



$$= \frac{1}{4\epsilon} + \frac{29}{8} - \frac{\pi^2}{6} + \left( \frac{525}{16} - 9\zeta_3 - \frac{13\pi^2}{8} \right) \epsilon$$

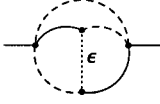
$$+ \left( \frac{7697}{32} - \frac{193\pi^2}{16} - \frac{119\pi^4}{360} - \frac{177\zeta_3}{2} + 4\pi^2 \ln 2 \right) \epsilon^2$$

V35a



$$\begin{aligned}
 & \text{Im } T3ae(-1, 1, 1, 0, 1, 1, 0, 0) / (\pi \mathcal{F}^4) & (B.34) \\
 & = -\frac{1}{12\epsilon} + \frac{49}{72} + \left( \frac{19\pi^2}{72} - \frac{2047}{432} \right) \epsilon \\
 & + \left( \frac{29\zeta_3}{2} - \frac{93667}{2592} + \frac{1045\pi^2}{432} - \frac{4\pi^2 \ln 2}{3} \right) \epsilon^2 \\
 & + \left( 155\zeta_3 - \frac{4353493}{15552} + 96A_4 + 4\ln^4 2 + \frac{42337\pi^2}{2592} \right. \\
 & \quad \left. - \frac{140\pi^2 \ln 2}{9} + \frac{8\pi^2 \ln^2 2}{3} - \frac{29\pi^4}{96} \right) \epsilon^3
 \end{aligned}$$

V45



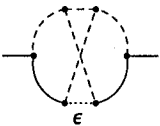
$$\begin{aligned}
 & \text{Im } T3ie(0, 1, 1, 1, 0, 0, 1, 1, 0) / (\pi \mathcal{F}^4) & (B.35) \\
 & = \left( \frac{1}{2} + \frac{\zeta_3}{2} + \frac{7\pi^2}{12} - \pi^2 \ln 2 \right) \epsilon + \left( \frac{31}{4} + 92A_4 + \frac{23\ln^4 2}{6} \right. \\
 & \quad \left. + \frac{155\pi^2}{24} - 4\pi^2 \ln 2 - \frac{10\pi^2 \ln^2 2}{3} - \frac{97\pi^4}{72} + \frac{91\zeta_3}{2} \right) \epsilon^2 \\
 & + \left( \frac{555}{8} + 368A_4 + 92A_5 + \frac{46\ln^4 2}{3} - \frac{23\ln^5 2}{30} + \frac{2119\pi^2}{48} \right. \\
 & \quad \left. - \frac{\pi^2 \ln 2}{2} - \frac{40\pi^2 \ln^2 2}{3} + \frac{10\pi^2 \ln^3 2}{9} - \frac{449\pi^4}{120} - \frac{457\pi^4 \ln 2}{180} \right. \\
 & \quad \left. + 478\zeta_3 - \frac{227\pi^2 \zeta_3}{8} - 369\zeta_5 \right) \epsilon^3 + X_{45}\epsilon^4
 \end{aligned}$$

V55



$$\begin{aligned}
 & \text{Im } T3be(0, 1, 1, 1, 1, 1, 0, 0, 0) / (\pi \mathcal{F}^4) & (B.36) \\
 & = \frac{1}{4\epsilon} + \frac{29}{8} - \frac{\pi^2}{6} + \left( \frac{517}{16} - \frac{23\zeta_3}{2} - \frac{11\pi^2}{24} - \pi^2 \ln 2 \right) \epsilon \\
 & + \left( \frac{7385}{32} + \frac{\ln^4 2}{2} + \frac{19\pi^2}{16} - 4\pi^2 \ln 2 - \frac{53\pi^4}{36} - 51\zeta_3 + 12A_4 \right) \epsilon^2 \\
 & + \left( \frac{93389}{64} + 48A_4 + 12A_5 + 2\ln^4 2 - \frac{\ln^5 2}{10} + \frac{1625\pi^2}{96} - \frac{\pi^2 \ln 2}{2} \right. \\
 & \quad \left. - \frac{9629\pi^4}{1440} + \frac{39\pi^4 \ln 2}{40} - \frac{349\zeta_3}{4} - \frac{121\pi^2 \zeta_3}{6} - \frac{10711\zeta_5}{16} \right) \epsilon^3 \\
 & + X_{55}\epsilon^4
 \end{aligned}$$

V60

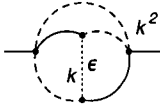


$$\begin{aligned}
 & \text{Im } T3ie(0, 1, 1, 1, 1, 1, 1, 0) / (\pi \mathcal{F}^4) & (B.37) \\
 & = -\frac{7\pi^4}{135} - \left( \frac{131\zeta_5}{6} + \frac{43\pi^2 \zeta_3}{18} + \frac{14\pi^4}{135} \right) \epsilon
 \end{aligned}$$

$$\text{Im } T3ie(-1, 1, 1, 1, 0, 0, 1, 1, 0) / (\pi \mathcal{F}^4) \quad (\text{B.38})$$

$$\begin{aligned}
&= \left( \frac{125}{48} - \frac{5\zeta_3}{2} - \frac{47\pi^2}{72} + \pi^2 \ln 2 \right) \epsilon + \left( \frac{12335}{288} - 92A_4 - 60\zeta_3 \right. \\
&\quad \left. - \frac{23\ln^4 2}{6} - \frac{1291\pi^2}{216} + \frac{23\pi^2 \ln 2}{6} + \frac{10\pi^2 \ln^2 2}{3} + \frac{35\pi^4}{36} \right) \epsilon^2 \\
&+ \left( \frac{91885}{216} - \frac{1058}{3}A_4 - 92A_5 + \frac{661\zeta_5}{8} - \frac{529\ln^4 2}{36} + \frac{23\ln^5 2}{30} \right. \\
&\quad + \frac{89\pi^2 \ln 2}{36} - \frac{57937\pi^2}{1296} + \frac{113\pi^2 \zeta_3}{4} - \frac{10\pi^2 \ln^3 2}{9} - \frac{3779\zeta_3}{8} \\
&\quad \left. + \frac{6641\pi^4}{4320} + \frac{457\pi^4 \ln 2}{180} + \frac{115\pi^2 \ln^2 2}{9} \right) \epsilon^3 + \left( \frac{17262961}{5184} \right. \\
&\quad + 1674H_6 - 92A_6 - \frac{2047}{9}A_4 - \frac{13627\pi^2 \ln 2}{216} - \frac{5069555\pi^2}{15552} \\
&\quad + \frac{529\ln^5 2}{180} - \frac{23\ln^6 2}{180} - \frac{1058}{3}A_5 - \frac{2047\ln^4 2}{216} + \frac{1162\pi^2}{3}A_4 \\
&\quad + \frac{445\pi^2 \ln^2 2}{54} - \frac{115\pi^2 \ln^3 2}{27} + \frac{197\pi^2 \ln^4 2}{12} + \frac{10511\pi^4 \ln 2}{1080} \\
&\quad - \frac{118861\pi^4}{6480} - \frac{2089\pi^4 \ln^2 2}{120} + \frac{1829\pi^6}{9072} - \frac{17161\zeta_3}{6} \\
&\quad \left. + \frac{9049\pi^2 \zeta_3}{32} + 45\pi^2 \zeta_3 \ln 2 + \frac{769\zeta_3^2}{4} - \frac{170873\zeta_5}{96} \right) \epsilon^4
\end{aligned}$$

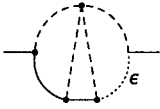
V45a



$$\text{Im } T3nee(0, 1, 1, 1, 1, -1, 1, 1, 0) / (\pi \mathcal{F}^4) \quad (\text{B.39})$$

$$\begin{aligned}
&= \frac{1}{4\epsilon} + \frac{19}{8} + \left( \frac{251}{16} - \frac{49\pi^2}{24} + \frac{\pi^4}{18} + \frac{15\zeta_3}{2} \right) \epsilon \\
&+ \left( \frac{3039}{32} - \frac{371\pi^2}{16} + \frac{557\pi^4}{360} - 7\zeta_3 + \frac{13\pi^2 \zeta_3}{2} - 55\zeta_5 \right) \epsilon^2 \\
&+ \left( \frac{36683}{64} - \frac{5663\pi^2}{32} + \frac{1179\pi^4}{160} - \frac{233\pi^6}{3240} - \frac{1873\zeta_3}{4} \right. \\
&\quad \left. + \frac{141\pi^2 \zeta_3}{4} + 51\zeta_3^2 + \frac{1279\zeta_5}{2} \right) \epsilon^3
\end{aligned}$$

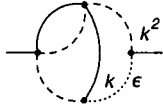
V70c



$$\text{Im T3be}(-1, 1, 1, 1, 1, 1, 0, 0, 0) / (\pi \mathcal{F}^4) \quad (\text{B.40})$$

$$\begin{aligned}
&= -\frac{1}{12\epsilon} - \frac{49}{72} + \left( \frac{3\zeta_3}{2} - \frac{631}{108} - \frac{13\pi^2}{24} + \pi^2 \ln 2 \right) \epsilon + \left( \frac{97\pi^4}{120} \right. \\
&\quad \left. + \frac{23\pi^2 \ln 2}{6} - \frac{34255}{648} - \frac{\ln^4 2}{2} - \frac{779\pi^2}{144} - 12A_4 + \frac{13\zeta_3}{12} \right) \epsilon^2 \\
&+ \left( \frac{\ln^5 2}{10} - \frac{6722599}{15552} - \frac{23 \ln^4 2}{12} - \frac{14479\pi^2}{432} - 46A_4 - 12A_5 \right. \\
&\quad \left. + \frac{89\pi^2 \ln 2}{36} + \frac{7313\pi^4}{2160} - \frac{39\pi^4 \ln 2}{40} - \frac{4505\zeta_3}{72} + \frac{167\pi^2 \zeta_3}{8} \right. \\
&\quad \left. + \frac{5057\zeta_5}{16} \right) \epsilon^3 + \left( \frac{23 \ln^5 2}{60} + \frac{91447\pi^4}{25920} - \frac{211553\pi^2}{1296} - 46A_5 \right. \\
&\quad \left. - \frac{89}{3}A_4 - 12A_6 - 159H_6 - \frac{89 \ln^4 2}{72} - \frac{\ln^6 2}{60} - \frac{13627\pi^2 \ln 2}{216} \right. \\
&\quad \left. + \frac{2105\zeta_3^2}{8} + \frac{5241\zeta_5}{4} + \frac{35\pi^2 \ln^4 2}{8} - \frac{299\pi^4 \ln 2}{80} + \frac{12389\pi^6}{5040} \right. \\
&\quad \left. + \frac{27979\pi^2 \zeta_3}{288} + 105\pi^2 A_4 - \frac{311\pi^4 \ln^2 2}{80} + 45\pi^2 \zeta_3 \ln 2 \right. \\
&\quad \left. - \frac{292507159}{93312} - \frac{259637\zeta_3}{432} \right) \epsilon^4
\end{aligned}$$

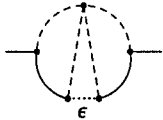
V55a



$$\text{Im T3ke}(0, 0, 1, 1, 1, 1, 1, 1, -1) / (\pi \mathcal{F}^4) \quad (\text{B.41})$$

$$\begin{aligned}
&= \left( \frac{35}{4} - \frac{\pi^2}{4} - \frac{\pi^4}{15} \right) \epsilon \\
&+ \left( \frac{1269}{8} - \frac{57\pi^2}{8} - \frac{4\pi^4}{15} - \frac{31\zeta_3}{2} + \frac{13\pi^2 \zeta_3}{3} - 94\zeta_5 \right) \epsilon^2 \\
&+ \left( \frac{27389}{16} - \frac{5401\pi^2}{48} - \frac{299\pi^4}{180} - \frac{163\pi^6}{1620} - \frac{597\zeta_3}{4} \right. \\
&\quad \left. + \frac{52\pi^2 \zeta_3}{3} + 6\zeta_3^2 - 376\zeta_5 \right) \epsilon^3
\end{aligned}$$

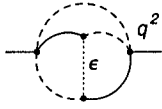
V80c



$$\text{Im } T3ie(0, 1, 1, 1, -1, 0, 1, 1, 0) / (\pi \mathcal{F}^4) \quad (\text{B.42})$$

$$\begin{aligned}
&= \left( \frac{31}{48} - \frac{11\zeta_3}{8} - \frac{10\pi^2}{9} + \frac{7\pi^2 \ln 2}{4} \right) \epsilon + \left( \frac{73 \ln 2 \pi^2}{12} + \frac{163\pi^4}{72} \right. \\
&\quad - 161A_4 - \frac{4775\pi^2}{432} + \frac{3331}{288} + \frac{35\pi^2 \ln^2 2}{6} - \frac{161 \ln^4 2}{24} \\
&\quad \left. - \frac{715\zeta_3}{8} \right) \epsilon^2 + \left( \frac{110561}{864} - \frac{1679}{3} A_4 - \frac{1679 \ln^4 2}{72} - 161A_5 \right. \\
&\quad + \frac{161 \ln^5 2}{120} - \frac{192857\pi^2}{2592} - \frac{85\pi^2 \ln 2}{36} + \frac{365\pi^2 \ln^2 2}{18} \\
&\quad - \frac{35\pi^2 \ln^3 2}{18} + \frac{18887\pi^4}{4320} + \frac{3199\pi^4 \ln 2}{720} - \frac{1665\zeta_3}{2} + \frac{397\pi^2 \zeta_3}{8} \\
&\quad \left. + \frac{18373\zeta_5}{32} \right) \epsilon^3 + \left( \frac{9443777}{5184} + \frac{2576}{9} A_4 - \frac{23}{3} A_5 - 23A_6 \right. \\
&\quad + \frac{837}{2} H_6 + \frac{322 \ln^4 2}{27} + \frac{23 \ln^5 2}{360} - \frac{23 \ln^6 2}{720} - \frac{1126049\pi^2}{15552} \\
&\quad + \frac{581\pi^2}{6} A_4 - \frac{2839\pi^2 \ln 2}{216} - \frac{280\pi^2 \ln^2 2}{27} + \frac{197\pi^2 \ln^4 2}{48} \\
&\quad - \frac{5\pi^2 \ln^3 2}{54} - \frac{288373\pi^4}{25920} + \frac{457\pi^4 \ln 2}{2160} + \frac{1829\pi^6}{36288} - \frac{9827\zeta_3}{24} \\
&\quad - \frac{2089\pi^4 \ln^2 2}{480} + \frac{5959\pi^2 \zeta_3}{96} + \frac{45\pi^2 \zeta_3 \ln 2}{4} + \frac{769\zeta_3^2}{16} \\
&\quad \left. - \frac{3433\zeta_5}{3} - \frac{3}{2} X_{45} \right) \epsilon^4
\end{aligned}$$

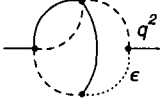
V45b



$$\text{Im T3be}(0, 1, 1, 1, 1, 1, -1, 0, 0) / (\pi \mathcal{F}^4) \quad (\text{B.43})$$

$$\begin{aligned}
&= -\frac{11}{24\epsilon} - \frac{197}{36} + \frac{\pi^2}{4} + \left( \frac{141\zeta_3}{8} - \frac{38273}{864} + \frac{3\pi^2}{16} + \frac{7\pi^2 \ln 2}{4} \right) \epsilon \\
&+ \left( \frac{1157\pi^4}{480} - \frac{786769}{2592} - \frac{7 \ln^4 2}{8} - \frac{385\pi^2}{72} + \frac{73\pi^2 \ln 2}{12} - 21A_4 \right. \\
&+ \left. \frac{1451\zeta_3}{24} \right) \epsilon^2 + \left( \frac{7 \ln^5 2}{40} - \frac{58965647}{31104} - \frac{71977\pi^2}{1728} - \frac{73 \ln^4 2}{24} \right. \\
&- \frac{85\pi^2 \ln 2}{36} + \frac{79547\pi^4}{8640} - \frac{273\pi^4 \ln 2}{160} + \frac{1177\zeta_3}{72} + \frac{1135\pi^2 \zeta_3}{32} \\
&+ \left. \frac{69323\zeta_5}{64} - 73A_4 - 21A_5 \right) \epsilon^3 + \left( \frac{317342731}{186624} - \frac{639301\pi^2}{10368} \right. \\
&+ \frac{14 \ln^4 2}{9} + \frac{\ln^5 2}{120} - \frac{\ln^6 2}{240} + \frac{112}{3} A_4 - A_5 - 3A_6 + \frac{105\pi^2}{4} A_4 \\
&- \frac{159}{4} H_6 - \frac{2839\pi^2 \ln 2}{216} + \frac{35\pi^2 \ln^4 2}{32} + \frac{2105\zeta_3^2}{32} - \frac{13\pi^4 \ln 2}{160} \\
&- \frac{311\pi^4 \ln^2 2}{320} + \frac{12389\pi^6}{20160} - \frac{206075\zeta_3}{432} - \frac{439081\pi^4}{51840} \\
&+ \left. \frac{505\pi^2 \zeta_3}{72} + \frac{45\pi^2 \zeta_3 \ln 2}{4} - \frac{30211\zeta_5}{64} - \frac{3}{2} X_{55} \right) \epsilon^4
\end{aligned}$$

V55b



## B.4 Three-loop eikonal topologies

$$\begin{aligned}
\text{E3} \quad & \int \frac{[d^D k_3][d^D k_4][d^D k_6] (2k_6 p)^{-a_9}}{(2k_3 p + i\delta)^{a_1} (2k_4 p + i\delta)^{a_2} k_3^{2a_3} (k_3 - k_4)^{2a_5}} \quad (\text{B.44}) \\
& \times \frac{1}{k_4^{2a_4} (k_6^2 + 1)^{a_6} [(k_3 + k_6)^2 + 1]^{a_7} [(k_4 + k_6)^2 + 1]^{a_8}}
\end{aligned}$$

$$\begin{aligned}
\text{E4} \quad & \int \frac{[d^D k_2][d^D k_7][d^D k_8] (2k_7 p)^{-a_9}}{(2k_2 p + i\delta)^{a_1} k_2^{2a_2} [(k_7 + k_8 + p) + 1]^{a_3} (k_8^2 + 2k_8 p)^{a_4}} \quad (\text{B.45}) \\
& \times \frac{1}{[(k_2 + k_7 + k_8 + p)^2 + 1]^{a_5} [(k_2 + k_8 + p)^2 + 1]^{a_6} k_7^{2a_7} k_8^{2a_8}}
\end{aligned}$$

## B.5 Three-loop eikonal master integrals

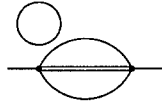
U1

$$\begin{aligned}
 & \text{E3}(0, 0, 0, 0, 0, 1, 1, 1, 0) / \mathcal{F}^3 \quad (\text{B.46}) \\
 & \begin{array}{c} \circ \\ \circ \\ \circ \end{array} = -\frac{1}{\epsilon^3} - \frac{3}{\epsilon^2} - \frac{6}{\epsilon} - 10 - 15\epsilon - 21\epsilon^2 - 28\epsilon^3
 \end{aligned}$$

$$\text{E3}(0, 1, 0, 0, 0, 1, 1, 1, 0) / (\mathcal{F}^3 \pi^2) \quad (\text{B.47})$$

$$\begin{aligned}
 & = \frac{16}{3} + \left( \frac{400}{9} - \frac{128 \ln 2}{3} \right) \epsilon + \left( \frac{6640}{27} + \frac{16\pi^2}{3} - \frac{3200 \ln 2}{9} \right. \\
 & \quad \left. + \frac{512 \ln^2 2}{3} \right) \epsilon^2 + \left( \frac{93520}{81} + \frac{400\pi^2}{9} - \frac{128\pi^2 \ln 2}{3} \right. \\
 & \quad \left. - \frac{53120 \ln 2}{27} + \frac{12800 \ln^2 2}{9} - \frac{4096 \ln^3 2}{9} - \frac{320\zeta_3}{3} \right) \epsilon^3 \\
 & \quad + \left( \frac{1217776}{243} + \frac{6640\pi^2}{27} - \frac{748160 \ln 2}{81} + \frac{32\pi^4}{5} - \frac{3200\pi^2 \ln 2}{9} \right. \\
 & \quad \left. + \frac{212480 \ln^2 2}{27} + \frac{512\pi^2 \ln^2 2}{3} - \frac{102400 \ln^3 2}{27} + \frac{8192 \ln^4 2}{9} \right. \\
 & \quad \left. - \frac{8000\zeta_3}{9} + \frac{2560\zeta_3 \ln 2}{3} \right) \epsilon^4
 \end{aligned}$$

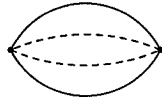
U2



$$\text{E3}(0, 0, 1, 1, 0, 0, 1, 1, 0) / \mathcal{F}^3 \quad (\text{B.48})$$

$$\begin{aligned}
 & = \frac{1}{3\epsilon^3} + \frac{7}{6\epsilon^2} + \frac{25}{12\epsilon} - \frac{5}{4} + \frac{8\zeta_3}{3} + \left( \frac{28\zeta_3}{3} - \frac{959}{48} - \frac{2\pi^4}{15} \right) \epsilon \\
 & \quad + \left( \frac{50\zeta_3}{3} - \frac{10493}{96} - \frac{7\pi^4}{15} + 48\zeta_5 \right) \epsilon^2 \\
 & \quad + \left( \frac{32\zeta_3^2}{3} - \frac{85175}{192} - \frac{5\pi^4}{6} - \frac{4\pi^6}{21} - \frac{5\zeta_3}{3} + 168\zeta_5 \right) \epsilon^3 \\
 & \quad + \left( \frac{\pi^4}{12} - \frac{610085}{384} - \frac{2\pi^6}{3} - \frac{959\zeta_3}{6} - \frac{16\pi^4\zeta_3}{15} + 300\zeta_5 \right. \\
 & \quad \left. + \frac{112\zeta_3^2}{3} + 664\zeta_7 \right) \epsilon^4
 \end{aligned}$$

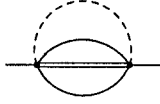
U3





$$E3(1, 0, 0, 1, 0, 0, 1, 1, 0) / (\mathcal{F}^3 \pi^2) \quad (B.49)$$

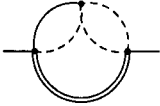
U4



$$\begin{aligned}
&= -\frac{1024}{45} \epsilon + \left( \frac{16384 \ln 2}{45} - \frac{223232}{675} \right) \epsilon^2 \\
&+ \left( \frac{3571712 \ln 2}{675} - \frac{31154176}{10125} - \frac{1024\pi^2}{15} - \frac{131072 \ln^2 2}{45} \right) \epsilon^3 \\
&+ \left( \frac{498466816 \ln 2}{10125} - \frac{3591815168}{151875} - \frac{223232\pi^2}{225} + \frac{16384\zeta_3}{9} \right. \\
&\quad \left. - \frac{28573696 \ln^2 2}{675} + \frac{2097152 \ln^3 2}{135} + \frac{16384\pi^2 \ln 2}{15} \right) \epsilon^4 \\
&+ \left( \frac{57469042688 \ln 2}{151875} - \frac{374934913024}{2278125} - \frac{31154176\pi^2}{3375} \right. \\
&\quad - \frac{131072\pi^4}{675} + \frac{3571712\pi^2 \ln 2}{225} - \frac{3987734528 \ln^2 2}{10125} \\
&\quad - \frac{131072\pi^2 \ln^2 2}{15} + \frac{457179136 \ln^3 2}{2025} - \frac{8388608 \ln^4 2}{135} \\
&\quad \left. + \frac{3571712\zeta_3}{135} - \frac{262144\zeta_3 \ln 2}{9} \right) \epsilon^5
\end{aligned}$$

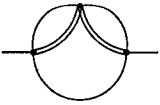
$$E3(0, 1, 1, 0, 1, 1, 0, 1, 0) / (\mathcal{F}^3 \pi^2) \quad (B.50)$$

U5



$$\begin{aligned}
&= -\frac{32}{3} + (128 \ln 2 - 128) \epsilon \\
&+ \left( 1536 \ln 2 - 1024 - \frac{320\pi^2}{9} - 768 \ln^2 2 \right) \epsilon^2 + \left( \frac{1280\pi^2 \ln 2}{3} \right. \\
&\quad \left. + 12288 \ln 2 - \frac{20992}{3} - \frac{1280\pi^2}{3} - 9216 \ln^2 2 + 3072 \ln^3 2 \right. \\
&\quad \left. + \frac{2048\zeta_3}{3} \right) \epsilon^3 + \left( 83968 \ln 2 - 44544 - \frac{10240\pi^2}{3} \right. \\
&\quad \left. + 5120\pi^2 \ln 2 - 73728 \ln^2 2 - 2560\pi^2 \ln^2 2 + 36864 \ln^3 2 \right. \\
&\quad \left. - 9216 \ln^4 2 + 8192\zeta_3 - 8192\zeta_3 \ln 2 - \frac{4864\pi^4}{45} \right) \epsilon^4
\end{aligned}$$

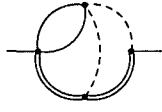
U6



$$E3(1, 1, 0, 0, 0, 1, 1, 1, 0) / (\mathcal{F}^3 \pi^2) \quad (B.51)$$

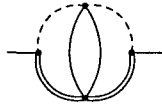
$$= -\frac{1}{6\epsilon} - \frac{5}{12} + \left( \frac{7}{8} + \frac{\pi^2}{6} \right) \epsilon + \left( \frac{599}{48} + \frac{5\pi^2}{12} - 8\zeta_3 \right) \epsilon^2$$

U7



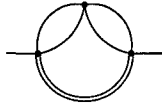
$$\begin{aligned} & \text{E3}(1, 1, 1, 0, 1, 1, 0, 1, 0) / \mathcal{F}^3 \quad (\text{B.52}) \\ &= -\frac{\pi^2}{9\epsilon^2} + \left( \frac{2\zeta_3}{3} - \frac{5\pi^2}{9} \right) \frac{1}{\epsilon} + \frac{10\zeta_3}{3} - \frac{19\pi^2}{9} - \frac{11\pi^4}{270} \\ &+ \left( \frac{38\zeta_3}{3} - \frac{65\pi^2}{9} - \frac{11\pi^4}{54} - \frac{8\pi^2\zeta_3}{9} + \frac{8\zeta_5}{3} \right) \epsilon \end{aligned}$$

U8



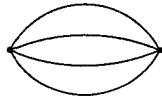
$$\begin{aligned} & \text{E3}(1, 1, 1, 1, 0, 0, 1, 1, 0) / \mathcal{F}^3 \quad (\text{B.53}) \\ &= -\frac{\pi^2}{9\epsilon^2} - \left( \frac{5\pi^2}{9} + \frac{4\zeta_3}{3} \right) \frac{1}{\epsilon} - \frac{19\pi^2}{9} - \frac{4\pi^4}{135} - \frac{20\zeta_3}{3} \\ &- \left( \frac{65\pi^2}{9} + \frac{4\pi^4}{27} + \frac{76\zeta_3}{3} + \frac{8\pi^2\zeta_3}{9} + \frac{16\zeta_5}{3} \right) \epsilon \\ &- \left( \frac{211\pi^2}{9} + \frac{76\pi^4}{135} - \frac{94\pi^6}{2835} + \frac{260\zeta_3}{3} + \frac{40\pi^2\zeta_3}{9} \right. \\ &\left. + \frac{32\zeta_3^2}{3} + \frac{80\zeta_5}{3} \right) \epsilon^2 \end{aligned}$$

U9



$$\begin{aligned} & \text{E4}(1, 0, 1, 1, 1, 1, 0, 0, 0) / (\mathcal{F}^3 \pi^2) \quad (\text{B.54}) \\ &= -\frac{32}{3} + \left( \frac{256 \ln 2}{3} - \frac{448}{3} - \frac{64\pi}{3} \right) \epsilon \end{aligned}$$

U0



$$\begin{aligned} & \text{E4}(0, 0, 1, 1, 1, 1, 0, 0, 0) / \mathcal{F}^3 \quad (\text{B.55}) \\ &= \frac{2}{\epsilon^3} + \frac{23}{3\epsilon^2} + \frac{35}{2\epsilon} + \frac{275}{12} + \left( \frac{112\zeta_3}{3} - \frac{189}{8} \right) \epsilon \\ &+ \left( 256A_4 - \frac{14917}{48} - \frac{136\pi^4}{45} - \frac{32\pi^2 \ln^2 2}{3} + 280\zeta_3 \right. \\ &\left. + \frac{32 \ln^4 2}{3} \right) \epsilon^2 + \left( 1920A_4 - \frac{48005}{32} + 1536A_5 - \frac{68\pi^4}{3} \right. \\ &\left. + \frac{272\pi^4 \ln 2}{15} - 80\pi^2 \ln^2 2 + 80 \ln^4 2 - \frac{64 \ln^5 2}{5} + \frac{64\pi^2 \ln^3 2}{3} \right. \\ &\left. + \frac{4060\zeta_3}{3} - 1240\zeta_5 \right) \epsilon^3 \end{aligned}$$

# Appendix C

## Semi-leptonic $b$ -quark decay results

### C.1 Integrated decay rate

The parameterization of results is according to Eq. 7.2. The one-gluon correction  $X_1$  is presented in Eq. 7.3, and the second-order correction  $X_2$  is parameterized as in Eq. 7.4. Through  $\mathcal{O}(\rho^7)$ , the results are

$$\begin{aligned}
 X_L = & -\frac{1009}{288} + \frac{8\zeta_3}{3} + \frac{77\pi^2}{216} + \left\{ \frac{118}{3} - \frac{4\pi^2}{3} + \frac{52}{3} \ln \rho - 8 \ln^2 \rho \right\} \rho^2 \quad (\text{C.1}) \\
 & + \left\{ \frac{64 \ln 2}{3} - \frac{112}{9} + \frac{32}{3} \ln \rho \right\} \pi^2 \rho^3 \\
 & + \left\{ 76\zeta_3 - \frac{5\pi^2}{3} - 33 + \left( 39 - \frac{16}{3}\pi^2 \right) \ln \rho + 52 \ln^2 \rho - 32 \ln^3 \rho \right\} \rho^4 \\
 & + \left\{ \frac{64 \ln 2}{3} - \frac{1216}{45} + \frac{32}{3} \ln \rho \right\} \pi^2 \rho^5 \\
 & + \left\{ \frac{344}{27} + \frac{28\pi^2}{27} - \frac{1564}{27} \ln \rho + 24 \ln^2 \rho \right\} \rho^6 + \frac{40}{21} \pi^2 \rho^7,
 \end{aligned}$$

$$\begin{aligned}
 X_C = & -\frac{1009}{288} + \frac{8\zeta_3}{3} + \frac{77\pi^2}{216} - \frac{5}{4} \pi^2 \rho \quad (\text{C.2}) \\
 & + \left\{ \frac{145}{3} + \frac{16\pi^2}{3} + \frac{52}{3} \ln \rho - 8 \ln^2 \rho \right\} \rho^2 + \left\{ \frac{569}{36} + \frac{64}{3} \ln \rho \right\} \pi^2 \rho^3 \\
 & + \left\{ 196\zeta_3 + \frac{\pi^2}{6} - \frac{4483}{36} + \left( \frac{599}{6} + \frac{74\pi^2}{3} \right) \ln \rho + 44 \ln^2 \rho - 32 \ln^3 \rho \right\} \rho^4 \\
 & + \left\{ \frac{50}{3} \ln \rho - \frac{172}{9} \right\} \pi^2 \rho^5 + \left\{ -\frac{33982}{225} - \frac{232\pi^2}{27} + \frac{11836}{135} \ln \rho \right. \\
 & \left. - \frac{64}{9} \ln^2 \rho \right\} \rho^6 + \left\{ \frac{44}{3} + 18 \ln \rho \right\} \pi^2 \rho^7,
 \end{aligned}$$

$$\begin{aligned}
X_H &= \frac{16987}{576} - \frac{64\zeta_3}{3} - \frac{85\pi^2}{216} + \left\{ \frac{8\pi^2}{3} - \frac{1198}{45} \right\} \rho^2 & (C.3) \\
&+ \left\{ \frac{156901877}{2116800} - \frac{11\pi^2}{18} - 64\zeta_3 - \left( \frac{186689}{2520} - \frac{20\pi^2}{3} \right) \ln \rho \right\} \rho^4 \\
&+ \left\{ \frac{189825233}{7144200} - \frac{52\pi^2}{27} - \frac{181627}{14175} \ln \rho + \frac{16}{5} \ln^2 \rho \right\} \rho^6 \\
&+ \left\{ \frac{629309}{1403325} - \frac{4\zeta_3}{3} + \frac{19\pi^2}{72} - \left( \frac{4741}{9072} + \frac{\pi^2}{9} \right) \ln \rho \right\} \rho^8,
\end{aligned}$$

$$\begin{aligned}
X_A &= \frac{11047}{2592} - \frac{223\zeta_3}{36} - \frac{515\pi^2}{81} + \frac{53\pi^2 \ln 2}{6} + \frac{67\pi^4}{720} & (C.4) \\
&+ \left\{ \frac{497\pi^2}{108} - \frac{2089}{8} + 86\zeta_3 - 8\pi^2 \ln 2 + \frac{121\pi^4}{540} - 105 \ln \rho - 36 \ln^2 \rho \right\} \rho^2 \\
&+ \left\{ \frac{752}{9} - \frac{112\pi}{3} \right\} \pi^2 \rho^3 + \left\{ \frac{16586}{27} - \frac{1139\pi^2}{24} - \frac{795\zeta_3}{2} + \frac{415\pi^2 \zeta_3}{3} \right. \\
&\quad - 4 \ln^4 2 + 935\zeta_5 - 96\text{Li}_4 \frac{1}{2} + 13\pi^2 \ln 2 - 8\pi^2 \ln^2 2 \\
&\quad - \left. \left( \frac{19459}{18} + \frac{71\pi^2}{3} - 246\zeta_3 + 60\pi^2 \ln 2 - \frac{40\pi^4}{3} \right) \ln \rho - 144 \ln^3 \rho \right. \\
&\quad + \left. (99 + 4\pi^2) \ln^2 \rho - \frac{349\pi^4}{72} \right\} \rho^4 + \left\{ \frac{67448}{675} - \frac{776\pi}{15} + 160 \ln \rho \right\} \pi^2 \rho^5 \\
&+ \left\{ \frac{4859\zeta_3}{12} - \frac{1732}{9} - \frac{14921\pi^2}{216} + \frac{89\pi^2 \ln 2}{6} - \frac{10\pi^4}{3} \right. \\
&\quad - \left. \left( \frac{3635}{18} + 136\zeta_3 - \frac{833\pi^2}{18} \right) \ln \rho + \left( \frac{1862}{9} - \frac{34\pi^2}{3} \right) \ln^2 \rho \right\} \rho^6 \\
&+ \left\{ \frac{86\pi}{7} - \frac{469304}{11025} + \frac{1376}{45} \ln \rho \right\} \pi^2 \rho^7,
\end{aligned}$$

$$\begin{aligned}
X_{NA} &= \frac{154927}{10368} - \frac{383\zeta_3}{72} + \frac{95\pi^2}{162} - \frac{53\pi^2 \ln 2}{12} + \frac{101\pi^4}{1440} & (C.5) \\
&+ \left\{ 4\pi^2 \ln 2 - \frac{1537}{16} - 43\zeta_3 - \frac{1181\pi^2}{216} + \frac{539\pi^4}{1080} - \frac{185}{3} \ln \rho + 22 \ln^2 \rho \right\} \rho^2 \\
&+ \left\{ \frac{556}{3} + \frac{56\pi}{3} - \frac{1136 \ln 2}{3} - \frac{124}{3} \ln \rho \right\} \pi^2 \rho^3 \\
&+ \left\{ \frac{727\pi^2}{48} - \frac{23807}{864} - \frac{535\zeta_5}{2} - \frac{615\zeta_3}{4} + 48\text{Li}_4 \frac{1}{2} + 2 \ln^4 2 - \frac{215\pi^2 \zeta_3}{6} \right. \\
&\quad - \frac{13\pi^2 \ln 2}{2} + 4\pi^2 \ln^2 2 + \frac{1777\pi^4}{720} + (5\pi^2 - 185) \ln^2 \rho + 88 \ln^3 \rho \\
&\quad + \left. \left( \frac{577}{36} - 39\zeta_3 - \frac{10\pi^4}{3} - 15\pi^2 + 30\pi^2 \ln 2 \right) \ln \rho \right\} \rho^4
\end{aligned}$$

$$\begin{aligned}
& + \left\{ \frac{140348}{675} - \frac{1136 \ln 2}{3} + \frac{388\pi}{15} - \frac{1492}{15} \ln \rho \right\} \pi^2 \rho^5 + \left\{ \frac{394001}{1296} + \frac{7\pi^4}{6} \right. \\
& + \frac{6509\pi^2}{144} - \frac{5435\zeta_3}{24} - \frac{89\pi^2 \ln 2}{12} + \left( \frac{4829}{72} + 80\zeta_3 - \frac{1037\pi^2}{36} \right) \ln \rho \\
& \left. - \left( 78 - \frac{20\pi^2}{3} \right) \ln^2 \rho \right\} \rho^6 + \left\{ \frac{461402}{33075} - \frac{43\pi}{7} - \frac{5072}{315} \ln \rho \right\} \pi^2 \rho^7.
\end{aligned}$$

## C.2 Moments of lepton energy distribution

The moments are defined as follows:

$$\langle \hat{E}_l^n \rangle = \int (E_l/m_b)^n d\Gamma, \quad (\text{C.6})$$

where  $E_l$  is the energy of the (massless) lepton in the rest frame of decaying  $b$ -quark, and integration is performed over the whole phase space of the decay products. Through  $\mathcal{O}(\rho^7)$ , the corrections to the first two moments are

$$\begin{aligned}
\langle \hat{E}_l^{1,2} \rangle &= \Gamma_0 \left( L_0^{(1,2)} + C_F \left( \frac{\alpha_s}{\pi} \right) L_1^{(1,2)} + C_F \left( \frac{\alpha_s}{\pi} \right)^2 L_2^{(1,2)} + \dots \right), \quad (\text{C.7}) \\
L_0^{(1)} &= \frac{7}{20} - \frac{15}{4} \rho^2 - (6 + 18 \ln \rho) \rho^4 + (10 - 6 \ln \rho) \rho^6, \\
L_1^{(1)} &= \frac{319}{300} - \frac{7\pi^2}{40} + \left( \frac{5\pi^2}{24} - \frac{301}{16} - \frac{45}{4} \ln \rho \right) \rho^2 + 8\pi^2 \rho^3 \\
&\quad - \left( \frac{1255}{12} + 6\pi^2 + 18 \ln \rho + 48 \ln^2 \rho \right) \rho^4 + \frac{328}{15} \pi^2 \rho^5 \\
&\quad - \left( \frac{3515}{36} + 2\pi^2 - \frac{238}{3} \ln \rho + 24 \ln^2 \rho \right) \rho^6, \\
L_0^{(2)} &= \frac{2}{15} - \frac{9}{5} \rho^2 - \left( \frac{13}{2} + 12 \ln \rho \right) \rho^4 + (8 - 8 \ln \rho) \rho^6, \\
L_1^{(2)} &= \frac{59}{150} - \frac{\pi^2}{15} - \left( \frac{24061}{2400} - \frac{7\pi^2}{40} + \frac{27}{5} \ln \rho \right) \rho^2 + 4\pi^2 \rho^3 \\
&\quad - \left( \frac{22223}{288} + \frac{49\pi^2}{12} + \frac{737}{24} \ln \rho + 30 \ln^2 \rho \right) \rho^4 + \frac{104}{5} \pi^2 \rho^5 \\
&\quad - \left( \frac{22775}{216} + \frac{34}{9} \pi^2 - \frac{1259}{18} \ln \rho + \frac{104}{3} \ln^2 \rho \right) \rho^6 + \frac{44}{15} \pi^2 \rho^7, \\
L_2^{(1,2)} &= T_R \left( N_L L_L^{(1,2)} + N_H L_H^{(1,2)} + N_C L_C^{(1,2)} \right) + C_F L_A^{(1,2)} + C_A L_{NA}^{(1,2)}.
\end{aligned}$$

$$\begin{aligned}
L_A^{(1)} = & -\frac{4166983}{10368000} + \frac{2971\zeta_3}{2400} - \frac{10471499\pi^2}{5184000} + \frac{4481\pi^2 \ln 2}{1800} + \frac{469\pi^4}{14400} \quad (C.8) \\
& + \left\{ \frac{3833\pi^2}{864} - \frac{10399277}{62208} + \frac{1885\zeta_3}{36} - \frac{19\pi^2 \ln 2}{4} + \frac{533\pi^4}{2880} \right. \\
& \left. - \left( \frac{1851}{32} - \frac{5\pi^2}{8} \right) \ln \rho - \frac{135}{8} \ln^2 \rho \right\} \rho^2 + \left\{ \frac{533}{12} - \frac{56\pi}{3} \right\} \pi^2 \rho^3 \\
& + \left\{ \frac{2805\zeta_5}{4} - \frac{93943}{3456} - \frac{2381\zeta_3}{12} - 100 \operatorname{Li}_4 \frac{1}{2} - \frac{25 \ln^4 2}{6} - \frac{72059\pi^2}{1728} \right. \\
& + \frac{415\pi^2 \zeta_3}{4} - \frac{31\pi^2 \ln 2}{3} - \frac{22\pi^2 \ln^2 2}{3} + \frac{67\pi^4}{270} + \left( 5\pi^2 - \frac{2813}{48} \right) \ln^2 \rho \\
& \left. + \left( \frac{437\zeta_3}{2} - \frac{28227}{32} - \frac{141\pi^2}{16} - 49\pi^2 \ln 2 + 10\pi^4 \right) \ln \rho - 96 \ln^3 \rho \right\} \rho^4 \\
& + \left\{ \frac{808049}{4500} - \frac{15428\pi}{225} + \frac{1298}{9} \ln \rho \right\} \pi^2 \rho^5 + \left\{ \frac{5397469}{86400} - \frac{43879\pi^2}{576} \right. \\
& + \frac{46835\zeta_3}{144} - 76 \operatorname{Li}_4 \frac{1}{2} - \frac{19 \ln^4 2}{6} + \frac{935\zeta_5}{4} + \frac{415\pi^2 \zeta_3}{12} + \frac{1225\pi^2 \ln 2}{36} \\
& \left. - \frac{1999\pi^4}{360} + \left( \frac{7111\pi^2}{144} - \frac{2006251}{4320} + \frac{71\zeta_3}{12} - \frac{56\pi^2 \ln 2}{3} + \frac{10\pi^4}{3} \right) \ln \rho \right. \\
& \left. + \left( \frac{43027}{144} - \frac{59\pi^2}{12} \right) \ln^2 \rho - \frac{841}{12} \ln^3 \rho \right\} \rho^6 \\
& - \left\{ \frac{305663}{18900} - \frac{736}{15} \ln \rho + \frac{23\pi}{9} \right\} \pi^2 \rho^7,
\end{aligned}$$

$$\begin{aligned}
L_C^{(1)} = & -\frac{22339}{12000} + \frac{14\zeta_3}{15} + \frac{869\pi^2}{4320} - \frac{21\pi^2}{40} \rho + \left\{ \frac{289889}{8640} + \frac{4217\pi^2}{2592} \right. \quad (C.9) \\
& \left. - \frac{10\zeta_3}{9} + \frac{65}{8} \ln \rho - \frac{15}{4} \ln^2 \rho \right\} \rho^2 + \left\{ \frac{677}{72} + \frac{32}{3} \ln \rho \right\} \pi^2 \rho^3 \\
& + \left\{ \frac{436\zeta_3}{3} + \frac{233\pi^2}{27} - \frac{22627}{864} + \left( \frac{1107}{10} + \frac{49\pi^2}{3} \right) \ln \rho + \frac{341}{20} \ln^2 \rho \right. \\
& \left. - \frac{64}{3} \ln^3 \rho \right\} \rho^4 - \left\{ \frac{1045}{108} - \frac{1141}{45} \ln \rho \right\} \pi^2 \rho^5 + \left\{ 70\zeta_3 - \frac{4740833}{18000} \right. \\
& \left. - \frac{10847\pi^2}{1080} + \left( \frac{770687}{5400} + 6\pi^2 \right) \ln \rho - \frac{2999}{90} \ln^2 \rho - \frac{14}{3} \ln^3 \rho \right\} \rho^6 \\
& + \left\{ \frac{23}{3} + 9 \ln \rho \right\} \pi^2 \rho^7,
\end{aligned}$$

$$\begin{aligned}
L_{NA}^{(1)} = & \frac{254191031}{41472000} - \frac{1699\zeta_3}{480} + \frac{40667\pi^2}{518400} - \frac{4481\pi^2 \ln 2}{3600} + \frac{707\pi^4}{28800} \quad (C.10) \\
& + \left\{ \frac{1921\pi^4}{17280} - \frac{1397029}{31104} - \frac{2119\zeta_3}{96} - \frac{9049\pi^2}{5184} + \frac{19\pi^2 \ln 2}{8} - \frac{925}{32} \ln \rho \right. \\
& \left. + \frac{165}{16} \ln^2 \rho \right\} \rho^2 + \left\{ \frac{6577}{72} - \frac{568 \ln 2}{3} + \frac{28\pi}{3} - \frac{62}{3} \ln \rho \right\} \pi^2 \rho^3 \\
& + \left\{ \frac{25 \ln^4 2}{12} - \frac{31577}{384} - \frac{1605\zeta_5}{8} - \frac{7529\zeta_3}{48} + 50\text{Li}_4 \frac{1}{2} - \frac{7549\pi^2}{3456} + \frac{191\pi^4}{216} \right. \\
& + \frac{31\pi^2 \ln 2}{6} + \frac{11\pi^2 \ln^2 2}{3} - \frac{215\pi^2 \zeta_3}{8} + \left( \frac{19\pi^2}{12} - \frac{2785}{32} \right) \ln^2 \rho \\
& \left. - \left( \frac{7283}{192} + \frac{239\zeta_3}{4} + \frac{5\pi^4}{2} + \frac{383\pi^2}{32} - \frac{49\pi^2 \ln 2}{2} \right) \ln \rho + \frac{365}{6} \ln^3 \rho \right\} \rho^4 \\
& + \left\{ \frac{502243}{1800} - \frac{120664 \ln 2}{225} + \frac{7714\pi}{225} - \frac{325}{3} \ln \rho \right\} \pi^2 \rho^5 \\
& + \left\{ \frac{86452559}{259200} - \frac{41119\zeta_3}{144} - \frac{535\zeta_5}{8} - \frac{1225\pi^2 \ln 2}{72} + 38 \text{Li}_4 \frac{1}{2} - \frac{215\pi^2 \zeta_3}{24} \right. \\
& + \left( \frac{665431}{8640} + \frac{104\zeta_3}{3} - \frac{8305\pi^2}{216} + \frac{28\pi^2 \ln 2}{3} - \frac{5\pi^4}{6} \right) \ln \rho + \frac{425}{12} \ln^3 \rho \\
& \left. - \left( \frac{5089}{32} - \frac{209\pi^2}{36} \right) \ln^2 \rho + \frac{135677\pi^2}{2592} + \frac{19 \ln^4 2}{12} + \frac{3293\pi^4}{2160} \right\} \rho^6 \\
& + \left\{ \frac{367559}{37800} + \frac{23\pi}{18} - \frac{368}{15} \ln \rho \right\} \pi^2 \rho^7,
\end{aligned}$$

$$\begin{aligned}
L_L^{(1)} = & -\frac{22339}{12000} + \frac{14\zeta_3}{15} + \frac{869\pi^2}{4320} + \left\{ \frac{47977}{1728} - \frac{3451\pi^2}{2592} + \frac{65}{8} \ln \rho \right. \quad (C.11) \\
& \left. - \frac{15}{4} \ln^2 \rho - \frac{10\zeta_3}{9} \right\} \rho^2 + \left\{ \frac{32 \ln 2}{3} - \frac{56}{9} + \frac{16}{3} \ln \rho \right\} \pi^2 \rho^3 + \left\{ \frac{6961}{216} \right. \\
& \left. + 48\zeta_3 - \frac{23\pi^2}{36} + \left( \frac{2225}{36} - \frac{11\pi^2}{2} \right) \ln \rho + \frac{68}{3} \ln^2 \rho - \frac{68}{3} \ln^3 \rho \right\} \rho^4 \\
& + \left\{ \frac{1312 \ln 2}{45} - \frac{23648}{675} + \frac{656}{45} \ln \rho \right\} \pi^2 \rho^5 + \left\{ \frac{157}{36} + 16\zeta_3 + \frac{275\pi^2}{108} \right. \\
& \left. - \left( \frac{7631}{108} + \frac{11\pi^2}{6} \right) \ln \rho + 55 \ln^2 \rho - \frac{34}{3} \ln^3 \rho \right\} \rho^6 - \frac{4}{3} \pi^2 \rho^7,
\end{aligned}$$

$$\begin{aligned}
L_H^{(1)} = & \frac{183544301}{12960000} - \frac{32\zeta_3}{3} - \frac{2959\pi^2}{21600} + \left\{ \frac{3269\pi^2}{2592} - \frac{12888643}{1555200} \right. \quad (C.12) \\
& \left. - \frac{32\zeta_3}{9} \right\} \rho^2 + \left\{ \frac{223106533}{6048000} - \left( \frac{385801}{7200} - 5\pi^2 \right) \ln \rho - 44\zeta_3 \right. \\
& \left. + \frac{79\pi^2}{72} \right\} \rho^4 + \left\{ \frac{50963353921}{1143072000} - \frac{44\zeta_3}{3} - \frac{521\pi^2}{216} + \frac{28}{15} \ln^2 \rho \right. \\
& \left. - \left( \frac{9167647}{453600} - \frac{10\pi^2}{9} \right) \ln \rho \right\} \rho^6.
\end{aligned}$$

$$\begin{aligned}
L_A^{(2)} &= \frac{2243831419}{3110400000} + \frac{193\zeta_3}{400} - \frac{13810213\pi^2}{12960000} + \frac{751\pi^2 \ln 2}{600} & (C.13) \\
&+ \frac{67\pi^4}{5400} + \left\{ \frac{8327\zeta_3}{300} - \frac{14297393}{144000} + \frac{10078087\pi^2}{5184000} - \frac{1111\pi^2 \ln 2}{600} \right. \\
&\quad \left. + \frac{18719\pi^4}{86400} - \left( \frac{24601}{800} - \frac{21\pi^2}{40} \right) \ln \rho - \frac{81}{10} \ln^2 \rho \right\} \rho^2 \\
&+ \left\{ \frac{42041}{1800} - \frac{28\pi}{3} \right\} \pi^2 \rho^3 + \left\{ \frac{935\zeta_5}{2} - \frac{736761143}{2488320} - \frac{1979683\pi^2}{64800} \right. \\
&\quad \left. - \frac{8587\zeta_3}{120} + \frac{24859\pi^4}{10800} - \frac{1309\pi^2 \ln 2}{90} - 112 \operatorname{Li}_4 \frac{1}{2} - \frac{14 \ln^4 2}{3} \right. \\
&\quad \left. + \frac{415\pi^2 \zeta_3}{6} - \frac{16\pi^2 \ln^2 2}{3} - \left( \frac{37703}{400} - 4\pi^2 \right) \ln^2 \rho - 60 \ln^3 \rho \right. \\
&\quad \left. + \left( 165\zeta_3 + \frac{11\pi^2}{15} - \frac{19945373}{28800} - 34\pi^2 \ln 2 + \frac{20\pi^4}{3} \right) \ln \rho \right\} \rho^4 \\
&+ \left\{ \frac{152381}{750} - \frac{1658\pi}{25} + \frac{337}{3} \ln \rho \right\} \pi^2 \rho^5 + \left\{ \frac{4314339253}{77760000} + \frac{4301\zeta_5}{10} \right. \\
&\quad \left. + \frac{174697\zeta_3}{720} - \frac{1064}{5} \operatorname{Li}_4 \frac{1}{2} - \frac{133 \ln^4 2}{15} - \frac{929239\pi^2}{10800} + \frac{4543\pi^2 \ln 2}{120} \right. \\
&\quad \left. + \frac{1909\pi^2 \zeta_3}{30} + \frac{26\pi^2 \ln^2 2}{15} - \frac{20483\pi^4}{5400} + \left( \frac{205769}{900} + \frac{31\pi^2}{180} \right) \ln^2 \rho \right. \\
&\quad \left. + \left( \frac{1511\zeta_3}{12} + \frac{102913\pi^2}{2160} - \frac{135412429}{216000} - \frac{76\pi^2 \ln 2}{3} + \frac{92\pi^4}{15} \right) \ln \rho \right. \\
&\quad \left. - \frac{10927}{108} \ln^3 \rho \right\} \rho^6 + \left\{ \frac{152734133}{3307500} - \frac{92497\pi}{3150} + \frac{17179}{225} \ln \rho \right\} \pi^2 \rho^7, \\
L_L^{(2)} &= -\frac{2860547}{3888000} + \frac{16\zeta_3}{45} + \frac{2711\pi^2}{32400} + \left\{ \frac{6639137}{432000} - \frac{3323\pi^2}{4320} \right. & (C.14) \\
&\quad \left. - \frac{14\zeta_3}{15} + \frac{39}{10} \ln \rho - \frac{9}{5} \ln^2 \rho \right\} \rho^2 + \left\{ \frac{16 \ln 2}{3} - \frac{28}{9} + \frac{8}{3} \ln \rho \right\} \pi^2 \rho^3 \\
&+ \left\{ \frac{118639}{2304} + \frac{563\zeta_3}{18} - \frac{2659\pi^2}{12960} + \left( \frac{22837}{432} - \frac{139\pi^2}{36} \right) \ln \rho + \frac{26}{3} \ln^2 \rho \right. \\
&\quad \left. - \frac{44}{3} \ln^3 \rho \right\} \rho^4 + \left\{ -\frac{7484}{225} + \frac{416 \ln 2}{15} + \frac{208}{15} \ln \rho \right\} \pi^2 \rho^5 \\
&+ \left\{ \frac{38879}{3888} + 29\zeta_3 + \frac{562\pi^2}{135} - \left( \frac{5477}{108} + \frac{71\pi^2}{27} \right) \ln \rho + \frac{548}{9} \ln^2 \rho \right. \\
&\quad \left. - \frac{424}{27} \ln^3 \rho \right\} \rho^6 + \left\{ -\frac{43894}{4725} + \frac{176 \ln 2}{45} + \frac{88}{45} \ln \rho \right\} \pi^2 \rho^7,
\end{aligned}$$



$$\begin{aligned}
L_{NA}^{(2)} = & \frac{11889210281}{6220800000} - \frac{6481\zeta_3}{4800} + \frac{360197\pi^2}{2160000} - \frac{751\pi^2 \ln 2}{1200} + \frac{101\pi^4}{10800} \quad (C.15) \\
+ & \left\{ \frac{105797\pi^2}{1728000} - \frac{4476829}{216000} - \frac{100079\zeta_3}{9600} + \frac{1111\pi^2 \ln 2}{1200} - \frac{2317\pi^4}{57600} \right. \\
& - \frac{111}{8} \ln \rho + \frac{99}{20} \ln^2 \rho \left. \right\} \rho^2 + \left\{ \frac{162359}{3600} - \frac{284 \ln 2}{3} + \frac{14\pi}{3} \right. \\
& - \left. \frac{31}{3} \ln \rho \right\} \pi^2 \rho^3 + \left\{ \frac{7 \ln^4 2}{3} - \frac{199241813}{2488320} - \frac{101091\pi^2}{12800} - \frac{535\zeta_5}{4} \right. \\
& - \frac{8029\zeta_3}{60} + 56 \operatorname{Li}_4 \frac{1}{2} - \frac{215\pi^2 \zeta_3}{12} + \frac{1309\pi^2 \ln 2}{180} + \frac{8\pi^2 \ln^2 2}{3} - \frac{73\pi^4}{7200} \\
& + \left( 17\pi^2 \ln 2 - \frac{6261931}{172800} - 54\zeta_3 - \frac{28543\pi^2}{2880} - \frac{5\pi^4}{3} \right) \ln \rho \\
& + \frac{233}{6} \ln^3 \rho + \left( \frac{\pi^2}{3} - \frac{91541}{2400} \right) \ln^2 \rho \left. \right\} \rho^4 + \left\{ \frac{699899}{2700} - \frac{39032 \ln 2}{75} \right. \\
& + \left. \frac{829\pi}{25} - \frac{951}{10} \ln \rho \right\} \pi^2 \rho^5 + \left\{ \frac{45759868247}{155520000} - \frac{2461\zeta_5}{20} - \frac{24617\zeta_3}{80} \right. \\
& + \frac{532}{5} \operatorname{Li}_4 \frac{1}{2} + \frac{133 \ln^4 2}{30} + \frac{11752123\pi^2}{259200} - \frac{989\pi^2 \zeta_3}{60} - \frac{4543\pi^2 \ln 2}{240} \\
& - \frac{13\pi^2 \ln^2 2}{15} + \frac{1049\pi^4}{1200} + \left( \frac{769\pi^2}{180} - \frac{585113}{3600} \right) \ln^2 \rho + \frac{10669}{216} \ln^3 \rho \\
& + \left. \left( \frac{26790779}{432000} - \frac{1873\zeta_3}{120} - \frac{18041\pi^2}{432} + \frac{38\pi^2 \ln 2}{3} - \frac{23\pi^4}{15} \right) \ln \rho \right\} \rho^6 \\
+ & \left\{ \frac{10396613}{245000} - \frac{131687}{3150} \ln \rho - \frac{17732 \ln 2}{225} + \frac{92497\pi}{6300} \right\} \pi^2 \rho^7,
\end{aligned}$$

$$\begin{aligned}
L_C^{(2)} = & -\frac{2860547}{3888000} + \frac{16\zeta_3}{45} + \frac{2711\pi^2}{32400} - \frac{7}{30} \pi^2 \rho + \left\{ \frac{8115737}{432000} \right. \quad (C.16) \\
& - \left. \frac{14\zeta_3}{15} + \frac{12869\pi^2}{21600} + \frac{39}{10} \ln \rho - \frac{9}{5} \ln^2 \rho \right\} \rho^2 + \left\{ \frac{2801}{540} + \frac{16}{3} \ln \rho \right\} \pi^2 \rho^3 \\
+ & \left\{ \frac{190411}{11520} + \frac{1763\zeta_3}{18} + \frac{2855\pi^2}{324} + \left( \frac{184727}{2160} + \frac{187\pi^2}{18} \right) \ln \rho + \frac{13}{2} \ln^2 \rho \right. \\
& - \left. \frac{40}{3} \ln^3 \rho \right\} \rho^4 + \left\{ -\frac{259}{72} + \frac{343}{15} \ln \rho \right\} \pi^2 \rho^5 + \left\{ \frac{4049\zeta_3}{45} - \frac{44096992}{151875} \right. \\
& - \frac{28061\pi^2}{3240} + \left( \frac{9184187}{81000} + \frac{1433\pi^2}{270} \right) \ln \rho - \frac{74923}{1350} \ln^2 \rho \\
& - \left. \frac{604}{135} \ln^3 \rho \right\} \rho^6 + \left\{ \frac{779}{216} + \frac{413}{45} \ln \rho \right\} \pi^2 \rho^7,
\end{aligned}$$

$$\begin{aligned}
L_H^{(2)} &= \frac{268942501}{38880000} - \frac{16\zeta_3}{3} - \frac{1117\pi^2}{21600} + \left\{ \frac{1451\pi^2}{2400} - \frac{8658049}{1440000} \right\} \rho^2 \quad (\text{C.17}) \\
&+ \left\{ \frac{2299\pi^2}{1620} - \frac{1409209633}{95256000} - \frac{16\zeta_3}{9} + \left( \frac{10\pi^2}{3} - \frac{49107}{1400} \right) \ln \rho \right\} \rho^4 \\
&+ \left\{ \frac{663872846659}{17146080000} - \frac{664\zeta_3}{45} - \frac{6599\pi^2}{3240} + \frac{16}{15} \ln^2 \rho \right. \\
&\quad \left. + \left( \frac{14\pi^2}{9} - \frac{147148321}{6804000} \right) \ln \rho \right\} \rho^6.
\end{aligned}$$

### C.3 Moments of hadronic energy distribution

Hadronic energy moments are defined similarly to Eq. C.6,

$$\langle \hat{E}_h^n \rangle = \int (E_h/m_b)^n d\Gamma, \quad (\text{C.18})$$

where  $E_h$  is the total energy of hadrons (quarks and gluons) in the rest frame of  $b$ -quark. The corrections to the first two moments are

$$\begin{aligned}
\langle \hat{E}_h^{1,2} \rangle &= \Gamma_0 \left( H_0^{(1,2)} + C_F \left( \frac{\alpha_s}{\pi} \right) H_1^{(1,2)} + C_F \left( \frac{\alpha_s}{\pi} \right)^2 H_2^{(1,2)} + \dots \right), \quad (\text{C.19}) \\
H_0^{(1)} &= \frac{7}{20} - \frac{5}{4} \rho^2 + (8 + 6 \ln \rho) \rho^4 - (8 - 6 \ln \rho) \rho^6, \\
H_1^{(1)} &= \frac{1381}{1200} - \frac{7\pi^2}{40} - \left( \frac{31}{48} + \frac{5}{24} \pi^2 + \frac{15}{4} \ln \rho \right) \rho^2 \\
&+ \left( \frac{2009}{36} + 4\pi^2 + \frac{158}{3} \ln \rho + 18 \ln^2 \rho \right) \rho^4 - \frac{352}{15} \pi^2 \rho^5 \\
&+ \left( \frac{665}{6} + 4\pi^2 - \frac{278}{3} \ln \rho + 34 \ln^2 \rho \right) \rho^6, \\
H_0^{(2)} &= \frac{2}{15} - \frac{\rho^2}{5} - 2\rho^4 - 8\rho^6 \ln \rho, \\
H_1^{(2)} &= \frac{2257}{4800} - \frac{\pi^2}{15} + \left( \frac{2731}{2400} - \frac{3\pi^2}{20} - \frac{3}{5} \ln \rho \right) \rho^2 \\
&- \left( \frac{12335}{576} + \frac{271}{24} \ln \rho \right) \rho^4 + \frac{48}{5} \pi^2 \rho^5 \\
&- \left( \frac{16661}{216} + \frac{52\pi^2}{9} - \frac{275}{18} \ln \rho + \frac{116}{3} \ln^2 \rho \right) \rho^6 + \frac{48}{5} \pi^2 \rho^7, \\
H_2^{(1,2)} &= T_R \left( N_L H_L^{(1,2)} + N_H H_H^{(1,2)} + N_C H_C^{(1,2)} \right) + C_F H_A^{(1,2)} + C_A H_{NA}^{(1,2)}.
\end{aligned}$$

$$\begin{aligned}
H_A^{(1)} &= \frac{1923913}{192000} - \frac{11069\zeta_3}{900} - \frac{3459451\pi^2}{1296000} + \frac{7621\pi^2 \ln 2}{1800} + \frac{469\pi^4}{14400} \quad (C.20) \\
&+ \left\{ \frac{477455}{10368} - \frac{683\zeta_3}{36} - \frac{8387\pi^2}{1296} + \frac{101\pi^2 \ln 2}{72} + \frac{521\pi^4}{1728} - \frac{45}{8} \ln^2 \rho \right. \\
&- \left. \left( \frac{77}{32} + \frac{5\pi^2}{8} \right) \ln \rho \right\} \rho^2 - \frac{71}{9} \pi^2 \rho^3 + \left\{ \frac{5846795}{10368} - \frac{1683\zeta_5}{4} \right. \\
&+ \frac{371\zeta_3}{12} + 192 \operatorname{Li}_4 \frac{1}{2} + 8 \ln^4 2 + \frac{22969\pi^2}{576} - \frac{249\pi^2 \zeta_3}{4} + \frac{131\pi^2 \ln 2}{6} \\
&+ 2\pi^2 \ln^2 2 - \frac{24541\pi^4}{4320} + (175 - 3\pi^2) \ln^2 \rho + 36 \ln^3 \rho \\
&+ \left. \left( \frac{446473}{864} - \frac{299\zeta_3}{2} + \frac{751\pi^2}{144} + 19\pi^2 \ln 2 - 6\pi^4 \right) \ln \rho \right\} \rho^4 \\
&+ \left\{ \frac{16592\pi}{225} - \frac{256859}{1125} - \frac{1112}{9} \ln \rho \right\} \pi^2 \rho^5 + \left\{ \frac{67 \ln^4 2}{6} - \frac{4900411}{21600} \right. \\
&- 6\pi^2 \ln^2 2 - \frac{1811\zeta_3}{9} + 268 \operatorname{Li}_4 \frac{1}{2} + \frac{108127\pi^2}{1296} - \frac{1603\pi^2 \ln 2}{36} \\
&- \frac{249\pi^2 \zeta_3}{4} - \frac{1683\zeta_5}{4} + \frac{20467\pi^4}{4320} - \left. \left( \frac{6503}{18} + \frac{17\pi^2}{18} \right) \ln^2 \rho \right. \\
&+ \left. \left( \frac{1216693}{2160} - \frac{437\zeta_3}{3} - \frac{9085\pi^2}{216} + \frac{50\pi^2 \ln 2}{3} - 6\pi^4 \right) \ln \rho \right. \\
&+ \left. \frac{959}{9} \ln^3 \rho \right\} \rho^6 + \left\{ \frac{152\pi}{9} - \frac{7213}{4725} - \frac{288}{5} \ln \rho \right\} \pi^2 \rho^7, \\
H_L^{(1)} &= -\frac{587}{216000} + \frac{14\zeta_3}{15} - \frac{91\pi^2}{4320} + \left\{ \frac{10\zeta_3}{9} - \frac{1903}{192} + \frac{2299\pi^2}{2592} \right. \quad (C.21) \\
&+ \left. \frac{65}{24} \ln \rho - \frac{5}{4} \ln^2 \rho \right\} \rho^2 - \left\{ \frac{8237}{108} + 20\zeta_3 + \frac{11\pi^2}{4} - 3 \ln^2 \rho \right. \\
&- 8 \ln^3 \rho - \left. \left( \frac{67\pi^2}{18} - \frac{7907}{108} \right) \ln \rho \right\} \rho^4 + \left\{ \frac{25472\pi^2}{675} - \frac{1408\pi^2 \ln 2}{45} \right. \\
&- \left. \frac{704\pi^2}{45} \ln \rho \right\} \rho^5 + \left\{ \frac{5317}{324} - \frac{98\zeta_3}{3} - \frac{437\pi^2}{108} - \frac{187}{3} \ln^2 \rho \right. \\
&+ \left. \left( \frac{6673}{108} + \frac{29\pi^2}{18} \right) \ln \rho + \frac{122}{9} \ln^3 \rho \right\} \rho^6 + \frac{32}{9} \pi^2 \rho^7, \\
H_H^{(1)} &= \frac{5935307}{4320000} - \frac{1013\pi^2}{7200} + \left\{ \frac{32\zeta_3}{9} - \frac{12976493}{1555200} + \frac{1051\pi^2}{2592} \right\} \rho^2 \quad (C.22) \\
&+ \left\{ \frac{70247839}{18144000} + \frac{40\zeta_3}{3} - \frac{409\pi^2}{216} + \left( \frac{118439}{7200} - \frac{5\pi^2}{3} \right) \ln \rho \right\} \rho^4 \\
&+ \left\{ \frac{76\zeta_3}{3} - \frac{55527105509}{1143072000} + \frac{137\pi^2}{72} \right. \\
&+ \left. \left( \frac{5891303}{453600} - \frac{8\pi^2}{9} \right) \ln \rho - \frac{4}{5} \ln^2 \rho \right\} \rho^6,
\end{aligned}$$

$$\begin{aligned}
H_{NA}^{(1)} &= \frac{888707}{864000} + \frac{763\zeta_3}{240} + \frac{4523\pi^2}{9600} - \frac{7621\pi^2 \ln 2}{3600} + \frac{707\pi^4}{28800} \quad (C.23) \\
&+ \left\{ \frac{4423\pi^2}{5184} - \frac{111587}{5184} + \frac{41\zeta_3}{8} - \frac{101\pi^2 \ln 2}{144} + \frac{127\pi^4}{3456} - \frac{925}{96} \ln \rho \right. \\
&+ \left. \frac{55}{16} \ln^2 \rho \right\} \rho^2 + \frac{71}{18} \pi^2 \rho^3 + \left\{ \frac{653675}{6912} + \frac{963\zeta_5}{8} + \frac{3157\zeta_3}{24} - 96 \operatorname{Li}_4 \frac{1}{2} \right. \\
&- 4 \ln^4 2 + \frac{74909\pi^2}{3456} + \frac{129\pi^2 \zeta_3}{8} - \frac{131\pi^2 \ln 2}{12} - \pi^2 \ln^2 2 + \frac{6749\pi^4}{8640} \\
&+ \left( \frac{138511}{1728} + \frac{263\zeta_3}{4} + \frac{1633\pi^2}{288} - \frac{19\pi^2 \ln 2}{2} + \frac{3\pi^4}{2} \right) \ln \rho - 22 \ln^3 \rho \\
&+ \left( \frac{3\pi^2}{4} - \frac{41}{8} \right) \ln^2 \rho \left. \right\} \rho^4 + \left\{ \frac{141856 \ln 2}{225} - \frac{434371}{1350} - \frac{8296\pi}{225} \right. \\
&+ \left. \frac{1604}{15} \ln \rho \right\} \pi^2 \rho^5 + \left\{ -\frac{753878}{2025} + \frac{963\zeta_5}{8} + \frac{21725\zeta_3}{72} - 134 \operatorname{Li}_4 \frac{1}{2} \right. \\
&- \frac{67 \ln^4 2}{12} - \frac{35077\pi^2}{648} + \frac{129\pi^2 \zeta_3}{8} + \frac{1603\pi^2 \ln 2}{72} + 3\pi^2 \ln^2 2 \\
&- \frac{1271\pi^4}{1728} + \left( \frac{13229}{72} - \frac{40\pi^2}{9} \right) \ln^2 \rho - \frac{428}{9} \ln^3 \rho \\
&+ \left( \frac{18919\pi^2}{432} - \frac{190883}{4320} + \frac{58\zeta_3}{3} - \frac{25\pi^2 \ln 2}{3} + \frac{3\pi^4}{2} \right) \ln \rho \left. \right\} \rho^6 \\
&- \left\{ \frac{58627}{9450} + \frac{76\pi}{9} - \frac{144}{5} \ln \rho \right\} \pi^2 \rho^7,
\end{aligned}$$

$$\begin{aligned}
H_C^{(1)} &= -\frac{587}{216000} + \frac{14\zeta_3}{15} - \frac{91\pi^2}{4320} - \frac{11}{40} \pi^2 \rho + \left\{ \frac{10\zeta_3}{9} - \frac{10979}{960} \right. \quad (C.24) \\
&+ \left. \frac{5215\pi^2}{2592} + \frac{65}{24} \ln \rho - \frac{5}{4} \ln^2 \rho \right\} \rho^2 - \frac{145}{72} \pi^2 \rho^3 \\
&- \left\{ \frac{47791}{864} + \frac{166\zeta_3}{3} + \frac{1469\pi^2}{108} + \left( \frac{41047}{540} - \frac{40\pi^2}{9} \right) \ln \rho \right. \\
&- \left. \frac{81}{20} \ln^2 \rho - 8 \ln^3 \rho \right\} \rho^4 + \left\{ \frac{121}{108} - \frac{1189}{45} \ln \rho \right\} \pi^2 \rho^5 + \left\{ \frac{14573071}{54000} \right. \\
&- \frac{214\zeta_3}{3} + \frac{11063\pi^2}{1080} - \left( \frac{504223}{5400} + \frac{40\pi^2}{9} \right) \ln \rho + \frac{4511}{90} \ln^2 \rho \\
&+ \left. \frac{46}{9} \ln^3 \rho \right\} \rho^6 - \left\{ \frac{13}{3} + \frac{7}{3} \ln \rho \right\} \pi^2 \rho^7,
\end{aligned}$$

$$\begin{aligned}
H_A^{(2)} &= \frac{173600731}{10368000} - \frac{7601\zeta_3}{450} - \frac{749837\pi^2}{162000} + \frac{6359\pi^2 \ln 2}{900} + \frac{67\pi^4}{5400} \quad (C.25) \\
&+ \left\{ \frac{2507267051}{62208000} - \frac{155491\zeta_3}{7200} - \frac{3121867\pi^2}{324000} + \frac{931\pi^2 \ln 2}{100} + \frac{8141\pi^4}{43200} \right. \\
&+ \left. \left( \frac{2671}{800} - \frac{9\pi^2}{20} \right) \ln \rho - \frac{9}{10} \ln^2 \rho \right\} \rho^2 - \frac{31}{20} \pi^2 \rho^3 \\
&+ \left\{ \frac{655\zeta_3}{12} - \frac{139149493}{497664} - 72 \operatorname{Li}_4 \frac{1}{2} - 3 \ln^4 2 + \frac{77263\pi^2}{25920} + \frac{\pi^2 \ln 2}{9} \right. \\
&+ \left. \frac{683\pi^4}{480} + \left( 24\zeta_3 - \frac{533743}{2880} + \frac{385\pi^2}{96} \right) \ln \rho - \frac{297}{10} \ln^2 \rho \right\} \rho^4 \\
&+ \left\{ \frac{840013}{6750} - \frac{736\pi}{25} + \frac{74}{3} \ln \rho \right\} \pi^2 \rho^5 + \left\{ 748\zeta_5 - \frac{22232371}{3888000} \right. \\
&- \frac{1715\zeta_3}{24} - 304 \operatorname{Li}_4 \frac{1}{2} - \frac{38 \ln^4 2}{3} - \frac{631637\pi^2}{8640} + \frac{332\pi^2 \zeta_3}{3} \\
&+ \frac{47\pi^2 \ln 2}{3} + \frac{4\pi^2 \ln^2 2}{3} - \frac{23\pi^4}{135} + \left( 4\pi^2 - \frac{2803}{720} \right) \ln^2 \rho \\
&+ \left. \left( \frac{1345\zeta_3}{6} - \frac{46390957}{64800} + \frac{1139\pi^2}{108} - \frac{82\pi^2 \ln 2}{3} + \frac{32\pi^4}{3} \right) \ln \rho \right. \\
&- \left. \frac{5909}{54} \ln^3 \rho \right\} \rho^6 + \left\{ \frac{3928186}{33075} - \frac{100768\pi}{1575} + \frac{1958}{15} \ln \rho \right\} \pi^2 \rho^7, \\
H_{NA}^{(2)} &= -\frac{61912411}{10368000} + \frac{10517\zeta_3}{1440} + \frac{3448421\pi^2}{1728000} - \frac{6359\pi^2 \ln 2}{1800} \quad (C.26) \\
&+ \frac{101\pi^4}{10800} + \left\{ \frac{2243\zeta_3}{288} - \frac{1498563551}{124416000} + \frac{1200733\pi^2}{345600} - \frac{931\pi^2 \ln 2}{200} \right. \\
&- \left. \frac{1397\pi^4}{86400} - \frac{37}{24} \ln \rho + \frac{11}{20} \ln^2 \rho \right\} \rho^2 + \frac{31}{40} \pi^2 \rho^3 + \left\{ \frac{3 \ln^4 2}{2} - \frac{1343\zeta_3}{48} \right. \\
&- \frac{12028871}{248832} + 36 \operatorname{Li}_4 \frac{1}{2} - \frac{42821\pi^2}{6480} - \frac{\pi^2 \ln 2}{18} - \frac{649\pi^4}{2880} + \frac{713}{80} \ln^2 \rho \\
&- \left. \left( \frac{5641}{2880} + 12\zeta_3 + \frac{7\pi^2}{4} \right) \ln \rho \right\} \rho^4 + \left\{ \frac{346663}{2700} - \frac{7088 \ln 2}{25} + \frac{368\pi}{25} \right. \\
&- \left. \frac{557}{15} \ln \rho \right\} \pi^2 \rho^5 + \left\{ \frac{1555625867}{15552000} - 214\zeta_5 - \frac{29699\zeta_3}{144} + 152 \operatorname{Li}_4 \frac{1}{2} \right. \\
&+ \frac{19 \ln^4 2}{3} + \frac{241783\pi^2}{25920} - \frac{86\pi^2 \zeta_3}{3} - \frac{47\pi^2 \ln 2}{6} - \frac{2\pi^2 \ln^2 2}{3} + \frac{29\pi^4}{90} \\
&+ \left. \left( \frac{41\pi^2 \ln 2}{3} - \frac{2909911}{259200} - \frac{847\zeta_3}{12} - \frac{11051\pi^2}{432} - \frac{8\pi^4}{3} \right) \ln \rho \right. \\
&+ \left. \frac{5333}{108} \ln^3 \rho + \left( \frac{11\pi^2}{6} - \frac{43129}{480} \right) \ln^2 \rho \right\} \rho^6 \\
&+ \left\{ \frac{24856319}{165375} - \frac{7088 \ln 2}{25} + \frac{50384\pi}{1575} - \frac{8041}{105} \ln \rho \right\} \pi^2 \rho^7,
\end{aligned}$$

$$\begin{aligned}
H_L^{(2)} = & \frac{1222633}{972000} + \frac{16\zeta_3}{45} - \frac{1873\pi^2}{12960} + \left\{ \frac{4\zeta_3}{5} - \frac{90893}{6750} + \frac{77\pi^2}{60} \right. & (C.27) \\
& + \left. \frac{13}{30} \ln \rho - \frac{1}{5} \ln^2 \rho \right\} \rho^2 + \left\{ \frac{37481}{2304} + \frac{97\zeta_3}{6} - \frac{173\pi^2}{432} - 4 \ln^2 \rho \right. \\
& + \left. \left( \frac{97\pi^2}{36} - \frac{7711}{432} \right) \ln \rho \right\} \rho^4 + \left\{ \frac{64 \ln 2}{5} - \frac{976}{75} + \frac{32}{5} \ln \rho \right\} \pi^2 \rho^5 \\
& + \left\{ \frac{126685}{7776} + \frac{140\zeta_3}{3} + \frac{83\pi^2}{24} + \left( \frac{143}{8} - \frac{71\pi^2}{27} \right) \ln \rho + \frac{338}{9} \ln^2 \rho \right. \\
& - \left. \frac{448}{27} \ln^3 \rho \right\} \rho^6 + \left\{ \frac{64 \ln 2}{5} - \frac{11552}{525} + \frac{32}{5} \ln \rho \right\} \pi^2 \rho^7,
\end{aligned}$$

$$\begin{aligned}
H_C^{(2)} = & \frac{1222633}{972000} + \frac{16\zeta_3}{45} - \frac{1873\pi^2}{12960} - \frac{7}{120} \pi^2 \rho + \left\{ \frac{4\zeta_3}{5} - \frac{201241}{13500} \right. & (C.28) \\
& + \left. \frac{23\pi^2}{15} + \frac{13}{30} \ln \rho - \frac{1}{5} \ln^2 \rho \right\} \rho^2 - \frac{41}{108} \pi^2 \rho^3 \\
& + \left\{ \frac{827507}{34560} + \frac{89\zeta_3}{6} + \frac{109\pi^2}{54} + \left( \frac{91\pi^2}{36} - \frac{6157}{432} \right) \ln \rho - \frac{49}{20} \ln^2 \rho \right\} \rho^4 \\
& + \left\{ \frac{97}{24} + \frac{47}{5} \ln \rho \right\} \pi^2 \rho^5 + \left\{ \frac{904\zeta_3}{9} - \frac{139542091}{972000} - \frac{9653\pi^2}{3240} - \frac{176}{27} \ln^3 \rho \right. \\
& + \left. \left( \frac{152\pi^2}{27} - \frac{15077}{16200} \right) \ln \rho - \frac{5647}{135} \ln^2 \rho \right\} \rho^6 - \left\{ \frac{55}{18} - \frac{106}{15} \ln \rho \right\} \pi^2 \rho^7,
\end{aligned}$$

$$\begin{aligned}
H_H^{(2)} = & \frac{10203257}{19440000} - \frac{581\pi^2}{10800} + \left\{ \frac{469\pi^2}{10800} - \frac{2937091}{6480000} \right\} \rho^2 & (C.29) \\
& + \left\{ 56\zeta_3 - \frac{785928293}{10584000} + \frac{17\pi^2}{24} - \frac{47}{1050} \ln \rho \right\} \rho^4 \\
& + \left\{ \frac{41353841743}{1714608000} - \frac{176\zeta_3}{9} - \frac{113\pi^2}{324} + \left( 2\pi^2 - \frac{2993309}{136080} \right) \ln \rho \right\} \rho^6.
\end{aligned}$$

## C.4 Decay rate in model with vector couplings

For studies of the logarithmic structure of answers, we calculated the decay rate where quark weak interaction vertex is substituted as

$$\frac{ig_w}{2\sqrt{2}} \gamma_\mu (1 - \gamma_5) \rightarrow \frac{ig_w}{2} \gamma_\mu. \quad (C.30)$$

Using the same parameterization as in Eq. 7.2 and 7.4 with the substitution of  $X_i \rightarrow V_i$ , the results through  $\mathcal{O}(\rho^5)$  become:

$$V_0 = 1 - 2\rho - 8\rho^2 - \{18 + 24 \ln \rho\} \rho^3 \quad (\text{C.31})$$

$$V_1 = \frac{25}{8} - \frac{\pi^2}{2} + \{\pi^2 - 10 - 3 \ln \rho\} \rho - \{34 + 24 \ln \rho\} \rho^2 \quad (\text{C.32})$$

$$\begin{aligned}
& + \{13\pi^2 - 90 - 81 \ln \rho - 36 \ln^2 \rho\} \rho^3 \\
& + \left\{ 24\pi^2 - \frac{273}{2} + 36 \ln \rho - 72 \ln^2 \rho \right\} \rho^4 \\
& + \left\{ 13\pi^2 - \frac{369}{2} + 135 \ln \rho - 72 \ln^2 \rho \right\} \rho^5, \\
V_{NA} = & \frac{154927}{10368} - \frac{383\zeta_3}{72} + \frac{95\pi^2}{162} - \frac{53\pi^2 \ln 2}{12} + \frac{101\pi^4}{1440} \quad (\text{C.33}) \\
& + \left\{ \frac{6091\pi^2}{1296} - \frac{38485}{972} + \frac{325\zeta_3}{36} + \frac{\pi^2 \ln 2}{6} - \frac{293\pi^4}{2160} - \frac{185}{24} \ln \rho \right. \\
& + \left. \frac{11}{4} \ln^2 \rho \right\} \rho + \left\{ 4\pi^2 \ln 2 - \frac{1537}{16} - 43\zeta_3 - \frac{1181\pi^2}{216} + \frac{539\pi^4}{1080} \right. \\
& - \left. \frac{185}{3} \ln \rho + 22 \ln^2 \rho \right\} \rho^2 + \left\{ \ln^4 2 - \frac{38465}{144} - \frac{321\zeta_5}{2} - \frac{629\zeta_3}{4} \right. \\
& + 24 \text{Li}_4 \frac{1}{2} + \frac{24569\pi^2}{144} - \frac{2221\pi^2 \ln 2}{6} - \frac{43\pi^2 \zeta_3}{2} + 4\pi^2 \ln^2 2 \\
& + \frac{56\pi^3}{3} - \frac{73\pi^4}{240} - \left( \frac{73}{4} + 3\pi^2 \right) \ln^2 \rho + 55 \ln^3 \rho \\
& + \left. \left( 32\pi^2 \ln 2 - 128\zeta_3 - \frac{5417}{72} - \frac{111\pi^2}{2} - 2\pi^4 \right) \ln \rho \right\} \rho^3 \\
& + \left\{ \frac{58501\pi^2}{144} - \frac{23807}{864} - \frac{535\zeta_5}{2} - \frac{615\zeta_3}{4} + 48 \text{Li}_4 \frac{1}{2} - \frac{4583\pi^2 \ln 2}{6} \right. \\
& - \frac{215\pi^2 \zeta_3}{6} + 2 \ln^4 2 + 4\pi^2 \ln^2 2 + \frac{152\pi^3}{3} + (5\pi^2 - 185) \ln^2 \rho \\
& + \left. \left( \frac{577}{36} - 39\zeta_3 - \frac{437\pi^2}{3} + 30\pi^2 \ln 2 - \frac{10\pi^4}{3} \right) \ln \rho + 88 \ln^3 \rho \right. \\
& + \left. \frac{1777\pi^4}{720} \right\} \rho^4 + \left\{ \frac{112163}{432} - \frac{321\zeta_5}{2} - \frac{1027\zeta_3}{4} + 12 \text{Li}_4 \frac{1}{2} + \frac{\ln^4 2}{2} \right. \\
& + \frac{2848193\pi^2}{10800} - \frac{43\pi^2 \zeta_3}{2} - \frac{2395\pi^2 \ln 2}{6} + 4\pi^2 \ln^2 2 + \frac{388\pi^3}{15} \\
& + \left. \left( \frac{25015}{144} + \frac{63\zeta_3}{2} - \frac{2077\pi^2}{15} + 33\pi^2 \ln 2 - 2\pi^4 \right) \ln \rho + \frac{119\pi^4}{36} \right. \\
& + \left. \left( 10\pi^2 - \frac{1133}{4} \right) \ln^2 \rho + 87 \ln^3 \rho \right\} \rho^5,
\end{aligned}$$

$$\begin{aligned}
V_A = & \frac{11047}{2592} - \frac{223\zeta_3}{36} - \frac{515\pi^2}{81} + \frac{53\pi^2 \ln 2}{6} + \frac{67\pi^4}{720} & (C.34) \\
+ & \left\{ \frac{1997\pi^2}{648} - \frac{81149}{1944} + \frac{317\zeta_3}{18} - \frac{\pi^2 \ln 2}{3} - \frac{211\pi^4}{1080} - \frac{9}{4} \ln^2 \rho \right. \\
+ & \left. \left( \frac{3\pi^2}{2} - \frac{123}{8} \right) \ln \rho \right\} \rho + \left\{ \frac{497\pi^2}{108} - \frac{2089}{8} + 86\zeta_3 - 8\pi^2 \ln 2 \right. \\
+ & \left. \frac{121\pi^4}{540} - 105 \ln \rho - 36 \ln^2 \rho \right\} \rho^2 + \left\{ \frac{4667\pi^2}{72} - \frac{16943}{36} + 561\zeta_5 \right. \\
- & \frac{37\zeta_3}{2} - 48 \operatorname{Li}_4 \frac{1}{2} - 2 \ln^4 2 + 83\pi^2 \zeta_3 - 17\pi^2 \ln 2 - 8\pi^2 \ln^2 2 \\
- & \left. \frac{112\pi^3}{3} + \left( 8\pi^4 + 328\zeta_3 + \frac{125\pi^2}{6} - \frac{50969}{72} - 64\pi^2 \ln 2 \right) \ln \rho \right. \\
+ & \left. \left( 12\pi^2 - \frac{747}{4} \right) \ln^2 \rho - 63 \ln^3 \rho + \frac{449\pi^4}{120} \right\} \rho^3 \\
+ & \left\{ \frac{16586}{27} - \frac{795\zeta_3}{2} - 96 \operatorname{Li}_4 \frac{1}{2} + \frac{13223\pi^2}{72} + 13\pi^2 \ln 2 + \frac{415\pi^2 \zeta_3}{3} \right. \\
+ & 935\zeta_5 - 4 \ln^4 2 - 8\pi^2 \ln^2 2 - \frac{304\pi^3}{3} - \frac{349\pi^4}{72} + (99 + 4\pi^2) \ln^2 \rho \\
+ & \left. \left( \frac{40\pi^4}{3} - \frac{19459}{18} + 246\zeta_3 + \frac{361\pi^2}{3} - 60\pi^2 \ln 2 \right) \ln \rho - 144 \ln^3 \rho \right\} \rho^4 \\
+ & \left\{ \frac{14036}{27} + 561\zeta_5 + \frac{109\zeta_3}{2} - 24 \operatorname{Li}_4 \frac{1}{2} - \ln^4 2 + \frac{264109\pi^2}{5400} + 83\pi^2 \zeta_3 \right. \\
+ & 41\pi^2 \ln 2 - 8\pi^2 \ln^2 2 - \frac{776\pi^3}{15} - \frac{1093\pi^4}{90} + \left( \frac{1395}{4} - 8\pi^2 \right) \ln^2 \rho \\
- & \left. 141 \ln^3 \rho + \left( 81\zeta_3 - \frac{8456}{9} + \frac{401\pi^2}{2} - 66\pi^2 \ln 2 + 8\pi^4 \right) \ln \rho \right\} \rho^5,
\end{aligned}$$

$$\begin{aligned}
V_L = & -\frac{1009}{288} + \frac{8\zeta_3}{3} + \frac{77\pi^2}{216} + \left\{ \frac{215}{18} - \frac{16\zeta_3}{3} - \frac{43\pi^2}{54} \right. & (C.35) \\
+ & \left. \frac{13}{6} \ln \rho - \ln^2 \rho \right\} \rho + \left\{ \frac{118}{3} - \frac{4\pi^2}{3} + \frac{52}{3} \ln \rho - 8 \ln^2 \rho \right\} \rho^2 \\
+ & \left\{ \frac{163}{2} + 48\zeta_3 - \frac{293\pi^2}{18} + \left( \frac{93}{2} + \frac{20\pi^2}{3} \right) \ln \rho - \ln^2 \rho - 20 \ln^3 \rho \right. \\
+ & \left. \frac{64\pi^2 \ln 2}{3} \right\} \rho^3 + \left\{ 76\zeta_3 - 33 - \frac{133\pi^2}{3} + (39 + 16\pi^2) \ln \rho \right. \\
+ & \left. 52 \ln^2 \rho - 32 \ln^3 \rho + \frac{128\pi^2 \ln 2}{3} \right\} \rho^4 + \left\{ \frac{1}{2} + 36\zeta_3 - \frac{2417\pi^2}{90} \right. \\
+ & \left. \frac{64\pi^2 \ln 2}{3} + \left( \frac{14\pi^2}{3} - \frac{195}{2} \right) \ln \rho + 109 \ln^2 \rho - 36 \ln^3 \rho \right\} \rho^5,
\end{aligned}$$



$$V_H = \frac{16987}{576} - \frac{64\zeta_3}{3} - \frac{85\pi^2}{216} + \left\{ \frac{35\pi^2}{54} - \frac{4109}{216} + \frac{32\zeta_3}{3} \right\} \rho \quad (\text{C.36})$$

$$+ \left\{ \frac{8\pi^2}{3} - \frac{1198}{45} \right\} \rho^2$$

$$+ \left\{ \frac{9\pi^2}{2} - 16\zeta_3 - \frac{30043}{1080} + \left( \frac{20\pi^2}{3} - \frac{1193}{18} \right) \ln \rho \right\} \rho^3$$

$$+ \left\{ \frac{156901877}{2116800} - 64\zeta_3 - \frac{11\pi^2}{18} + \left( \frac{20\pi^2}{3} - \frac{186689}{2520} \right) \ln \rho \right\} \rho^4$$

$$+ \left\{ \frac{24416711}{352800} - 24\zeta_3 - \frac{9\pi^2}{2} + \left( 6\pi^2 - \frac{9883}{140} \right) \ln \rho \right\} \rho^5,$$

$$V_C = -\frac{1009}{288} + \frac{8}{3}\zeta_3 + \frac{77}{216}\pi^2 + \left\{ \frac{94}{9} - \frac{16\zeta_3}{3} - \frac{167\pi^2}{108} \right\} \rho \quad (\text{C.37})$$

$$+ \left\{ \frac{13}{6} \ln \rho - \ln^2 \rho \right\} \rho + \left\{ \frac{145}{3} + \frac{22\pi^2}{3} + \frac{52}{3} \ln \rho - 8 \ln^2 \rho \right\} \rho^2$$

$$+ \left\{ 68 + 120\zeta_3 + \left( \frac{129}{2} + \frac{106\pi^2}{3} \right) \ln \rho - \ln^2 \rho - 20 \ln^3 \rho \right.$$

$$\left. + \frac{1061\pi^2}{36} \right\} \rho^3 + \left\{ 196\zeta_3 - \frac{4483}{36} + \left( \frac{599}{6} + \frac{158\pi^2}{3} \right) \ln \rho + 44 \ln^2 \rho \right.$$

$$\left. - \frac{121\pi^2}{18} - 32 \ln^3 \rho \right\} \rho^4 + \left\{ 200\zeta_3 - \frac{20557}{72} + \left( \frac{98\pi^2}{3} + \frac{686}{3} \right) \ln \rho \right.$$

$$\left. - 36 \ln^2 \rho - 12 \ln^3 \rho - \frac{185\pi^2}{6} \right\} \rho^5.$$

## C.5 Charm mass in $b \rightarrow u$ transitions

In case of semi-leptonic decay  $b \rightarrow u\ell\bar{\nu}$  the correction due to  $c$ -quarks is calculated similarly to  $X_C$  of Eq. 7.4, with massless propagators corresponding to  $u$ -quark. Through  $\mathcal{O}(\rho^7)$ , the result (with the same pre-factors as  $X_C$ ) is

$$U_C = -\frac{1009}{288} + \frac{8\zeta_3}{3} + \frac{77\pi^2}{216} - \frac{5}{4}\pi^2\rho + \left\{ 21 + \frac{8\pi^2}{3} \right\} \rho^2 \quad (\text{C.38})$$

$$+ \left\{ \frac{64 \ln 2}{3} - \frac{95}{36} + \frac{32}{3} \ln \rho \right\} \pi^2 \rho^3$$

$$+ \left\{ 48\zeta_3 - \frac{4375}{36} - \frac{25\pi^2}{6} + \left( \frac{365}{6} + 6\pi^2 \right) \ln \rho - 8 \ln^2 \rho \right\} \rho^4$$

$$- \frac{112}{15}\pi^2\rho^5 + \left\{ \frac{7804}{675} + \frac{8}{5} \ln \rho - \frac{64}{9} \ln^2 \rho + \frac{64\pi^2}{27} \right\} \rho^6 - \frac{24}{7}\pi^2\rho^7.$$